

Determination of pullout resistance of galvanized-steel strips within select South African soils based on their free draining potential in mechanically stabilized earth wall backfill conditions

by

Kyle Hoffman



Thesis presented in fulfilment of the requirements for the degree of Master of Engineering in the Faculty of Civil Engineering at Stellenbosch University

Supervisor: Nanine Fouché

Candidate: Kyle Hoffman

December 2019



UNIVERSITEIT • STELLENBOSCH • UNIVERSITY
jou kennisvenoot • your knowledge partner

Plagiaatverklaring / Plagiarism Declaration

- 1 Plagiaat is die oorneem en gebruik van die idees, materiaal en ander intellektuele eiendom van ander persone asof dit jou eie werk is.
Plagiarism is the use of ideas, material and other intellectual property of another's work and to present it as my own.
- 2 Ek erken dat die pleeg van plagiaat 'n strafbare oortreding is aangesien dit 'n vorm van diefstal is.
I agree that plagiarism is a punishable offence because it constitutes theft.
- 3 Ek verstaan ook dat direkte vertalings plagiaat is.
I also understand that direct translations are plagiarism.
- 4 Dienooreenkomstig is alle aanhalings en bydraes vanuit enige bron (ingesluit die internet) volledig verwys (erken). Ek erken dat die woordelike aanhaal van teks sonder aanhalingstekens (selfs al word die bron volledig erken) plagiaat is.
Accordingly all quotations and contributions from any source whatsoever (including the internet) have been cited fully. I understand that the reproduction of text without quotation marks (even when the source is cited) is plagiarism.
- 5 Ek verklaar dat die werk in hierdie skryfstuk vervat, behalwe waar anders aangedui, my eie oorspronklike werk is en dat ek dit nie vantevore in die geheel of gedeeltelik ingehandig het vir bepunting in hierdie module/werkstuk of 'n ander module/werkstuk nie.
I declare that the work contained in this assignment, except where otherwise stated, is my original work and that I have not previously (in its entirety or in part) submitted it for grading in this module/assignment or another module/assignment.

K. Hoffman	25/09/2019
Voorletters en van / Initials and surname	Datum / Date

Declaration

By submitting this thesis electronically, I declare that the entirety of the work contained therein is my own, original work, that I am the sole author thereof (save to the extent explicitly otherwise stated), that reproduction and publication thereof by Stellenbosch University will not infringe any third party rights and that I have not previously in its entirety or in part submitted it for obtaining any qualification.

September 2019

Copyright © 2019 Stellenbosch University

All rights reserved

Abstract

The design requirements stipulate that for a mechanically stabilized earth (MSE) wall, the backfill used should be classified as free draining and non-plastic (McKittrick, 1978). For this reason, there is a lack of research involving testing of materials that are cohesive and non-free draining as they could potentially fail to adhere to the design requirements. Using *Fusion 360*, a pullout apparatus was designed and tested in silico for safe working loads through the use of finite element analysis. The pullout apparatus was then constructed and used to quantify the pullout resistance of steel strips within South African soils with varying free draining potentials. The materials tested consisted of a Greywacke crusher dust, Cape Flats sand and a micaceous residual granite from Malmesbury. These materials represented a range of permeabilities from the medium permeability of the crusher dust (1.2×10^{-4} m/s), to the low permeability of the Cape Flats sand (3.3×10^{-5} m/s) and the very low permeability of the micaceous residual granite (7.8×10^{-6} m/s).

A total of 24 pullout tests were performed at four discrete applied vertical stresses, those being 0 kPa, 50 kPa, 100 kPa and 150 kPa (excluding self-weight of the soil as those are factored on a per soil basis). In order to compare the soils, the use of a maximum pullout force versus applied vertical stress plot was constructed. This showed that both the granular free draining materials (the crusher dust and Cape Flats sand) out-performed the micaceous residual granite. This was evidenced by the gradient of the pullout force versus effective stress graph for each respective soil. The non-plastic materials, namely the crusher dust and the Cape Flats sand, presented a gradient of 1.1 and 0.9 respectively while the micaceous residual granite had a gradient of 0.4. The steeper gradients of the granular materials provide an indication as to their improved pullout resistance at higher vertical stresses as compared to that of the micaceous residual granite.

A common method of characterizing the performance of a given backfill's pullout resistance is to compare the measured pullout factor (F_m^*) to that of an estimated pullout factor (F_e^*) determined at the same relative vertical stress. The performance of the granular materials was superior to that of the micaceous residual granite. All calculated F_m^* values for the granular materials plotted well above the estimated F_e^* values. This was not the case for the micaceous residual granite, as any F_m^* value calculated for a simulated depth greater than 4 m fell below the estimation curve. A factor of safety (FoS) plot was constructed from the measured pullout force and the estimated pullout force (derived from the estimated F_e^* values). For the granular materials, as wall height increases, the FoS trends towards a value greater than 1 while the micaceous residual granite plots below 1. This shows that the estimated performance for granular materials used within MSE walls are typically conservative while the opposite is true for the plastic non-free draining materials.

When comparing the data obtained from both the pullout tests and the soil classification tests, the results support the design requirement of MSE walls that granular free draining materials should be used within backfills. Even though the micaceous residual granite passed all soil shear strength and grading parameters, it fell well below the AASHTO estimation boundary. This indicates that if the correct precautions are not taken, any structure which uses the micaceous residual granite as a backfill to construct an MSE wall has a high potential for failure.

Opsomming

Die ontwerpvereistes vir meganies gestabiliseerde grondmure ('MSE' mure) stipuleer dat die opvulling wat gebruik word, geklassifiseer moet word as vry-dreinerend en nie-plasties. Aangesien die gebruik van kohesie en nie-vry-dreinerende materiale nie voldoen aan die vereistes nie, is daar 'n gebrek aan navorsing rondom die gebruik van sulke materiale as opvulling.

In hierdie studie was die program *Fusion 360* gebruik om 'n uittrek-apparaat te ontwerp en om die ontwerp te toets vir veilige werkladings deur die gebruik van eindige elementanalise. Die volledige apparaat was verder gebruik om die uittrekweerstand van staalstroke binne Suid-Afrikaanse grondsoorte met vry-dreinerende potensiaal te bepaal. Die grondsoorte was as volg: 'n growwak breker stof (crusher dust), sand vanaf die Kaapse Vlakte, en 'n mika bevattende residuele graniet vanaf Malmesbury. Die deurlaatbaarheid van hierdie grondsoorte het 'n reeks van waardes getoon: die breker stof met medium deurlaatbaarheid (1.2×10^{-4} m/s), die Kaapse Vlakte sand met lae deurlaatbaarheid (3.3×10^{-5} m/s), en die mika bevattende oorblywende graniet met besonderse lae deurlaatbaarheid (7.8×10^{-6} m/s).

Die uittrektoetse was by vier verskillende toegepaste vertikale spannings uitgevoer (0 kPa, 50 kPa, 100 kPa en 150 kPa) met 'n geheel van 24 toetse. Die uittrekweerstand van die grondsoorte was vergelyk deur die gebruik van grafieke met maksimum uittrekweerstand teenoor toegepaste vertikale spanning. Beide die korrelagtige vry-dreinerende materiale (breker stof en sand) het beter gevaar as die graniet in terme van die helling van die grafieke. Die breker stof en sand het onderskeidelik oor 'n helling van 1.1 en 0.9 beskik, terwyl die graniet 'n helling van 0.4 gehad het. Die groter hellings van die twee korrelagtige materiale stem ooreen met beter uittrekweerstand onder hoër vertikale spanning.

Die uittrekweerstand van grondversterkings word dikwels evalueer deur om die gemete uittrek faktor (F_m^*) te vergelyk met die geskatte uittrek faktor (F_e^*) wat bepaal word by dieselfde vertikale spanning. Die korrelagtige materiale het beter presteer as die residuele graniet. Al die berekende F_m^* waardes vir die korrelagtige materiale was ver bo die geskatte F_e^* waardes geleë. Hierdie was egter nie die geval vir die residuele graniet nie aangesien al die F_m^* waardes by 'n diepte groter 4 m onder die kurwe geleë was. Die gemete uittrekweerstand en die geskatte uittrekweerstand (gebaseer op die geskatte F_e^* waardes) was gebruik om 'n veiligheidsfaktor grafiek te teken. Soos die hoogte van die muur toeneem, is die tendens vir die veiligheidsfaktor van die korrelagtige materiale na 'n waarde groter as 1, terwyl die graniet se veiligheidsfaktor onder 1 bly. Dit dien as bewyse dat die beraamde prestasie van korrelagtige materiale binne 'MSE' mure oor die algemeen konserwatief is, terwyl die teenoorgestelde waar is in die geval van plastiese nie-vry-dreinerende materiale.

Wanneer die resultate van die uittrektoetse en die grondsoort klassifikasie toetse in ag geneem word, leen dit ondersteuning aan die aanvanklike ontwerpvereistes dat korrelagtige vry-dreinerende materiale gebruik moet word as opvulling vir 'MSE' mure. Al het die graniet die nodige grondsoort skuifkrag en graderings grense geslaag, was dit ver onder die AASHTO skattinggrens geleë. Dus dui dit aan dat enige struktuur wat hierdie graniet grondsoort gebruik as opvulling vir 'n 'MSE' muur 'n hoë potensiaal het om te faal as die regte voorsorgmaatreëls nie in plek gestel is nie.

Acknowledgments

I would like to extend my gratitude to the following groups and individuals, without whom this dissertation would not have been possible:

To my supervisor, Nanine Fouché, thank you for always being there for assistance and guidance.

To Colin, Gavin, Dion and Oom Johan, your technical assistance and knowhow is truly an invaluable asset to all those studying at Stellenbosch University.

To the team in office S477, thanks for all the great memories and helping keep us all sane through the tough times.

To my loving wife Ingrid Jacobs-Hoffman, without you being there as my source of strength, this dissertation would have never come to be, thank you for everything.

Dear Dad, This one's for you.

Table of Contents

Declaration	i
Abstract	ii
Opsomming	iii
Acknowledgments	iv
List of Figures.....	x
List of Tables.....	xiv
1 Introduction	1
1.1 Background.....	1
1.2 Problem statement	1
1.3 Unique research contributions	1
1.4 Outline of this study	2
1.5 Limitations of research	2
1.6 Brief chapter overviews.....	3
2 Literature Review	4
2.1 Introduction	4
2.2 History and development of mechanically stabilized earth walls.....	4
2.2.1 Original idea of stress transfer within a soil mass	4
2.2.2 Improved soil stress transfer models	6
2.2.3 The modern definition of reinforced soil concepts	8
2.3 Design of modern MSE walls.....	10
2.4 Soil Permeability	12
2.5 Modern standards on backfill conditions.....	13
2.6 Determining pullout resistance of a soil reinforcement.....	17
2.6.1 In-situ pullout tests in South Africa.....	17
2.6.2 Laboratory pullout tests	19
2.6.3 Estimating pullout resistance	21
3 Pullout apparatus	23
3.1 Introduction	23
3.2 Aim and objectives	23

3.3	Design phase.....	23
3.3.1	Initial study.....	23
3.3.2	Design prototyping.....	24
3.3.3	Primary design parameters.....	27
3.3.4	Testing of the design.....	28
4	Construction phase.....	33
4.1.1	Material preparation.....	33
4.1.2	Assembly of the materials.....	34
4.1.3	Wooden inserts.....	36
4.1.4	Steel strip coupling.....	37
4.2	Stressing equipment.....	38
4.2.1	Airbag.....	38
4.2.2	Hydraulic jack.....	41
4.3	Data acquisition.....	44
4.4	Cost breakdown.....	44
4.5	Conclusion.....	45
5	Methodology.....	46
5.1	Introduction.....	46
5.2	Aim and Objectives.....	46
5.3	Soil Samples.....	46
5.3.1	Crusher Dust.....	46
5.3.2	Cape Flats sand.....	46
5.3.3	Micaceous Residual Granite.....	47
5.4	Soil Classification.....	47
5.4.1	Maximum dry density and optimum moisture content.....	47
5.4.2	Soil particle size distribution.....	47
5.4.3	Atterberg limits.....	48
5.4.4	Permeability testing.....	48
5.4.5	Direct shear testing.....	51
5.5	Pullout testing.....	52

5.5.1	Steel Strip	52
5.5.2	Sample preparation	53
5.5.3	Pullout resistance testing	53
6	Results	57
6.1	Introduction	57
6.2	Soil Classification.....	57
6.2.1	Maximum dry density and optimum moisture content.....	57
6.2.2	Soil particle size distribution	58
6.2.3	Atterberg limits.....	60
6.2.4	Permeability testing	61
6.2.5	Direct shear testing	61
6.3	Pullout testing	64
6.3.1	Pullout resistance testing	64
6.3.2	Displacement during pullout testing.....	66
7	Discussion.....	69
7.1	Introduction	69
7.2	Soil classifications	69
7.2.1	Soil compaction	69
7.2.2	Soil permeability.....	69
7.2.3	Shear strength parameters.....	70
7.3	Pullout resistance testing	71
7.3.1	Condensing pullout resistance over time graphs	71
7.3.2	Analysis of pullout resistance data	72
7.3.3	Moisture content.....	74
7.3.4	Link to rate of shearing.....	74
7.3.5	Anomalies in pullout resistance trends	74
7.3.6	Pullout resistance factor comparison	75
7.3.7	Estimated factor of safety	77
8	Final Conclusions and Research Recommendations	79
8.1	Pullout apparatus	79

8.2	Pullout testing and soil classification	79
9	Bibliography	81
Appendix A.	Individual pullout test data	I
Appendix B.	Pullout apparatus assembly guide.....	IX
Appendix C.	Finite Element Analysis.....	XX

List of Figures

Figure 2-1. The effects of soil reinforcements on dilation caused by vertical stressing.....	4
Figure 2-2. Original Mohr circle described by Henry Vidal (1969).....	5
Figure 2-3. Failure envelope according to the SIGMA models constant prestress conditions (Hausmann and Lee, 1976).....	6
Figure 2-4. Failure envelope according to the SIGMA model's increasing prestress conditions (Hausmann and Lee, 1976).....	7
Figure 2-5. Normal pressure inducing friction on soil reinforcement	8
Figure 2-6. Frictional resistance versus passive resistance in steel strips.	8
Figure 2-7. Frictional resistance versus passive resistance in reinforcement grids.	9
Figure 2-8. Cross-section view of an MSE wall and all its elements	10
Figure 2-9. Soil reinforcement strips produced by Reinforced Earth.....	11
Figure 2-10. Materials suitable for backfill construction according to Reinforced Earth	15
Figure 2-11. Pullout resistance of in-situ materials in South Africa	19
Figure 2-12. Estimation of pullout factor with relation to depth and C_u (AASHTO, 2012).....	22
Figure 3-1. Small-scale model of pullout apparatus constructed using foam board.....	24
Figure 3-2. Construction of model – replicating steel channel using foam board.....	25
Figure 3-3 Construction of model - disassembly of apparatus into parts for easy transport and storage.	25
Figure 3-4. Construction of model - modular base assembly.....	26
Figure 3-5. Construction of model - steel channel orientation.....	26
Figure 3-6. Construction of model - zone of concern.....	27
Figure 3-7 Final pullout apparatus model designed using Autodesk Fusion 360.....	28
Figure 3-8. General stress strain relation of steel.	28
Figure 3-9. Finite Element Analysis of pullout apparatus lid at 300kPa. Deflection was observed to be roughly 1.7mm.....	30
Figure 3-10. Finite Element Analysis of pullout apparatus lid at 500 kPa. Deflection was observed to be roughly 2.9mm.....	30
Figure 3-11. Finite Element Analysis of pullout apparatus base assembly at its standard vertical position with a jack load of 50kN. Deflection was observed to be 16.5 mm.	31
Figure 3-12. Finite Element Analysis of pullout apparatus base assembly at the least ideal position with a jack load of 50kN. Deflection was observed to be 44.7mm.....	32
Figure 4-1. Plasma cutter.....	33
Figure 4-2. Steel bandsaw.	33
Figure 4-3. End-plates.	33
Figure 4-4. Prepared steel channels.....	33
Figure 4-5. General design of all load carrying beams.....	34
Figure 4-6. Center punch and top hat design.....	34
Figure 4-7. Side panel alignment.....	35

Figure 4-8. Top hat insert.	35
Figure 4-9. Magnetic mounting drill (magdrill).	35
Figure 4-10. Construction of pullout apparatus lid.	36
Figure 4-11. Wooden inserts used to reduce the internal dimension of the soil chamber.	37
Figure 4-12. Steel strip to threaded rod coupling.	37
Figure 4-13. Inner tube when deflated.	39
Figure 4-14. Inner tube when inflated.	39
Figure 4-15. Clamped test airbag.	39
Figure 4-16. Inflated test airbag.	39
Figure 4-17. Valve design.	40
Figure 4-18. Final bag dimensions.	40
Figure 4-19. Air pressure regulator.	40
Figure 4-20. Standard rate of pullout displacement.	41
Figure 4-21. Adjusted pullout method to achieve standardized rate of pullout.	41
Figure 4-22. Hydraulic jack and power pack.	42
Figure 4-23. Rate of displacement test setup.	42
Figure 4-24. Rate of displacement testing.	43
Figure 4-25. Hydraulic jack mount – front.	43
Figure 4-26. Hydraulic jack mount – back.	43
Figure 4-27. Data acquisition setup.	44
Figure 5-1. Permeability test apparatus (not to scale)	48
Figure 5-2. Permeameter cell assembly requirements.	49
Figure 5-3. Permeameter Cell.	50
Figure 5-4. 100 0mm Shear box components.	51
Figure 5-5. Shear box sample preparation.	51
Figure 5-6. Shear box layer compaction height.	51
Figure 5-7. Steel strip used for testing – dimensions.	52
Figure 5-8. Enlarged image of steel strip features.	52
Figure 5-9. Pullout testing sample preparation.	53
Figure 5-10. Soil chamber lined with HDPE plastic.	55
Figure 5-11. Soil heights used for compaction.	55
Figure 5-12. Compacted soil within the soil chamber.	55
Figure 5-13. HDPE lining on soil surface.	55
Figure 5-14. Airbag within the soil chamber.	55
Figure 5-15. HDPE plastic lining around airbag to reduce friction.	55
Figure 5-16. Soil chamber with bolted lid and air pressure regulator attached.	56
Figure 6-1. Dry density curve of the crusher dust.	57
Figure 6-2. Dry density curve of micaceous residual granite.	57

Figure 6-3. Dry density curve of Cape Flats sand	58
Figure 6-4. Particle size distribution of crusher dust in both pre- and post-pullout testing conditions	59
Figure 6-5. Particle size distribution of Cape Flats sand in both pre- and post-pullout testing conditions	59
Figure 6-6. Particle size distribution of micaceous residual granite in both pre- and post-pullout testing conditions	60
Figure 6-7. Failure envelope of the crusher dust in both pre- and post-pullout testing conditions	62
Figure 6-8. Failure envelope of the sieved crusher dust in both pre- and post-pullout testing conditions	62
Figure 6-9. Failure envelope of the Cape Flats sand in both pre- and post-pullout testing conditions	63
Figure 6-10. Failure envelope of the micaceous residual granite in both pre- and post-pullout testing conditions	63
Figure 6-11. Pullout resistance over time - Crusher dust	64
Figure 6-12. Pullout resistance over time - Cape Flats sand	65
Figure 6-13. Pullout resistance over time - Micaceous residual granite.....	65
Figure 6-14. Rate of displacement confirmation for crusher dust pullout testing	66
Figure 6-15. Displacement results indicating hydraulic jack mount deflection for the crusher dust tests	67
Figure 6-16. Rate of displacement confirmation for Cape Flats sand pullout testing	67
Figure 6-17. Displacement results indicating hydraulic jack mount deflection for the Cape Flats sand tests	67
Figure 6-18. Displacement data for micaceous residual granite pullout testing.....	68
Figure 6-19. Displacement results indicating hydraulic jack mount deflection for the micaceous residual granite tests.....	68
Figure 7-1. Determination of an average pullout resistance for a given pullout resistance versus time plot ..	71
Figure 7-2. Average peak pullout resistance measured for each soil type	73
Figure 7-3. Moisture content of embedment layer during pullout testing.....	74
Figure 7-4. Pullout resistance factor comparison for the crusher dust	76
Figure 7-5. Pullout resistance factor comparison for the Cape Flats sand	76
Figure 7-6. Pullout resistance factor comparison for the micaceous residual granite	77
Figure 7-7. Factor of safety versus wall height	78
Figure B-1. Base construction	XI
Figure B-2. Dot alignment method.....	XI
Figure B-3. Base plate positioning	XII
Figure B-4. Plate 'A' Alignment	XII
Figure B-5. Plate 'B' Alignment.....	XII
Figure B-6. Side panel assembly	XIII
Figure B-7. 'A' Alignment	XIII
Figure B-8. 'B' Alignment	XIII
Figure B-9. Lower back panel alignment	XIV
Figure B-10. Lower front panel alignment	XIV
Figure B-11. Lower load transfer sleeve	XV

Figure B-12. Load transfer sleeve slotted fixture	XV
Figure B-13. Upper back plate	XVI
Figure B-14. Upper front plate	XVI
Figure B-15. Completed soil chamber.....	XVII
Figure B-16. Completed soil chamber.....	XVII
Figure B-17. Final 'A' alignment	XVIII
Figure B-18. Final 'B' alignment	XVIII
Figure B-19. Upright support positions.....	XVIII
Figure B-20. Base mounting positions	XVIII
Figure B-21. Jack position 1.....	XIX
Figure B-22. Jack position 2.....	XIX
Figure B-23. Jack position 4.....	XIX
Figure B-24. Jack position 3.....	XIX
Figure C-1. Finite Element Analysis of pullout box lid at 300 kPa.	XX
Figure C-2. Finite Element Analysis of pullout box lid at 500 kPa.	XXI
Figure C-3. Finite Element Analysis of pullout box base assembly at its standard vertical position with a jack load of 50 kN.....	XXII
Figure C-4. Finite Element Analysis of pullout box base assembly at the least ideal position with a jack load of 50 kN.	XXIII

List of Tables

Table 2-1. Reinforcement types and their resistance characteristics	9
Table 2-2. Soil classification related to permeability based on Head (1992).	12
Table 2-3. Comparison of selection criteria of mechanical properties for backfill materials.....	14
Table 2-4. Reinforced Earth backfill material classifications, modified from Reinforced Earth (Smith, 2010)	15
Table 2-5. Summary of in-situ pullout tests in South Africa (summarized from Smith and Vadron, 1993)...	18
Table 2-6. Novel pullout tests for steel strips	20
Table 4-1. Cost breakdown of constructing pullout apparatus (excluding other equipment).....	45
Table 5-1. Summary of pullout testing conditions	54
Table 6-1. Atterberg limits of micaceous residual granite	60
Table 6-2. Summary of material permeability.....	61
Table 6-3. Summary of shear strength parameters for all soil materials	61
Table 7-1. Issues derived for shear strength tests	70
Table 7-2. Shear strength parameters of testing materials.....	70
Table 7-3. Summary of pullout resistance results including calculated F_m^* values.....	72
Table 7-4. Values required to determine F_e^*	75
Table 7-5. Factor of Safety for each material type with respect to wall height.....	77

1 Introduction

1.1 Background

The process of reinforcing a soil mass with non-soil inserts has been practiced for thousands of years (Berg, Christopher, & Samtani, 2009). Henri Vidal is regarded as the pioneer of modern soil reinforcement techniques owing to his work *The Principle of Reinforced Earth* (Vidal, 1969). Within his writing he describes his initial theory of improving the mechanical property of a soil through the use of reinforcement layers. This has since led to the global influence that reinforced earth currently has on the market of retaining structures.

Retaining structures have many different designs with the same aim of producing near vertical walls which use the retained soil as part of the overall design. Retaining walls can typically be differentiated depending on the type of soil reinforcements they use – those that use extensible reinforcement sheets (segmented block retaining walls) and those that use inextensible reinforcement strips (mechanically stabilized earth walls). Although there are many different standards and theories which try to quantify the relationship between construction and soil conditions within a backfill to that of the physical resistance of the strip-like reinforcements, it is generally accepted that the pullout resistance of the reinforcement is the best means to determine overall strength. The pullout resistance of soil reinforcements has successfully been quantified in both in-situ and laboratory pullout tests.

1.2 Problem statement

The design specifications that are followed during the construction of MSE walls stipulate that the backfill material should consist of a free draining non-plastic soil (McKittrick, 1978). For this reason, there is a lack of pullout resistance data on non-free draining/plastic backfill materials in literature. After 1978, the majority of pullout resistance tests in South Africa were performed in-situ through the use of monitoring panels. This has caused a further gap in the literature regarding pullout tests performed within the laboratory environment.

1.3 Unique research contributions

South African MSE walls are predominantly built using the methods and materials provided by the *Reinforced Earth* Company. By building a pullout test apparatus, South African soils can be tested locally through a range of backfill conditions to quantify their performance with regards to the pullout resistance of various soil reinforcements. This allows for South African soils which are either free draining or non-free draining to be subjected to laboratory pullout tests. The design of the pullout apparatus will be completed insuring that not only standardized horizontal testing can be performed, but also vertical micro pile pullout tests. The soil types which can be tested are not limited to a given specification, such as origin, particle size distribution or moisture content.

1.4 Outline of this study

The primary aim of this research project was to determine the pullout resistance of select South African soils with ranging drainage characteristics. The tests were performed in conditions which match backfill conditions directly after construction has taken place. This study is divided into two subsections, each of which focuses on an aspect of the main aim. The first section is aimed at the design and construction of a pullout apparatus and the second section focuses on soil classification and pullout testing of the South African soils.

The first section (Chapter 3) had the following objectives:

- Design and construct a pullout apparatus that can safely allow for pullout testing at a range of vertical stresses.
- Allow for additional apparatus orientations in order to alter the testing methods to non-standardized testing protocols.

The second section (Chapter 4) concentrates on the testing methodology of the overall study, including soil classification techniques and pullout testing (utilizing the pullout apparatus designed and constructed in Chapter 3). In order to achieve the aim of this section, the following objectives were set:

- Classify the testing materials through a range of standardized laboratory tests, such as shear strength tests, permeability tests and maximum dry density determination.
- To design a test protocol for the pullout testing.

1.5 Limitations of research

The limitations pertaining to this research project can be subdivided into two sections: those regarding the design process and those regarding the ability to obtain enough pullout results that are consistent and accurate. Limitations regarding the design process involved the development of the CAD (computer aided design) model. As there were no clear design constraints for the pullout apparatus, the limitation rather became a question of what is feasible to produce. This is a key point that many designers face of producing a product that is both functional and safe while also keeping costs as low as possible. In general, standardized soil characterization tests (e.g. those that determine maximum dry density, soil strength parameters and permeability) are rapid and easy to perform.

The difficulties regarding pullout testing are all based off of keeping consistence moisture contents for the given soil types. During the compaction and loading phases of the soil chamber, moisture loss can occur. This gives a short life span for a given batch of mixed material as extended periods of testing could leading to sub-optimum moisture for testing.

1.6 Brief chapter overviews

The structure of this thesis will be divided into seven unique chapters. Chapter 1 provides an outline of the entire research project, including a summary of the literature review, the aims and objectives as well as the limitations of this study. Chapter 2 provides a literature review on mechanically stabilized earth walls containing information regarding the history and design of MSE walls, and a look at South African standards regarding these structures. This chapter acts as a lead into Chapter 3, which outlines the pullout apparatus used to obtain the pullout resistance of soil reinforcements.

Chapter 3 describes the design and development of a pullout apparatus for the use of Stellenbosch University Geotechnical Engineering Department. This chapter provides insight into the initial design study and prototyping stage required in order to begin the construction phase of the pullout apparatus. A small conclusion is provided at the end of this chapter to ascertain whether the aims and objectives for the design and construction of the pullout apparatus were achieved. Chapter 4 consists of the methods and materials used performing the soil classification tests and pullout testing. These tests include direct shear, permeability, maximum dry density and sieve analysis. This chapter concludes in a similar way to Chapter 3, as it also assesses the outcome of this chapter in meeting the stated aims and objectives.

Chapter 5 and 6 contain the results and discussion, respectively, of the soil classification tests and pullout tests. Chapter 5 provides the original data in a clear condensed form, whereas the analysis thereof is done within Chapter 6. The discussion is orientated around structuring the data in such a way that the main aims and objectives of the research project can be easily assessed. The final conclusion is provided in Chapter 7 where the overall dissertation is discussed, and further improvements are given on both the pullout apparatus design as well as the testing procedure provided in Chapter 4.

2 Literature Review

2.1 Introduction

This chapter is structured around the design conditions of mechanically stabilized earth (MSE) walls based on what is provided in literature as well as what is directly related to structures present in South Africa. As South Africa's MSE walls are predominantly built by using the methods and materials provided by the *Reinforced Earth* company (Smith and Vadron, 1993) the main focus is therefore placed on the same methods and materials. This will include the history and development of the mechanics involved within a reinforced soil mass. The modern definition and design standards of MSE walls will be looked at with a specific focus on the required soil conditions within the backfill of the MSE walls as well as the reinforcements themselves. This will focus on the conditions which define whether the backfill material is considered free draining or not. A section will be based on the current standards used for testing the strength of MSE walls in both field and laboratory tests in which the pullout resistance of soil reinforcement strips is determined.

2.2 History and development of mechanically stabilized earth walls

2.2.1 Original idea of stress transfer within a soil mass

The idea of a mechanically stabilized soil mass is not a novel concept. The method of inserting some form of a non-soil element within a soil mass to improve the strength and stability of the soil has been around for thousands of years (Berg et al., 2009). Although in modern day soil mechanics, the idea on how MSE walls achieve their strength, in its simplest form, is based on the addition of a soil reinforcement (typically made of either steel, high strength plastic grids or woven plastic sheets) to a soil mass. The use of soil reinforcements therefore allows for an additional horizontal component to form within the soil which is caused by the friction between the reinforcement and soil (Ingold, 1982), hence restricting the horizontal strain caused by vertical stresses (Figure 2-1).

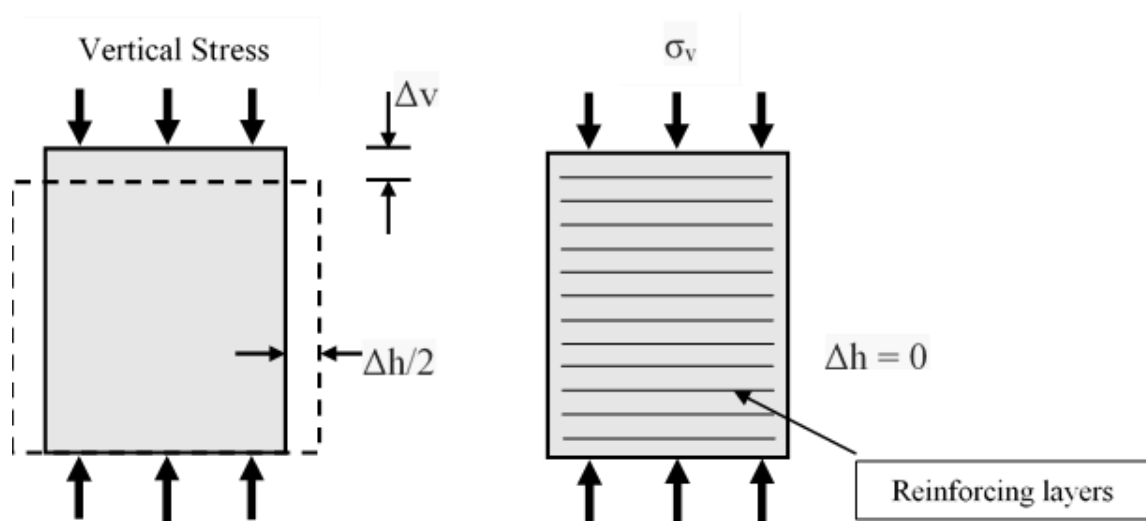


Figure 2-1. The effects of soil reinforcements on dilation caused by vertical stressing

Although other techniques were used to reinforce walls such as the addition of tie member rows within the soil retained by the retaining wall, such as the ‘ladder wall’ developed by Coyne in the 1930’s, it was only until the late 1960’s were the French ultimately defined the structure of a modern MSE wall (Jones, 1978). Henry Vidal was the French engineer to pioneer the field of reinforced earth techniques in his article written on the principles of reinforced earth (Vidal, 1969), which ultimately led to the development of his company, *Reinforced Earth*.

His theory based itself on a Mohr-coulomb failure envelope of a cohesionless material in which, for a given effective vertical stress (σ_1'), a minimum confining pressure is required (σ_3'). This is shown as the smaller Mohr circle in Figure 2-2. The minimum σ_3' required for stability is then defined as $\sigma_3' = \sigma_1' K_a$, where K_a is the active earth pressure. If the same material is then reinforced, the action of loading the soil induces tensile force within the reinforcement which acts as an additional confining pressure within the soil, a statement that was confirmed by Ingold (1982).

This changes the Mohr-circle to include a $\Delta\sigma_3'$ to the original σ_3' , which in turn shifts the maximum vertical effective stress required for failure to a much greater value (Figure 2-2). Therefore, as the vertical stress is increased, the induced $\Delta\sigma_3'$ will also increase, indicating that the reinforced soil mass is limited by either the bond strength of the soil/reinforcement or the tensile strength of the reinforcement itself (Vidal, 1969).

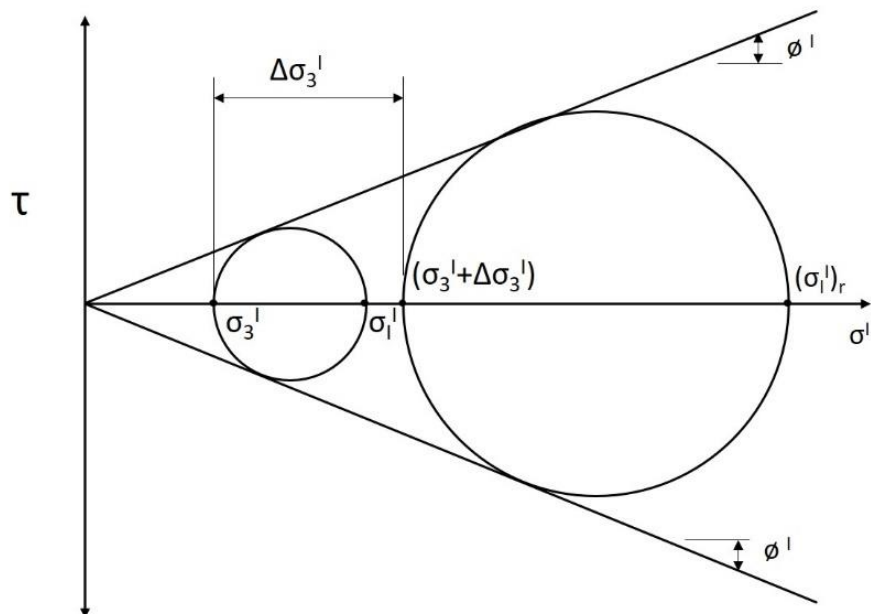


Figure 2-2. Original Mohr circle described by Henry Vidal (1969)

In later years, Vidal digressed from his original ideas and firmly subscribed to the ‘anisotropic cohesion concept’ in which the soil is described to act as a cohesive material as the tensile stresses induced by the applied vertical stress can be considered as cohesion within the soil mass. However, it has not been possible to define this cohesion in a way that allows for it to be used within the design of reinforced earth structures (Narain, 1978).

2.2.2 Improved soil stress transfer models

Theoretical models of an anisotropic homogenous reinforced earth material exist which are derived from the work done by Hausmann and Lee (1976). Hausmann and Lee (1976) described two theories, namely the SIGMA and TAU models, which define the strength of a soil mass in which the failure occurs when the soil mass experiences dilation in the direction of the reinforcement. The SIGMA model assumes that the reinforcement induces a normal confining pressure within the soil mass, whereas the TAU model assumes that the reinforcement induces a shear stress. For each model, a failure envelope is drawn for both methods of failure, those being the reinforcement rupturing, and the failure induced by loss of bond strength. Hausmann and Lee noted that for both the SIGMA and TAU models, the exhibited bond strengths are similar enough to limit all further considerations to that of the SIGMA model.

The SIGMA model is based on two separate stress conditions, the first being a constant prestress σ'_r which corresponds to the failure method of the soil mass being limited to the rupture of the reinforcement itself. The lateral expansion of the soil mass creates a pre-stress which is equivalent to the bond strength of the soil-reinforcement interface based on the ultimate tensile strength of the reinforcement. This allows the strength of the reinforced soil mass to originate from an added cohesion value c_r to the soil shown in Figure 2-3.

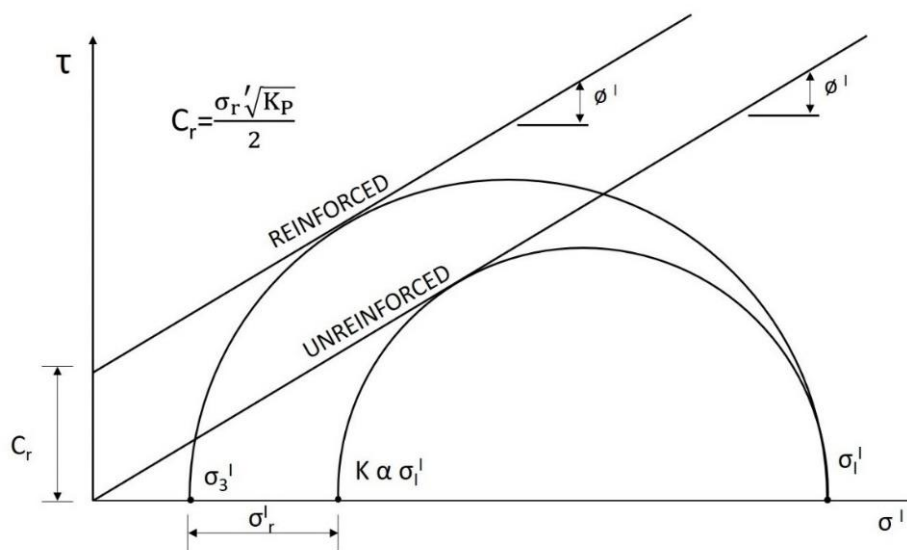


Figure 2-3. Failure envelope according to the SIGMA model constant prestress conditions (Hausmann and Lee, 1976)

The principle stresses were calculated as follows:

$$\sigma'_3 + \sigma'_r = \sigma'_1 K_a \quad (2.1)$$

Where:

$$\sigma'_1 \text{ (kPa)} = K_p \sigma'_3 + K_p \sigma'_r \quad (2.2)$$

The comparison of the respective Mohr circles allows for the definition of c_r to be as follows:

$$c_r \text{ (kPa)} = \sigma'_r \frac{\sqrt{K_a}}{2} \quad (2.3)$$

A further addition was made to include a soil mass of unit dimensions: height (H), breadth (B) with a reinforcement of cross-sectional area (A) and tensile strength (σ). This produced the final equation as follows:

$$c_r \text{ (kPa)} = \frac{\sigma A \sqrt{K_a}}{2BH} \quad (2.4)$$

The second stress condition defined in the SIGMA model is that which describes failure of the system related to bond strength failure or slippage of the reinforcement within the soil mass. This assumes that the relationship between bond strength and vertical stress are directly proportional, allowing for a frictional factor (F) to be included, thus defining the variable pre-stress conditions as follows:

$$\sigma'_r = \sigma'_1 F \quad (2.5)$$

Which has the effect of increasing the friction angle of the reinforced soil, as shown in Figure 2-4.

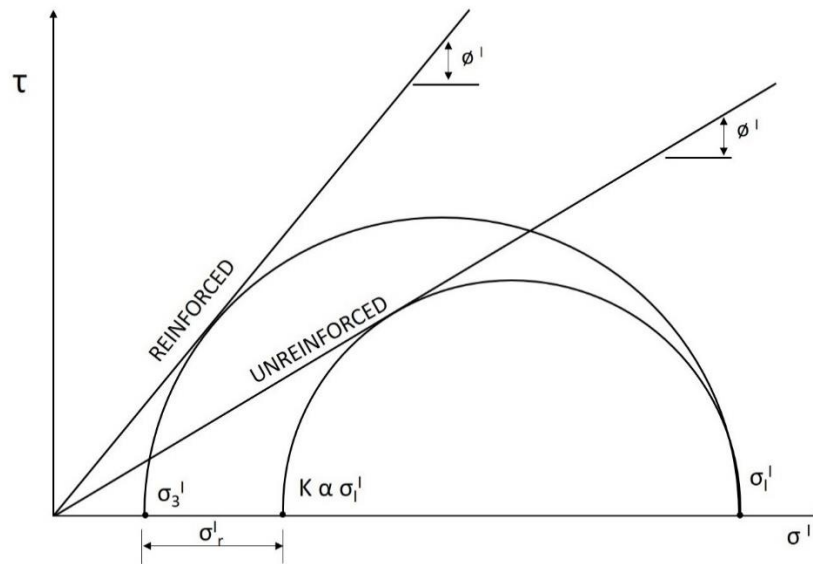


Figure 2-4. Failure envelope according to the SIGMA model's increasing prestress conditions (Hausmann and Lee, 1976)

This is described as follows:

$$\frac{\sigma'_3}{\sigma'_1} + F = K_a \quad (2.6)$$

As there are now two represented friction angles, the subscript "r" will refer to the reinforced soil mass friction angle. Expanding on 2.2.6, the following is derived:

$$\frac{\sigma'_3}{\sigma'_1} = K_{ar} = \frac{1 - \sin\phi'_r}{1 + \sin\phi'_r} \quad (2.7)$$

This in combination with Equation 2.2.6 and Equation 2.2.7 allows for the reinforced friction angle to be defined as follows:

$$\sin\phi'_r = \frac{K_a - F - 1}{F - K_a - 1} \quad (2.8)$$

2.2.3 The modern definition of reinforced soil concepts

The modern understanding of the stress transfer mechanism used in the design of these MSE walls are outlined by the U.S. Department of Transportation and Federal Highway Administration (FHWA). The FHWA (Berg et al., 2009) defines that a reinforced soil mass acts similarly to reinforced concrete structures as they both have improved mechanical properties. This is due to the reinforcement's placement being parallel to the principle strain direction. This allows for the reinforcement to compensate for the soil/concrete's inherent lack of tensile strength, allowing for the reinforced material to possess the following characteristics:

- Contiguous stress transfer occurs along the entire length of the reinforcement
- The reinforcements are spaced uniformly throughout the soil mass allowing for uniform stress/strain relationships to form throughout the soil mass.

The stress transfer mechanisms defined by the FHWA allows for the distinction between frictional resistance and passive resistance. The frictional resistance occurs both along the entire strips as well as due to the ribbed nature of the steel strips, where:

- The friction along the reinforcement surface is caused by the frictional surface bond induced by the normal pressure exerted by the soil on the reinforcement surface (Figure 2-5), and
- The steel ribs allow for friction to be caused in locations where there is a relative shear displacement of the soil. This displacement can allow for the shear stress to be transferred back onto the steel strip which in turn causes the additional friction (Wang, Jacobs, & Ziegler, 2016).

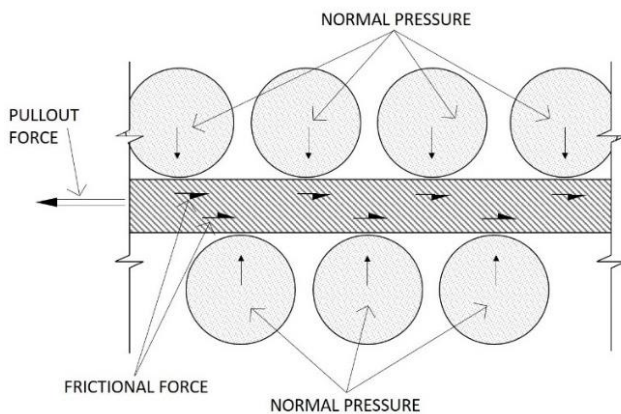


Figure 2-5. Normal pressure inducing friction on soil reinforcement

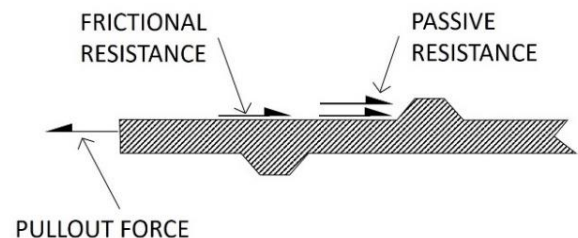


Figure 2-6. Frictional resistance versus passive resistance in steel strips.

The primary source of resistance in soil reinforcements such as steel strips (both ribbed and smooth), geotextiles/geosynthetics and geostraps is that of frictional resistance. The frictional resistance is also directly related to the length of the soil reinforcement. In some cases, such as in ribbed steel strips, both frictional resistance and passive resistance are actively present (Figure 2-6).

Passive resistance is considered the primary interaction for reinforcements such as bar mats, wire meshes and geogrids (those which possess a high cross machine stiffness). The resistance occurs through the development

of a bearing type stress on soil reinforcement sections which are orientated perpendicular to the normal direction of the reinforcement's movement (Figure 2-7).

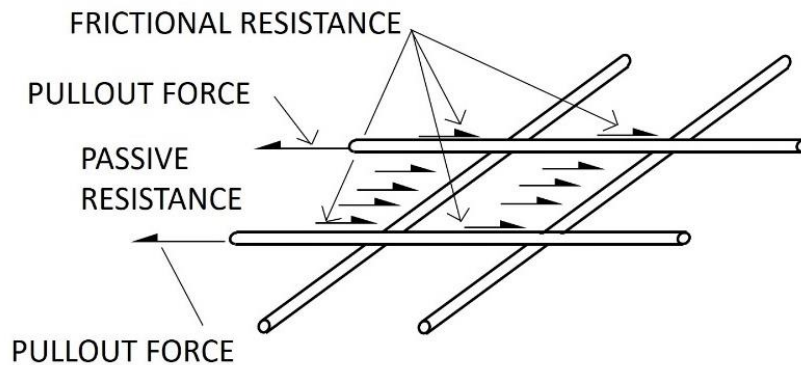


Figure 2-7. Frictional resistance versus passive resistance in reinforcement grids.

This allows for each soil reinforcement type to be described in terms of its primary resistance and secondary resistance (if applicable), as seen by the generic reinforcements described in Table 2-1.

Table 2-1. Reinforcement types and their resistance characteristics

Reinforcement Type	Load Transfer Mechanism*	
	Primary	Secondary
Smooth	Frictional	
Ribbed	Frictional	Passive
Extensible composite plastic strips	Frictional	
Geotextiles	Frictional	
Bar mats	Passive	Frictional
Welded wire meshes	Passive	Frictional
Geogrids	Passive	Frictional
Woven wire meshes	Passive	Frictional

*These load transfer mechanisms are only in reference to Figures 2.5, 2.6 and 2.7

The boundary between passive and frictional resistance in soil reinforcements that have an aperture (grid-like reinforcement) is dependent on the ratio between aperture size and particle size distribution of the soil. This is due to the fact that a large aperture size in conjunction with a large particle size allows for the dominant resistance to be that of passive resistance, yet a large aperture size with a small particle size will remove the majority of passive resistance and rely mainly on the frictional resistance.

2.3 Design of modern MSE walls

Retaining walls can be built using a range of soil reinforcements. These reinforcements are typically categorized as either extensible or inextensible. For segmented block retaining walls, a wide range of extensible reinforcements can be used, which consists of sheet-like reinforcements (such as geotextiles, geosynthetics and steel reinforcement meshes). For the design case of MSE walls, inextensible strip like reinforcements are typically used due to their design which allows for them to attach to the facing units of the wall.

According to the design of *Reinforced Earth*, MSE walls comprise of four main elements (Lee, 1978) (Figure 2-8):

- i. The engineered backfill, which accounts for the bulk mass of the system, resistance to compression under self-weight and vertical loading, as well as the shear strength of the system.
- ii. The embedded inextensible reinforcements.
- iii. The facing elements
- iv. Mechanical connections between the tensile reinforcements and the facing elements.

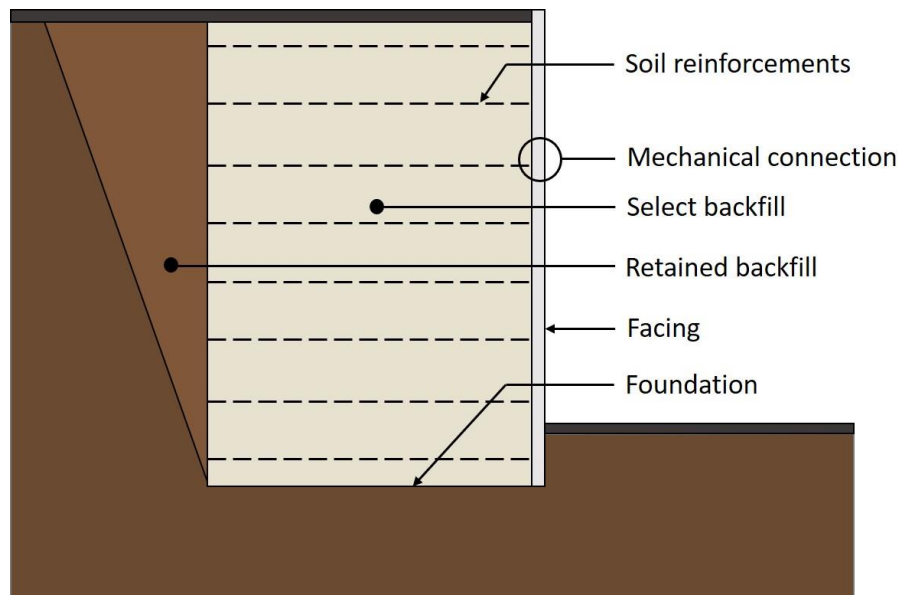


Figure 2-8. Cross-section view of an MSE wall and all its elements

Depending on the design requirements of the MSE wall, several soil inextensible reinforcements are available which have important differences in their designed use cases (Figure 2-9). The most common of them all being the high adherence strips, although no reason for this is provided in literature, the reason for its dominance might be due to ease of manufacturing. Due to this project's focus being on testing the resistance of ribbed steel strips, a focus will be placed on the literature that is orientated towards the design criteria and materials used within MSE walls that use strip reinforcement techniques.

Currently, *Reinforced Earth* produces the following types of soil strip-reinforcements used for the construction of MSE walls:

- High-adherence ribbed steel strips (Figure 2-9a)
- High adherence steel ladders (Figure 2-9b)
- Geosynthetic reinforcement strips (produced by GeoStrap®) (Figure 2-9c)

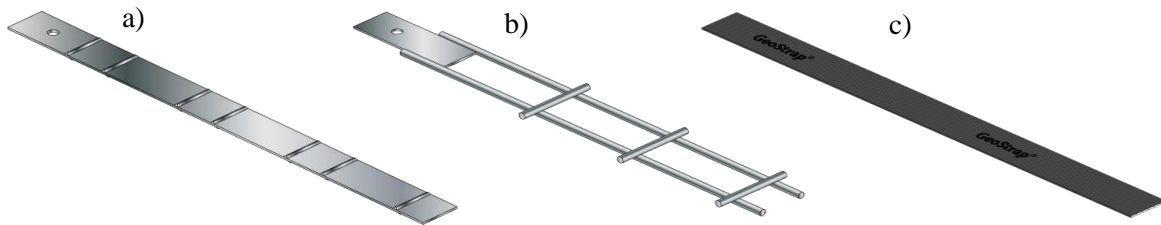


Figure 2-9. Soil reinforcement strips produced by Reinforced Earth (Source: <https://reinforcedearth.com/products/retaining-walls/mechanically-stabilized-earth-mse-retaining-walls/>)

For the strips shown above, the required backfill conditions are summarized by *Reinforced Earth* to be ideal when consisting of an open-graded material with low plasticity and fines content. These conditions typically allow for ease of compaction and high drainage potential. This definition is consistent within literature, as defined by Kenneth Lee (1978), where the concept of increasing tensile stress produced at higher vertical stresses is used to justify the use of granular free draining material. Lee (1978) places an emphasis on the nature of MSE wall constructions, namely their lack of external reinforcement. This construction technique requires there to be a direct transfer of effective normal stress from soil to the reinforcement. Any form of pore water pressure build-up would limit the rate of stress transfer.

Between the years of 1972 and 1978, *Reinforced Earth* constructed a total of 159 structures, 106 of them being specifically retaining walls. The construction characteristics of these walls were assessed by McKittrick (1978) and noted that, for these retaining walls, a vast range of fines content was measured from as low as 5% to as high as 40%. McKittrick (1978) noted that there was, however, evidence that out of all the backfill materials used, they were all classified as being non-plastic and free draining. This allows for a further question of what essentially defines a soil mass's ability to be classified as free draining.

2.4 Soil Permeability

All soils have an inherent permeability associated with them. This dictates water's ability to free flow through the soil mass through the interconnected pores between the soil particles (Craig, 2004) from a high point of energy to a low point of energy (Das, 2010). Within one dimension, the flow of water through a soil in saturated conditions follows Darcy's empirical law:

$$q = Aki \quad (2.9)$$

The above equation defines the flow rate (q in m^3/s) of water through a soil mass's interconnected pore space to be directly related to the soil's inherent permeability (k in m/s), the hydraulic gradient (i in m) and the surface area (A in m^2) of the soil through which the water is flowing. The coefficient of permeability is directly related to the average grain size of the soil (Das, 2010), as the smaller the average grain size, the smaller the interconnected pore spaces which ultimately leads to a restriction of water flow.

Various methods of determining a soil's permeability exist, all of which are based on two standardized testing procedures: the constant head test and the falling head test. Constant head tests are better suited for soils which possess a high coefficient of permeability, while falling head tests are best suited for soils which possess a low coefficient of permeability (Craig, 2004). The boundary between low and high permeability coefficients is not clearly defined as a specific value within literature. However, it is widely accepted that the differentiation exists in a range where k is a value between 10^{-4} m/s and 10^{-5} m/s. This is often noted as a change in the material's general soil classification from a fine silty sand to that of a clean sand or gravel.

In the Manual for Soil Laboratory Testing (Head, 1992), the differentiation is made at a value of 10^{-5} m/s. In the case of k being less than 10^{-5} m/s, it is recommended that a falling head cell should be used while a constant head cell should be used for all values larger than 10^{-5} m/s. Head (1992) also provides additions to the testing procedure by indicating that a larger soil sample is required for high permeability values, and the use of an odometer is required to determine incredibly low permeability values (these differentiations can be seen in Table 2-2).

Table 2-2. Soil classification related to permeability based on Head (1992).

Permeability range, k (m/s)	1 to 10^{-3}	10^{-3} to 10^{-5}	10^{-5} to 10^{-8}		10^{-8} to 10^{-12}
Permeability classification	High	Medium	Low	Very low	Practically impermeable
General soil type	Clean Gravels	Clean sand	Very fine silty sand		Intact clays
Test methods	Large constant head cell	Standard constant head cell	Falling head cell		Falling head test in odometer

In the book “Groundwater” (Freeze & Cherry, 1979), the authors defined a k value to 10^{-4} m/s at the transition from fine sand to silty sand. This material transition matches that of the material transition (and the k value associated with it) in Head (1992).

Considerable research has been performed in trying to quantify a soil’s permeability from only that of its particle size distribution. Such work includes the work done by Hazen (1930), where he determined that a soil’s coefficient of permeability could be calculated as follows:

$$k \text{ (cm/s)} = c D_{10}^2 \quad (2.10)$$

Where the D_{10} value is the effective particle size (that should be within the range of 0.1 mm to 3 mm to provide accurate results) and a constant value, c , which ranges from 1.0 to 1.5 depending on a soil’s classification. It should be noted that in text books such as Craig’s Soil Mechanics (Craig, 2004), the same equation is expressed in terms of m/s and omits the constant value (c). Other efforts have been made that expand the correlation between a soil’s particle size distribution to include extra factors, such as shown by the *Kozeny-Carman* equation (Equation 2.11), which was derived over a course of several publications by Kozeny and Carman (Das, 2010). The equation is given as follows:

$$k \text{ (m/s)} = \frac{2}{fS^2} \left(\frac{e^3}{1+e} \right) \quad (2.11)$$

Where f is an angularity factor of the material, S is the specific surface of the soil grains and e is the void ratio of the soil mass.

Considering this, there does, however, seem to be a disconnect between classifying fines according to particle size rather than by both size and mineralogy. A study outlined by Terzaghi (1948) shows that for sand-bentonite mixtures (typically used for seepage barriers) an increase in the clay content naturally limited the permeability as hydrated bentonite fills the pore spaces. This allows for the conclusion to be made that active clay minerals are better at inhibiting flow than inert fines such as those created by the mechanical grinding down of soil particles.

2.5 Modern standards on backfill conditions

There is no strict requirement for a backfill to possess a specific permeability. According to SANS 207 (2011), a backfill should allow for adequate draining through the use of a naturally free draining backfill or, in the event that cohesive materials are used for the backfill construction, to ensure that regular drainage layers are used to reduce pore water pressure buildup. However, a safe assumption can be made from the particle size distribution, which is partly outlined by the standards, that the generally granular composition required by these standards would allow for the backfills to be classified as free draining.

The U.S. Department of Transportation and Federal Highway Administration (FHWA) outlined the overall design requirements for backfill conditions based of AASHTO (2007). The requirements which they adhered to are those outlined as the ‘select granular fill material for the reinforced zone of walls’. Although the

requirements closely matched those of SANS 207 (2011), the FHWA also provides a sub section outlined as ‘marginal reinforced fill for MSE walls’. This sub-section focusses on the soil criteria found within backfill conditions which did not adhere to the granular fill material characteristics yet provided successful results.

This plays an important role in the construction of MSE walls as, during construction, the effective stress transfer within non-free draining materials is not immediate. This occurs if there is a build-up of material faster than what the layers below it can de-water, resulting in a build-up of pore water which will lead to a loss of both shear strength and soil-reinforcement bond strength (Jones, 1985). The entire self-weight of the system is also affected if a non-free draining backfill material is used. If a backfill is constructed using non-free draining materials, saturation will lead to the saturated unit weight being carried by the supporting foundation/soil base for an extended period of time and bearing capacity failure can occur (SANS 207, 2011).

The unique characteristic outlined by only the AASHTO (2007) granular fill standard is the required plasticity of the backfill material. Considering that plasticity is an indicator property that only clay minerals have, using this as a factor to define both the percentage of fines as well as a key indicator to free draining potential is incredibly important.

A summary of all backfill requirements can be found within Table 2-3, where the requirements are divided into five general categories. However, not all categories are addressed within the respective standards and are thus left empty. For the sections that are defined, the overall classifications are similar, if not identical.

Table 2-3. Comparison of selection criteria of mechanical properties for backfill materials

Back fill property		Standard			
		AASHTO (2007)	U.S. Department of Transportation, Federal Highway Administration.	SANS 207: 2011	<i>Reinforced Earth</i>
Percentage passing a given sieve size	100mm	100%	-	-	Refer to Figure 2-10
	37.5mm	-	-	100%	
	0.425mm	0-60%	-		
	0.075mm	0-15%	0-35%	0-15%	
Internal friction angle		$\geq 34^\circ$, for material passing the 2.0mm sieve	*analysed on individual basis to be deemed sufficient	-	-
Plasticity		≤ 6	< 20	-	
Electrochemical properties	pH	5 - 10	-	5 - 10	5 - 10
	resistivity	$> 30 \Omega \cdot m$	-	$> 100 \Omega \cdot cm$	$> 100 \Omega \cdot cm$
	Chlorides	$< 100ppm$	-	$< 0.02\%$	$< 100 ppm$
	Sulphates	$< 200ppm$	-	$< 0.1\%$	$< 1000 ppm$
Should not contain material of this type		Shale or soft (poor durability) particles	-	Materials susceptible to degradation in water	Refer to Table 2-4

According to *Reinforced Earth*, similar guidelines are given as to the backfill condition recommendations. The overall chemical properties are given in Table 2-3 whereas the soil particle distribution is given as a two dimensional range in Figure 2-10. The soil particle size distribution is divided into two main areas, those being the ‘granular usable’ and ‘conditionally usable’ areas. There is no clear definition as to what the conditionally usable area means with regards to its ability to perform as a backfill material. If a soil falls within this area, it might indicate that further testing is required as a material that contains up to 40% silt and clays might underperform in the required shear strength parameters for a backfill. Figure 2-10 also contains pink areas which indicate that if a particle size distribution falls within those areas, it is deemed insufficient to be used as a backfill material. *Reinforced Earth* does include four main categories into which a potential backfill material can be sorted into. These categories are provided in Table 2-4.

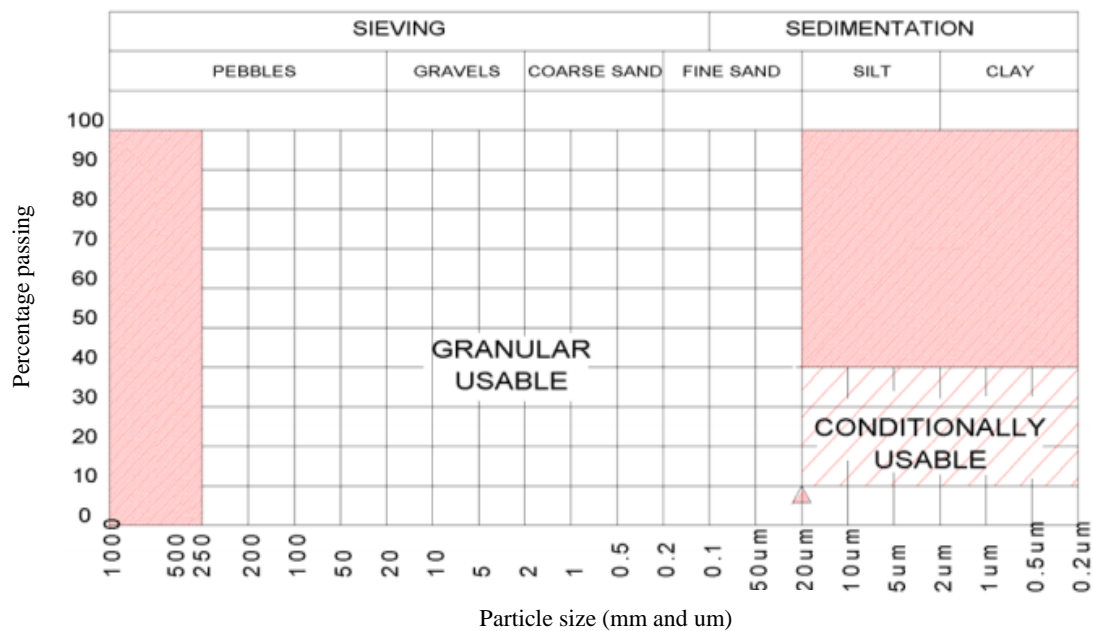


Figure 2-10. Materials suitable for backfill construction according to Reinforced Earth

Table 2-4. Reinforced Earth backfill material classifications, modified from Reinforced Earth (Smith, 2010)

Category	Description
“The best”	Free draining sand or gravel, typically containing <5% fines (75 micron sieve)
	Mine waste rock or tailings that have not been polluted during extraction
“Good”	Granular material according to Figure 2-10, this can include transported material or weathered residual rock.
“Satisfactory”	Intermediate material according to Figure 2-10. These include lateritic gravels or pebble markers.
	These materials are typically water sensitive (susceptible to swelling and collapsing due to porewater pressure build-up)
“Unacceptable”	Fill that fall within the clay and silt region of Figure 2-10. Material types such as shales and rock that have a tendency to oxidize in contact with air or water.

2.6 Determining pullout resistance of a soil reinforcement

An issue that is defined throughout the history of reinforcing soil masses, from the original testing performed to validate Vidal's proposed reinforced earth designs (Ingold, 1982) to the modern standards used in South Africa (SANS 207, 2011), is the determination of the bond strength between the backfill material and the reinforcement itself. Bond strength is directly related to the tensile stress induced by the loading of a reinforced soil. Therefore the 'pullout test' method is often used to characterise the force required to pull a reinforcement out of a soil mass as this provides a direct indication of the bond strength.

Initial studies attempted to use a standard direct shear test in which the lower half was fitted with a section of a ribbed steel reinforcement to determine the bond strength. However, the results were discarded as the test clearly lacked the ability to allow for tension within the reinforcement (Ingold, 1982). Some of the original pullout tests performed were those done by Schlosser and Elias (1978) where they defined two conditions to which MSE walls could be tested, those being in-situ tests and those tests that were performed on a reduced scale model (laboratory testing).

2.6.1 In-situ pullout tests in South Africa

In-situ tests have the benefit of providing data that has a direct correlation to the system that has just been constructed, allowing for an accurate assessment of post construction stability and quality of backfill construction. For in-situ testing, the installation of monitoring panels is required. These monitoring panels are of the same shape as the facing units of the MSE wall yet have several built-in access holes through which the steel strips can be accessed. This allows for multiple in-situ tests to be performed with a single monitoring panel (Smith & Vadron, 1993).

Monitoring panels have been a required addition to structures built by Reinforced Earth from 1978. This allowed for a total of 52 test sites to be included in a study on the durability of reinforcing ribbed steel strips in South Africa (Smith & Vadron, 1993). These tests included materials of the granular to fine-medium sands, some of which contained a silty fines content. Out of the 52 tests performed, only 34 of the tests had a recorded backfill grading description (which included the origin of the material used). These consisted of granular, intermediate to granular, intermediate and silty granular materials. For the scope of this project, only those tests performed which contain a backfill material description will be evaluated. A condensed list of pullout resistance measured for a given soil type is provided in Table 2-5.

According to all the standards discussed in Section 2.5, the minimum required length of a reinforcement strip is typically $0.7 H$, where H (in meters) is the height of the wall being tested. This allows for the height of the wall (a factor not included in the study by Smith and Vadron (1993)) to be assumed from the length of the steel strip used for testing of the pullout resistance. A further addition that was made to Table 2-5 is for the strip dimensions correction, as not all the strips are the same length and breadth. As such, a column was added correcting the maximum tensile strength from kN to kN/m^2 .

Table 2-5. Summary of in-situ pullout tests in South Africa (summarized from Smith and Vadron, 1993)

#	Grading Classification	Type of material	B (mm)	B (m)	L (m)	Max tensile strength (kN)	Estimated height of the wall (m)	Adjusted wall height, correcting for height of test panel (m)	Length corrected maximum tensile strength (kN)	Adjusted pullout resistance (kN/m ²)
1	Granular	Dump-rock from Mined Quartzite	60	0.06	5	185.5	7.143	6.143	37.10	309.17
2		Dump-rock from Mined Quartzite	60	0.06	5	115.5	7.143	6.143	23.10	192.50
3		Weathered Granite	40	0.04	5	79	7.143	6.143	15.80	197.50
4		Cape Dune Sand	40	0.04	5	77.8	7.143	6.143	15.56	194.50
5		Cape Dune Sand	40	0.04	5	82.5	7.143	6.143	16.50	206.25
6		Cape Dune Sand	40	0.04	5	76	7.143	6.143	15.20	190.00
7		Coarse River Sand	40	0.04	5	82.5	7.143	6.143	16.50	206.25
8		Slag from Dunswart iron and steel	40	0.04	5	89.4	7.143	6.143	17.88	223.50
9		Weathered Dolerite	60	0.06	10	262	14.286	13.286	26.20	218.33
10		Blast Slag furnace	60	0.06	5	152.9	7.143	6.143	30.58	254.83
11		Sandy Gravel	60	0.06	5	134.3	7.143	6.143	26.86	223.83
12		Sandy Gravel	40	0.04	5	101.9	7.143	6.143	20.38	254.75
13		Sandy Gravel	60	0.06	5	159.1	7.143	6.143	31.82	265.17
14		Sandy Gravel	40	0.04	5	128.6	7.143	6.143	25.72	321.50
15		Boulders remaining on 19.2mm sieve	50	0.05	5	151.8	7.143	6.143	30.36	303.60
16		Boulders remaining on 19.2mm sieve	50	0.05	5	152.2	7.143	6.143	30.44	304.40
17		Weathered dolerite	60	0.06	10	275	14.286	13.286	27.50	229.17
18		Dune sand / Top soil	40	0.04	4	86.1	5.714	4.714	21.53	269.06
19		Blast Furnace slag	60	0.06	5	149.2	7.143	6.143	29.84	248.67
20	Silty Granular	Laterite	40	0.04	5	81.5	7.143	6.143	16.30	203.75
21	Granular to intermediate	Dwyka Tillite	40	0.04	5	83.5	7.143	6.143	16.70	208.75
22		Dwyka Tillite	40	0.04	5	75.5	7.143	6.143	15.10	188.75
23		Sand Stone	40	0.04	5	67.75	7.143	6.143	13.55	169.38
24		Decomposed Tillite	40	0.04	5	102.7	7.143	6.143	20.54	256.75
25	Intermediate	Commercial Sand	80	0.08	3	87.8	4.286	3.286	29.27	182.92
26		Weathered Sandstone	40	0.04	5	78	7.143	6.143	15.60	195.00
27		Weathered Sandstone	40	0.04	5	80	7.143	6.143	16.00	200.00
28		Weathered Sandstone	40	0.04	5	80	7.143	6.143	16.00	200.00
29		Sandstone	60	0.06	5	197	7.143	6.143	39.40	328.33
30		Decomposed Granite	60	0.06	5	160	7.143	6.143	32.00	266.67
31		Dark red sand	40	0.04	5	96.2	7.143	6.143	19.24	240.50
32		Dune sand / Top soil	40	0.04	5	92.7	7.143	6.143	18.54	231.75
33		Dune sand / Top soil	60	0.06	5	104.4	7.143	6.143	20.88	174.00
34		Aeolian sand	80	0.08	3	79.5	4.286	3.286	26.50	165.63

If the average pullout resistance for a given strip's area (kN/m²) is plotted for each of the material types, it is clear to see that the granular fill material as well as the intermediate materials presented the highest pullout

resistance. This might be due to the lack of test data recorded for the lesser pullout capacity groups that fell within a given soil category, hence effecting the statistical relevance of how this data is provided in Figure 2-11.

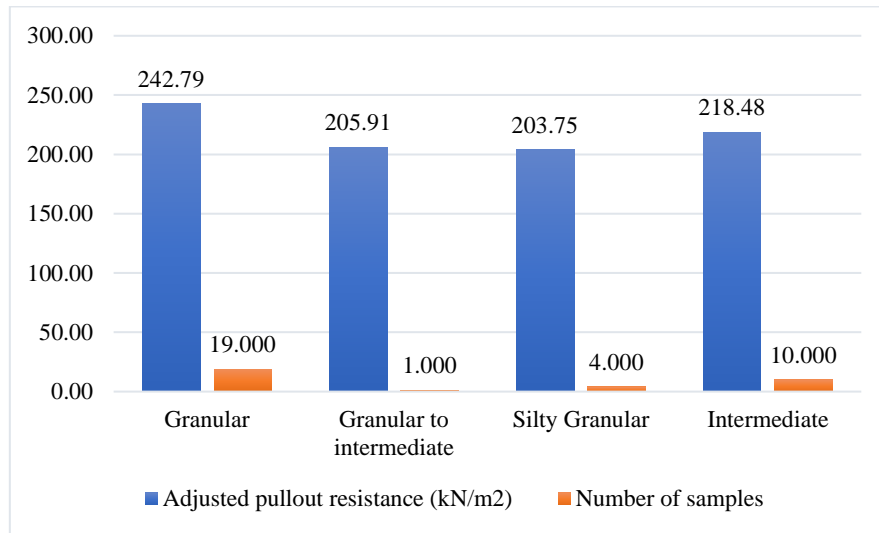


Figure 2-11. Pullout resistance of in-situ materials in South Africa

A limitation to the tests performed by Smith and Vadron (1993) is that these tests do not include the grading of the soil, as they are usually referred to as a ‘granular fill’ which gives no indication to the soil’s particle size distribution.

2.6.2 Laboratory pullout tests

This is the first area in which there is a lack of research regarding testing performed within South Africa. This might be due to the prevalence of in-situ testing (Smith & Vadron, 1993). Laboratory pullout testing is, however, common within the global space as pullout tests on soil reinforcements are performed in both small and large-scale testing apparatuses. The scale of the test is simply a description based on the size of the soil chamber in which the soil reinforcements are imbedded as well as the range of vertical stress which can be applied. Laboratory testing on ribbed steel strips are, however, not as common as extensible reinforcements. This might be due to other forms of retaining structures (those that use extensible reinforcement types) that are typically more common than MSE walls.

The benefit of having a laboratory pullout test apparatus is the ability to construct the backfill conditions in any way that suits the testing requirements. Thus a range of pullout tests can be performed on a given material prior to its use as a backfill material, allowing for an actual performance metric to be determined for that material. Table 2-6 gives an outline of the novel testing setups, both small and large scale, that have been performed in the past using steel strips. The tests performed by Weldu (2015) showed that soils with a higher coefficient of uniformity (C_u) value allowed for a higher pullout resistance. This was attributed to the density obtained being higher for materials with higher C_u values. The testing performed by Strahler, Walters and Stuedlein (2016) showed that closely spaced steel strips allowed for an increase in pullout resistance. The increased pullout resistance was attributed to an increased effective stress felt by the surrounding strips. The

tests performed by Jayawickrama et al. (2013, 2015) were based on quantifying the pullout resistance on both sand and gravels, all of which had varying C_u values. The results of his studies all used the AASHTO F* estimation method (Berg et al., 2009) as a verification to the values obtained.

Table 2-6. Novel pullout tests for steel strips

Author	Project title	Steel strip dimensions (Width x Thickness) (mm)	Soil chamber dimensions (L x B x H) (mm)		Vertical stresses
Weldu (2015)	The effects of a soil coefficient of uniformity on pullout resistance	50 x 5	1500 x 600 x 600		25 kPa to 138kPa
Strahler, Walters and Stuedlein (2016)	Frictional resistance of closely spaced reinforcement strips	50 x 6	2160 x 456 x 356	Single strip tests with a longer soil chamber	10kPa to 300kPa
			1520 x 1520 x 1830	Multiple pullout tests for a single soil chamber	10kPa to 300kPa
Jayawickrama et al. (2015)	Pullout resistance factors for steel strips in gravelly backfill	50 x 5	3600 x 3600 x 1200		30, 72, 120, and 240 kPa
Jayawickrama et al. (2013)	Pullout resistance factors for steel strips in sandy backfill	50 x 5	3600 x 3600 x 1200		5, 12, 20 and 40ft of vertical depth
Jayawickrama et al. (2012)	The effect of skewed/spayed steel strips within a backfill	50 x 5	3600 x 3600 x 1200	Degree of skew: 0°, 15° and 30°	5, 12, 20 and 40ft of vertical depth

There is a clear lack of testing within literature on non-free draining soils as only tests on granular materials have been performed. This includes the lack of testing done on granular materials in saturated conditions as well as laboratory testing as a whole within South Africa. This may be due to the fact that using non-free draining or plastic soils in backfills are clearly marked as materials with which caution should be taken. This then leads to the main aim of this study, which was to perform laboratory tests on both free draining granular and non-free draining plastic materials found within South Africa.

2.6.3 Estimating pullout resistance

Considering that in-situ testing has the caveat that it can only be performed on walls that have been successfully built, the use of laboratory testing is the only other direct test to determine a reinforcement's pullout resistance. However, the lack of availability of a laboratory pullout apparatus requires the ability to determine pullout resistance by other means. For this reason, the use of the AASHTO (2012) method to estimate the pullout factor is commonly used to calculate a soil reinforcement's pullout resistance at any given depth within a backfill.

For a given soil reinforcement, the pullout resistance (P_r) is generally characterized by Equation 2.12.

$$P_r(kN) = F^* \alpha \sigma'_v L_e C w \quad (2.12)$$

Where, F^* is the pullout resistance factor, α is a scale effect correction factor (typically 1 for ribbed steel strips), σ'_v is the effective vertical stress (kN/m^2) and the L_e factor describes the total length (in m) situated in the passive zone behind the failure surface with the C value being that of 2 as for each reinforcement type (as the resistance is measured on both the top and bottom for any given reinforcement), and w is the width (in m) of the strip being tested. For clarity, the pullout resistance factor will be given a subscript of either 'e' for factors which are derived from other soil properties (estimated) and 'm' for factors which are measured through pullout testing.

In order to determine the estimated pullout resistance factor F_e^* , a pullout factor versus depth plot is constructed with two separate depth conditions (AASHTO, 2012). This allows for the determination of F_e^* for any given depth of wall. At ground level, the value for F_e^* can be estimated using Equation 2.13.

$$F_e^* = 1.2 + \text{Log}(Cu) \leq 2.0 \quad (2.13)$$

Where Cu is the soil's coefficient of uniformity. This value changes linearly to a depth of 6 m from the top of the wall where the value is calculated using Equation 2.14.

$$F_e^* = \tan\phi \quad (2.14)$$

Where ϕ is the angle of internal friction of the backfill material. At any depth greater than 6 m below the top of the wall, the value of F_e^* remains constant. This relationship allows for any estimated F_e^* value to be determined for a given depth of backfill, as shown in Figure 2-12.

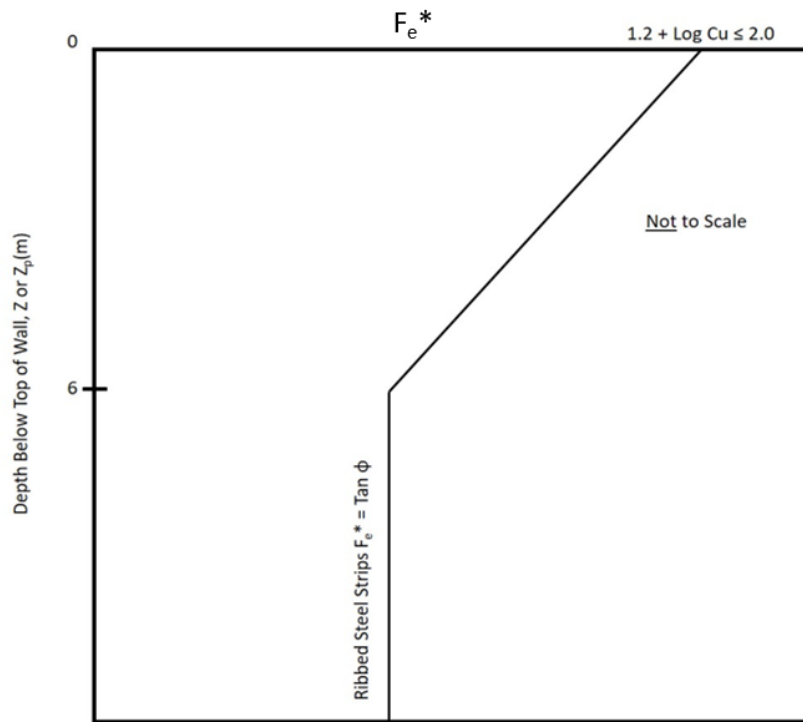


Figure 2-12. Estimation of pullout factor with relation to depth and Cu (AASHTO, 2012)

Using the estimated pullout resistance factor F_e^* is convenient as it allows for an estimated pullout resistance (P_r) to be calculated without the need for in-situ or laboratory testing. However, if laboratory pullout testing can be performed, a comparison of the measured pullout resistance factor F_m^* to that of the estimated pullout resistance factor F_e^* can be made. This method of comparison is often used within literature as a means of indicating the performance of the tested backfill, a method which *Reinforced Earth* has stated as being acceptable (Reinforced Earth Company, 1995).

The calculated pullout resistance factor is determined through changing the subject of Equation 2.12, allowing for the following:

$$F_m^* = \frac{P_r}{\alpha \sigma_v' L_e C w} \quad (2.15)$$

Where the P_r is the pullout resistance (kN) measured during laboratory pullout tests. In comparing the measured pullout resistance factor F_m^* to that of the estimated pullout resistance factor F_e^* , some insight can be gained as to the assumptions made regarding backfill conditions and their resistance to reinforcement pullout.

3 Pullout apparatus

3.1 Introduction

As the Stellenbosch University did not possess any relevant equipment which could be used for pullout testing, it was essential that a piece of equipment was designed and constructed to fulfill the requirements of pullout testing to meet the overall goals of this research project.

This chapter is divided into both the design and construction of the physical pullout apparatus and other subsystems required for use of the apparatus during testing. The design was influenced through referencing relevant literature as well as by means of trial and error to determine the best design for the required system. Appendix C contains an assembly guide for the pullout apparatus.

3.2 Aim and objectives

The aim of this chapter was to design a complete system for standardized pullout testing by meeting the following objectives:

- The overall dimensions need to meet the criteria set by ASTM (ASTM Standard D6706, 2013).
- The pullout apparatus needs to be strong enough to support a wide range of allowable effective stresses.
- The system needs to provide a cost effect solution that is reproducible without the need for specialized tools.
- The apparatus must be capable of being configured in such a way that other orientations/non-standardized testing can be performed.

3.3 Design phase

3.3.1 Initial study

The primary goal of this initial study was to create a rough design of an apparatus that can adequately handle the loads imposed through standardized horizontal pullout testing. This type of testing involves the preparation of soil samples within a soil chamber and determining its corresponding pullout resistance for a given effective vertical stress.

Two other non-standardized orientation states of testing were considered in the design of the apparatus. Firstly, the ability to have a modular mounting/positioning system for the hydraulic jack (which applies the pullout force) so that the system can be arranged in such a way to introduce an inclined pullout force on the testing material. Secondly, the ability of the entire apparatus to be set on its upright axis to enable the use of ‘micro-pile’ pullout testing.

Apart from the two design considerations described above, as well as the overall dimensions defined by the relevant ASTM standard, there are little to no limitations on the design and construction of a pullout apparatus. Previous studies on pullout testing which required the use of a pullout apparatus that meets the same ASTM standards are either incredibly large and cumbersome or too small and unequipped for testing high effective

stresses. One such design, as described by Taghavi & Mosallanezhad (2017), had five sides of the soil chamber completely welded shut with each face containing a perpendicular grid-like reinforcement making the walls roughly 150 mm thick with the intention of testing high effective stress. Other designs, such as that implemented by Esmaili, Hatami, & Miller (2014), only considered the testing of lower effective vertical stress and was constructed using a combination of wooden and Perspex side walls (in order to observe soil displacements) with steel angle irons as reinforcements. It was for these reasons that the pullout apparatus's dimensions and overall design was rather based on the design of Weldu (2015) as it would produce a suitable size for the apparatus as well as allow for the incorporation of the required setup orientations mentioned above. Lastly, an important influence on the final design was the fact that the apparatus does not have any dedicated floor space in the lab and thus should be designed in such a way that the apparatus is able to be disassembled and relocated at any given time.

3.3.2 Design prototyping

Prior to any form of CAD modelling, it was essential to understand the ultimate dimensions and construction constraints of the apparatus. This was achieved through the construction of a prototype using 4 mm thick foam board, as it was the fastest and most cost-effective way to gain an understanding of the overall construction. The foam board was used to construct a 5:1 small-scale replica of the pullout apparatus adhering to the initial design parameters (as defined in Section 3.3.1). The completed foam model can be seen in Figure 3-1.

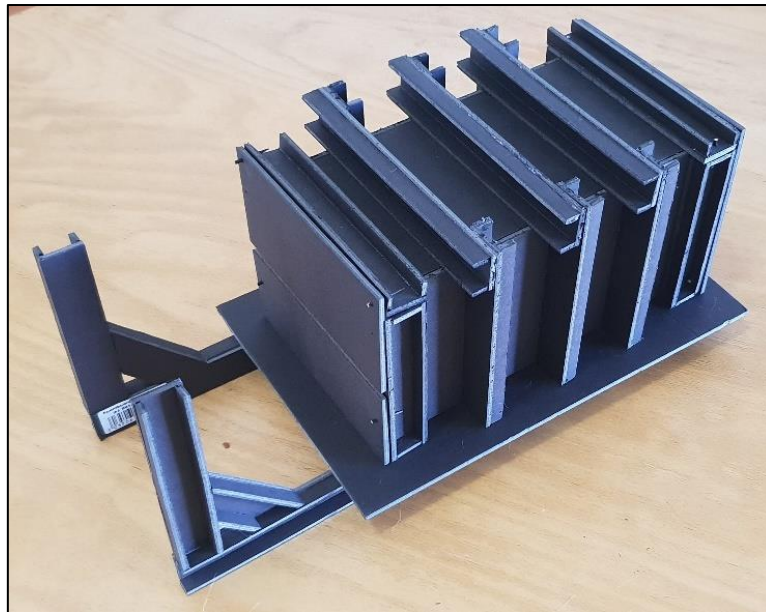


Figure 3-1. Small-scale model of pullout apparatus constructed using foam board

The design of the model was limited to the size of the raw materials that were available for construction of the actual pullout apparatus, those being 100 mm by 50 mm parallel flange steel channel and 5 mm thick cold-rolled steel sheets. The steel channels were replicated by cutting the foam board down into strips and constructing it into channels (Figure 3-2) that match the scaled-down external dimensions of the actual steel channel.

As the foam board used was 4 mm thick, it was impossible to create a scale model that perfectly matched the material dimensions used, therefore it was decided to use the external dimensions of the materials to keep consistent throughout the model's construction.

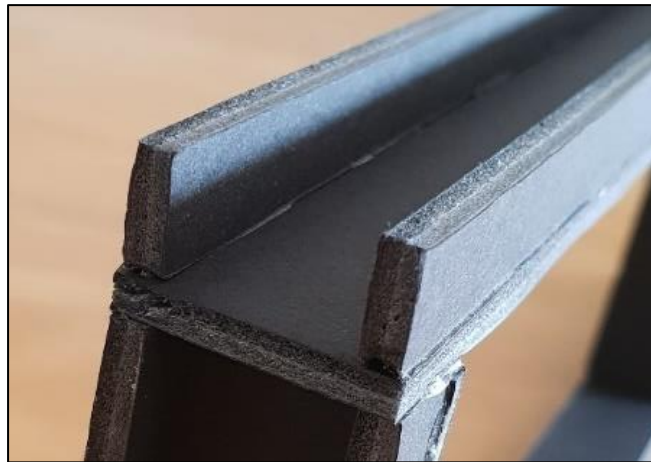


Figure 3-2. Construction of model – replicating steel channel using foam board.

Once the foam model was completed, several improvements were noted and implemented into the CAD model. The first key feature was the pullout apparatus's ability to disassemble, as this was an important feature necessary for movement and storage of the apparatus at any point in time (as mentioned before). The foam board model indicated that, for the most optimal disassembly of the apparatus, it should consist of having the main soil chamber capable of being dismantled into two side panels, a lid, a back panel, two separate sections of the front plate and the lower support structure which consists of the base assembly and jack support of the pullout apparatus (Figure 3-3).

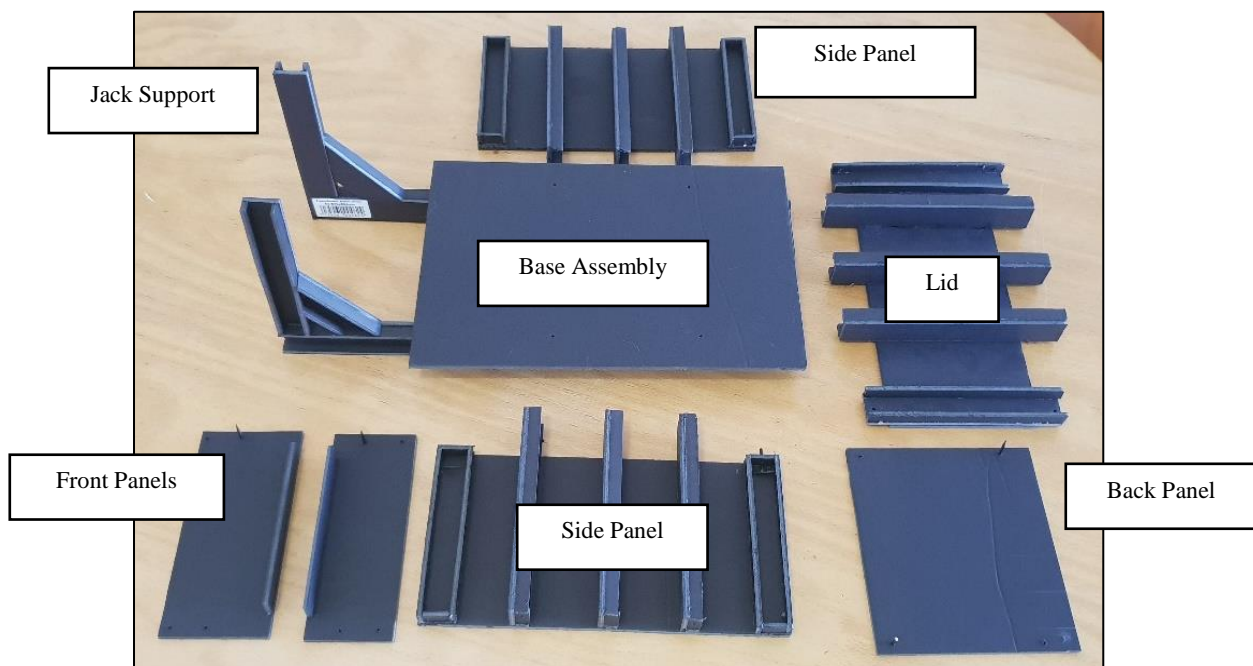


Figure 3-3 Construction of model - disassembly of apparatus into parts for easy transport and storage.

The base assembly on which the entire apparatus is seated was also designed to be modular (Figure 3-4). Each of the smaller cross members were designed to be bolted to the longer members. Five smaller cross members were used in the final design but only two were added on the foam model to save time on construction.

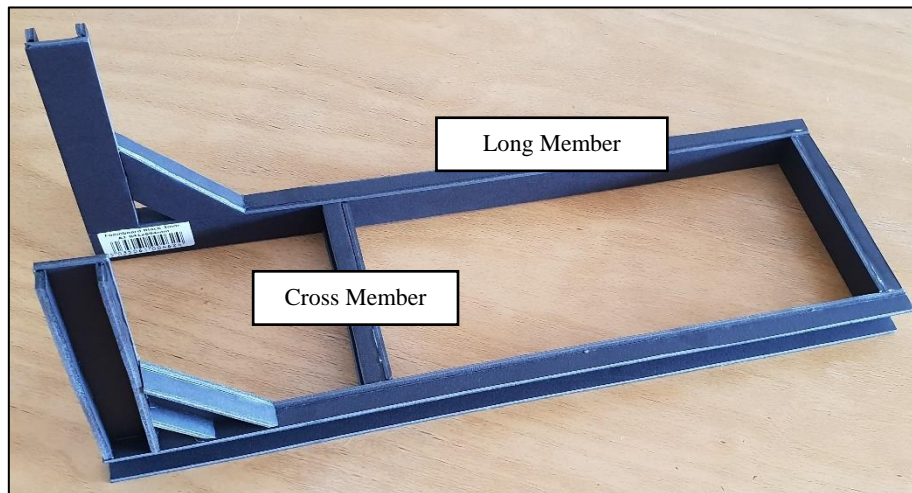


Figure 3-4. Construction of model - modular base assembly.

One of the design aspects that required consideration was the orientation of the steel channels of the side panels and lid. In the foam board model, the channels for the lid and the side panels were assembled in such a way that the short edge was attached to the plate steel in the mid sections but on the long edge for the outer channel sections as seen in Figure 3-5.

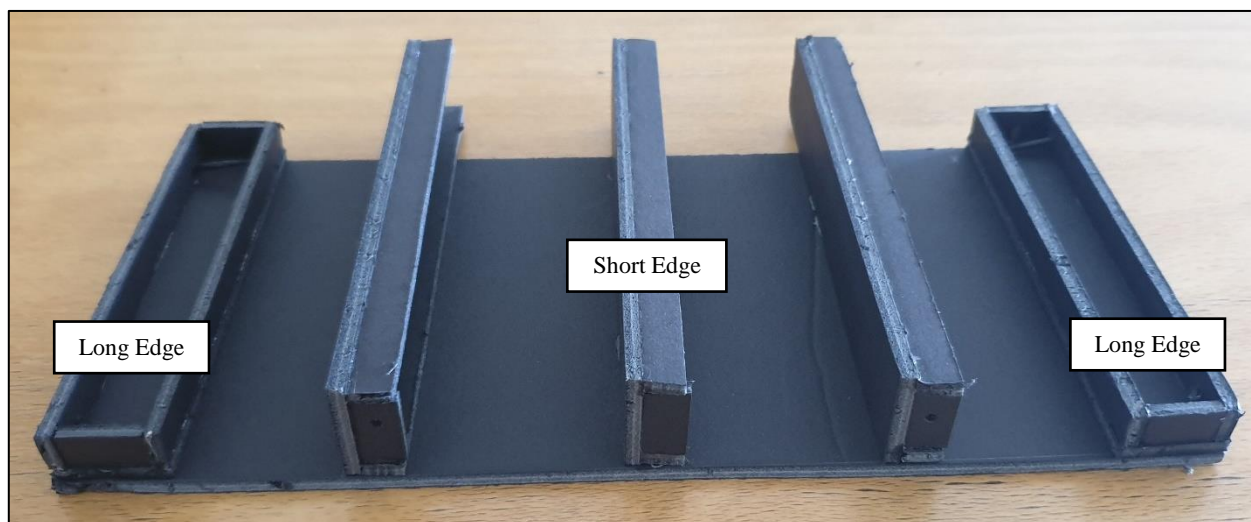


Figure 3-5. Construction of model - steel channel orientation.

This orientation was initially preferred as it would allow any loading applied by the airbag to be carried by the channel in a way that provides the highest resistance to bending motion. This, however, was adjusted during the final design to rather have the steel channels attach with their long ends to the steel plate, thereby allowing for 17.6% more supported surface area of the steel plate at the cost of the steel channel's ultimate resistance to bending.

The final addition to the apparatus was the implementation of an adjustable and removable lower half of the load transfer sleeve. This was needed as, during construction of the foam model, it became apparent that the area indicated in red in Figure 3-6 would be impossible to reach during compaction of the material in the apparatus. This concern is amplified when considering that the load transfer sleeve was not made to the original scale size and should extend further into the soil chamber

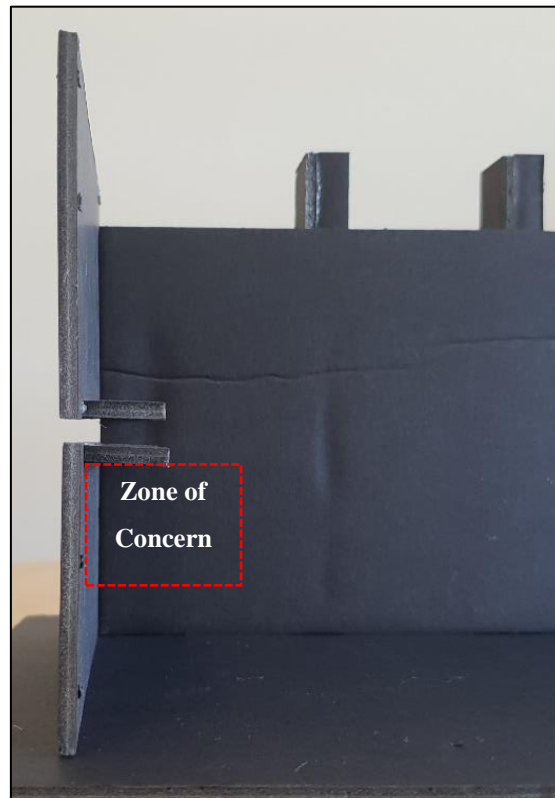


Figure 3-6. Construction of model - zone of concern.

Adjustability was achieved by implementing vertically slotted connection points to which the lower load transfer sleeve attaches, ensuring that the load transfer sleeve is always attached in such a way that it is in contact with the soil.

3.3.3 Primary design parameters

The primary guiding parameters adhered to during the pullout apparatus design, excluding those defined as additional use-cases for the apparatus, are defined by the ASTM standard for measuring geosynthetic pullout resistance in soil (ASTM Standard D6706, 2013). According to these standards, the length, width and depth are required to be a minimum of 610 mm, 460 mm and 305 mm respectively. These dimensions are proposed under the assumption that precautions must eliminate side wall friction which can be achieved, as suggested by the same standard, through lining the apparatus with a high-density plastic such as high-density polyethylene (HDPE) (ASTM Standard D6706, 2013).

Considering that the only limitations provided by literature are those defining the smallest internal dimensions of the soil chamber, it was decided to have the dimensions as large as possible while best utilizing the two sheets of 5 mm thick cold rolled steel available as building material. The dimensions were finalized to consist

of a length of 1205 mm and a depth/breadth of 600 mm. An advantage to maximizing the dimensions of the apparatus's soil-chamber is that the internal volume can easily be reduced through the use of wooden inserts (as will be discussed in Section 4.1.3).

The load transfer sleeve (which acts as the soil-geosynthetic interface) (ASTM Standard D6706, 2013) is required to extend a minimum of 150 mm into the soil chamber, rendering the effective length of the apparatus's soil chamber to be 1050 mm. The total internal soil chamber volume is thus 0.43 m³.

Autodesk Fusion 360 software was used during the conceptual design stage of the pullout apparatus as well as the final model to perform Finite Element Analysis (FEA) (Figure 3-7).

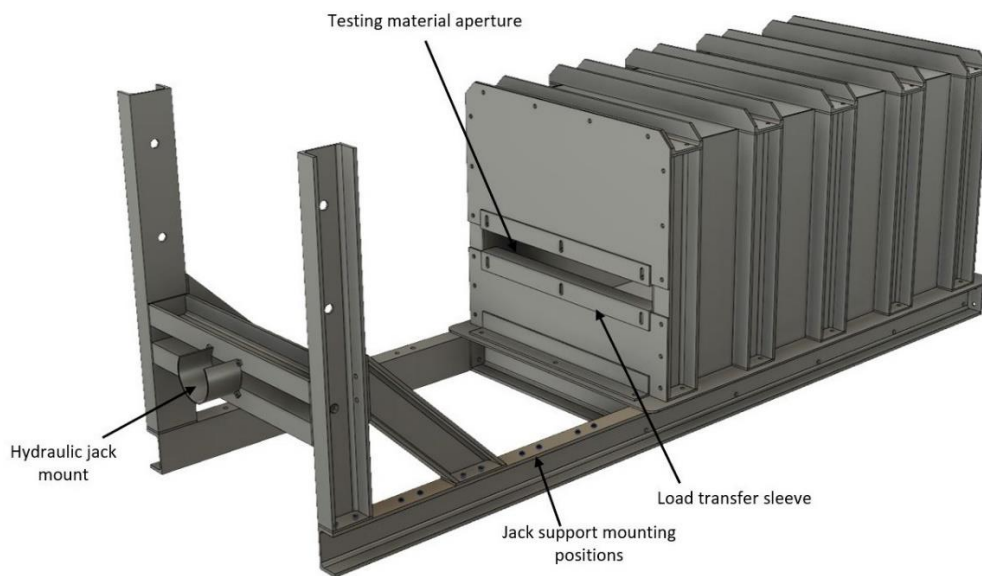


Figure 3-7 Final pullout apparatus model designed using Autodesk Fusion 360.

3.3.4 Testing of the design

To determine the safe range of testing pressures/loads the design was subjected to several Finite Element Analysis (FEA) scenarios using Autodesk Fusion 360 (Autodesk, 2018). Fusion 360 has the capability of performing FEA on any material or structure that acts within the linear stress strain region (Figure 3-8).

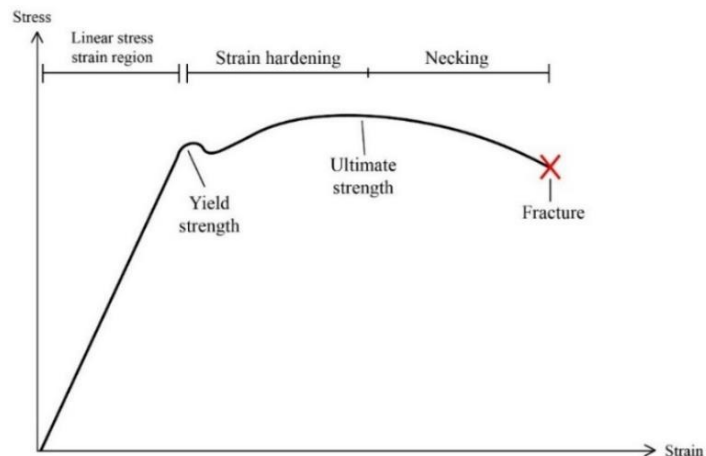


Figure 3-8. General stress strain relation of steel.

Other finer attributes, such as the mesh size used during the FEA, were manipulated within Fusion 360 to increase the accuracy of the results. A 3% mesh size per part was implemented to ensure that there is a minimum of 4 nodes on the shortest length of an object. Rather than applying a global mesh size, the scale per part option was used to allow the mesh to be generated individually per each independent part, thereby further increasing accuracy of the analysis. The use of Fusion 360's contact types allows for the accurate modeling of joints that are both free moving and welded together. For the apparatus's design, all welded contacts used the 'bonded' contact type, which causes the pieces to act as one part during the simulation. All joints that are connected using a bolt took advantage of the simulation's built-in 'bolted' feature, as well as defining the contact surface to act as the 'separation' contact type, which ensured that the pieces could slide with respect to each other yet are not able to penetrate each other.

The initial testing loads were derived from a similar study which also tested pullout resistance of steel strips (Weldu, 2015). The study found that on average, for an effective vertical stress of 70 kPa, the required pullout force was measured to approximately 20 kN. These values were increased by an arbitrary factor to 300 kPa and 50 kN respectively, in order to have a sufficient factor of safety (FoS) for standardized horizontal pullout tests. This was done to allow a wider range of loading for the other two use-cases for this apparatus design (outlined in Section 3.2).

The load which is used during the FEA has the purpose of simulating the applied vertical stress due to self-weight of the soil above the reinforcement, a conversion which is directly dependent on the density of the soil that is being tested. This means that for the maximum load applied of 300 kPa to a given soil with a density of 15 kN/m³, the corresponding wall height would be approximately 20 m high. The same can be done for a soil with a density of 25 kN/m³, which corresponds to the wall being 12 m high. Although not a requirement, a range of tests which can be performed at a large range of loading conditions will allow for a greater insight as to its performance within a MSE wall.

The following scenarios were identified as appropriate for testing as they provided both a proof of concept for the apparatus's safe working loads as well as defined loads that should be avoided as they could cause permanent deformation of the apparatus's structure (full FEA results can be found in Appendix C):

- 1) The lid construction was tested as being fixed in space and having the pressures applied at a maximum of 300 kPa. By isolating this component, it is possible to see the deformation of the part without the inherent benefit of stress migration to the side panels and thus, into the supporting frame.
 - a. After completing the FEA, it was concluded that the design for the lid is adequate as it only received a maximum of approximately 1.7 mm of deflection (Figure 3-9). This corroborates the decision to attach the channel beams to the plate steel using their long edge rather than short edge. Even though the resistance to a bending moment in the direction of the short edge is magnitudes stronger compared to that of the long edge, the effective area gained by having the channels in this orientation allows less pressure to be applied in the unsupported sheet steel, thereby leading to less displacement.

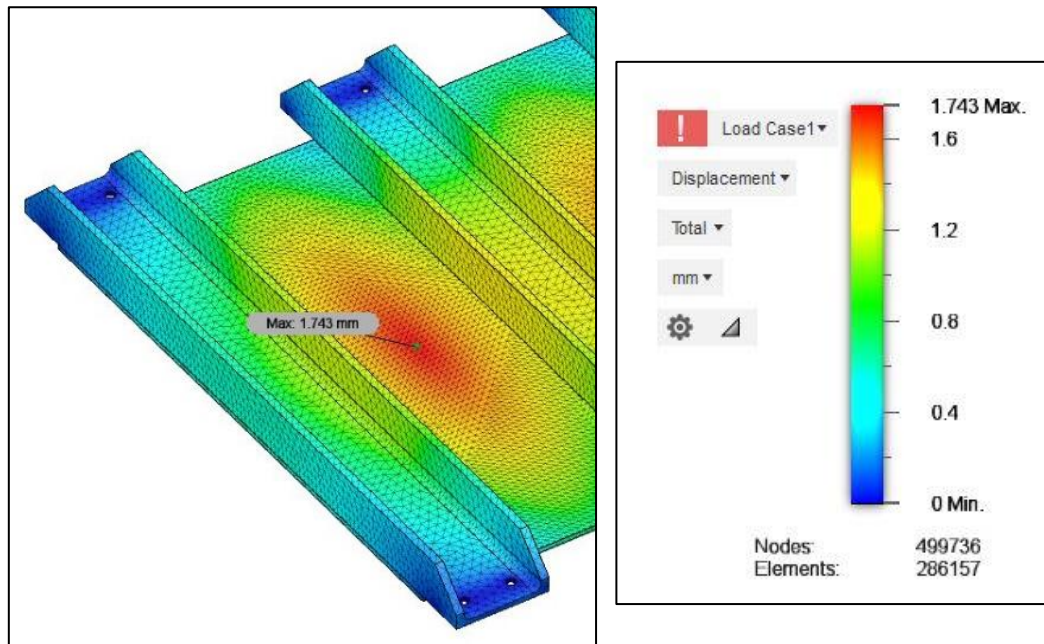


Figure 3-9. Finite Element Analysis of pullout apparatus lid at 300kPa. Deflection was observed to be roughly 1.7mm.

- b. A test of ultimate loading was performed at 500 kPa, which is an arbitrary value chosen to be approximately double the maximum working load. The deformation observed was only 2.9 mm (Figure 3-10) and is considered a safe level of deflection. However, when testing at these loads the more important issue becomes the possibility of the bolts (which hold the lid in place) to fail.

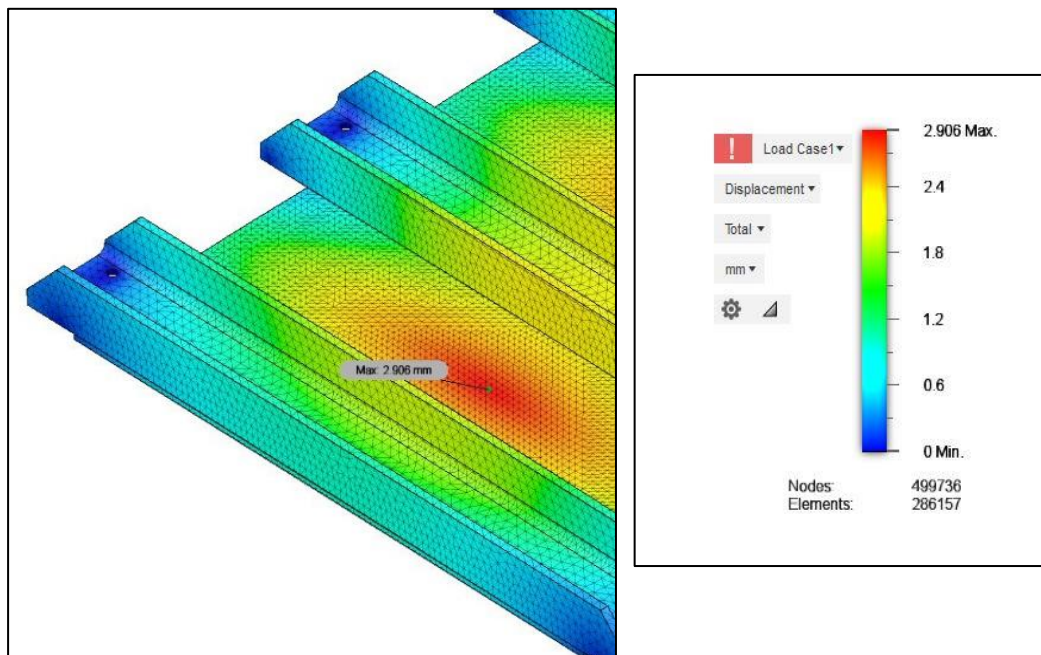


Figure 3-10. Finite Element Analysis of pullout apparatus lid at 500 kPa. Deflection was observed to be roughly 2.9mm.

- 2) Structural deformation of the base assembly caused by loading of the jack was performed by isolating the base assembly from the soil chamber, thereby removing the stabilizing force produced by the weight of the soil. Two scenarios of 50 kN jack load were tested:
- One scenario was having the jack situated at the standard vertical position to be used for horizontal pullout testing. During this setup, a deflection of 16.5 mm was observed (Figure 3-11). Although a deflection of 16.4 mm should not lead to permanent deformation, testing at this level of loading should be done sparingly.

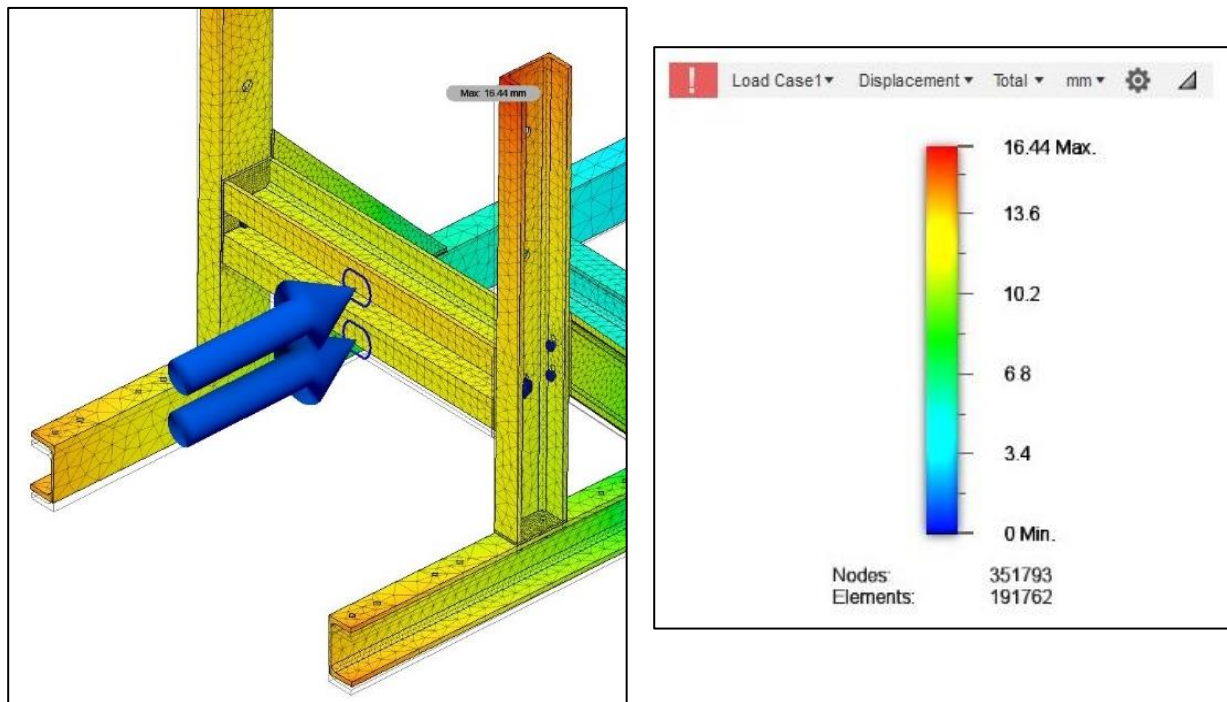


Figure 3-11. Finite Element Analysis of pullout apparatus base assembly at its standard vertical position with a jack load of 50kN. Deflection was observed to be 16.5 mm.

- The second scenario was created by inducing a 50 kN load to the jack at the worst position for loaded testing i.e. being at the furthest possible distance from the soil chamber as well as at its highest mounting position. During this setup, a deflection of 44.7 mm was observed (Figure 3-12). This level of deflection is considered unsafe as it could cause permanent deformation of the structure. When loading at such high loads under these setup conditions precautions should be taken to mount the entire structure to the floor, thereby distributing the load away from the structure itself and into the bolted connection to the floor.

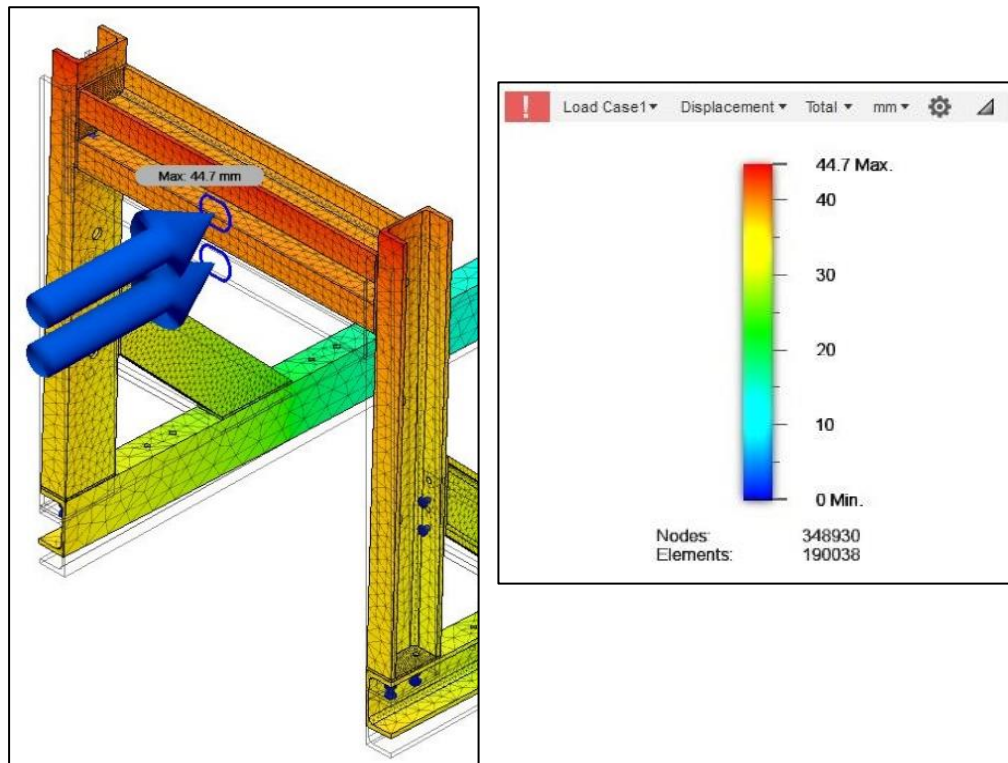


Figure 3-12. Finite Element Analysis of pullout apparatus base assembly at the least ideal position with a jack load of 50kN. Deflection was observed to be 44.7mm.

4 Construction phase

4.1.1 Material preparation

As the entire apparatus consisted of only two structural steel types, those being steel plate and steel channel, the preparation of the materials was simple. The entire process consisted of using a plasma cutter (Figure 4-1) to cut the steel plates into the required dimensions and the large steel bandsaw (Figure 4-2) to cut the channel sections down to size.



Figure 4-1. Plasma cutter.



Figure 4-2. Steel bandsaw.

A simplified way of considering how the design of this apparatus works is by considering the use of steel plate to retain the soil, while the steel channels are used as a load carrying beams which distribute the force applied to the steel plate by the soil to the entire apparatus frame. The preparation of the load carrying beams was completed by producing a total of 34 end-plates (Figure 4-3) using the plasma cutter and a drill press while the bandsaw was used to cut the channel sections to the desired lengths (Figure 4-4).



Figure 4-3. End-plates.



Figure 4-4. Prepared steel channels.

4.1.2 Assembly of the materials

The materials prepared in Section 4.1.1 were then assembled into the final pullout apparatus's structure. This involved attaching the completed load carrying beams (Figure 4-5) to both the walls of the apparatus's soil chamber as well as the base assembly.

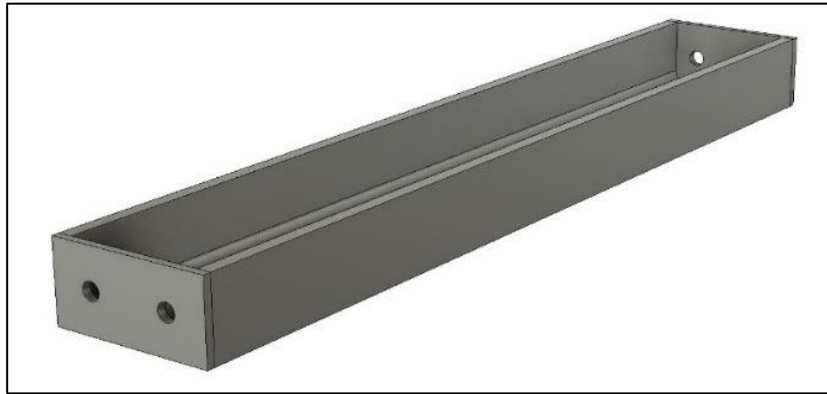


Figure 4-5. General design of all load carrying beams.

A major issue encountered during the construction phase was the loss of accurate reference edges on cut lines after use of the plasma cutter. Whenever the cutter head deviated off completely perpendicular to the work surface, an angled cut was produced. The resulting cut line was wavy and inaccurate for the standard means of measuring and marking.

For this reason, all markings made for drilling were made possible by incorporating relative positioning to the final orientation rather than on a piece-by-piece basis. Once the side panels had been constructed, they were positioned on the base assembly and with the use of a center punch and a 'top-hat' inserted into the corresponding bolt holes, the correct drill hole markings could be made. The 'top hat' works by narrowing and extending the bolt hole to a point where the center punch can be both longer, thinner, and use a finer point for center punching, as seen in Figure 4-6.

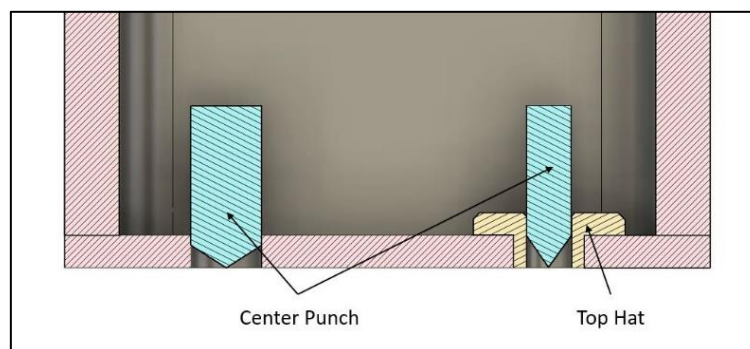


Figure 4-6. Center punch and top hat design.

In Figure 4-7 it can be seen how the side panel is aligned on the base assembly and clamped into position such that the bolt hole locations can be marked using the 'top hat' inserts (Figure 4-8).



Figure 4-7. Side panel alignment.



Figure 4-8. Top hat insert.

For all drilling operations on large pieces that could not be easily mounted in the drill-press, the use of a magnetic-mounting drill was incorporated (Figure 4-9). All holes drilled were drilled to a diameter 11 mm to ensure that the M10 bolts used would have sufficient play to make assembly easier.



Figure 4-9. Magnetic mounting drill (magdrill).

The construction of the lid also followed a similar process in which the ‘top hat’ inset was used to mark the drill hole locations for the lid on the channels. Once all holes were drilled, the steel plate used for the lid could be inserted into the apparatus’s soil chamber and clamped to the channels that had been pre-bolted to the side walls (Figure 4-10). This was done in order to keep the entire soil chamber as square as possible while the lid was welded together.



Figure 4-10. Construction of pullout apparatus lid.

4.1.3 Wooden inserts

An issue that became apparent after construction of the apparatus was that the total dimensions of the soil chamber meant that there was an insufficient amount of soil for each material type that is required to be tested. For this reason, wooden inserts were constructed and inserted into the soil chamber to reduce the internal dimensions. By reducing the dimensions of the apparatus’s soil chamber down to 400 mm in both depth and width, while leaving the length unchanged, there would be a sufficient amount of material for testing.

The reduced dimension still falls within the specifications defined by the ASTM standard. A clause is given by which if the side wall friction is reduced, the minimum dimension between the reinforcement and the side walls should be no less than 150 mm (ASTM D6706, 2013). The reduced width of 400 mm of the soil chamber also matches to the 400 mm width used by Lee and Bobet (2005) for their pullout testing.

The wooden inserts were constructed by cutting a single sheet of plywood into the dimensions of the apparatus’s soil chamber side panels and attaching a total of seven cross braces to prevent the plywood from bending during soil compaction and loading. The wooden insets were coated with waterproof paint to provide

some longevity during the testing procedure and then bolted to the side walls to ensure rigidity during use of the pullout apparatus (Figure 4-11).

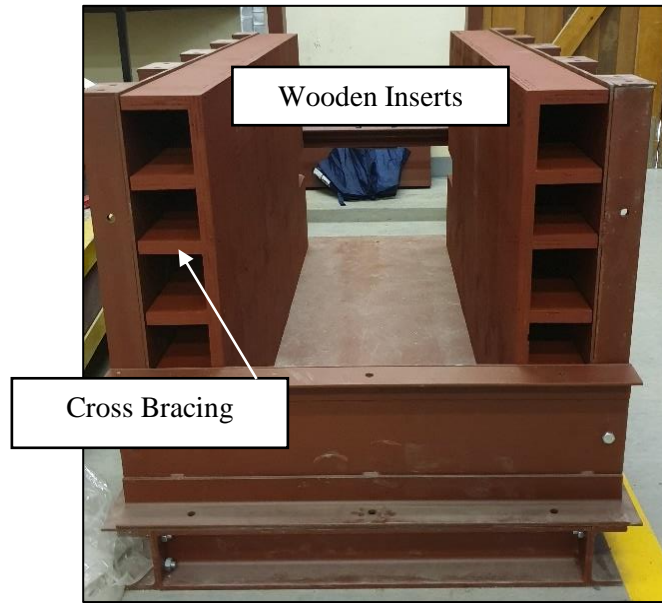


Figure 4-11. Wooden inserts used to reduce the internal dimension of the soil chamber.

4.1.4 Steel strip coupling

As the design of the pullout apparatus described thus far has mainly focused on its general use, the construction of an additional piece of specialized equipment was required to enable pullout testing using steel strips specifically. To allow the steel strip to connect to the hydraulic jack, a coupling was constructed from two steel washers and a stack of M20 bolts joined by two steel plates (Figure 4-12).



Figure 4-12. Steel strip to threaded rod coupling.

The coupling allows for pinned connection to the steel strip (fitted through the holes seen on the left of Figure 4-12) and a threaded connection to the threaded rod, this allows for a rigid connection between the steel strip and the hydraulic jack. An addition which is not shown in Figure 4-12 is a perpendicular plate which was welded to this coupling, which was done to allow for a rigid area of displacement to be measured from.

4.2 Stressing equipment

4.2.1 Airbag

4.2.1.1 Airbag prototyping

To apply an effective vertical stress in the soil chamber, an airbag which applies an even load over the surface of the soil was required. Thus, the required airbag should fill the soil chamber even when not fully inflated and also be capable of withstanding 35 psi of pressure (roughly 2.4 Bars) which equates to 241 kPa of effective vertical stress.

The first design option that was considered was the use of lay-flat hose which could be cut to the length of the apparatus's soil chamber and clamped at either end, allowing for a cylindrical airbag to be formed to which a standard inner tube valve could be attached for inflation. This, however, proved to be problematic as once the airbag is inflated, the surface area of the bag would change depending on multiple aspects such as initial cavity size of the void which the airbag is placed in, as well as the degree to which it is inflated to achieve the required overburden. As this would require prior knowledge of the surface area of contact such that the psi could be calculated, it would be impractical considering that the apparatus's soil chamber is completely sealed.

The second design option that was considered involved the use of PVC sheets (the same material from which lay-flat hoses are produced from) to construct a square airbag that would fit the internal dimensions of the apparatus. As lay-flat hoses are often rated for up to 6 Bars of pressure, this option would produce a sufficiently strong airbag for pullout testing. However, even with the use of high-frequency welding to seal overlaps on the material, the issue of having corners would still present points of failure for both air to escape as well as tearing to occur, something which is especially likely to occur at such high pressures.

The third option was to use a large capacity tyre inner tube typically used for farming equipment. The advantage of this material is that it is rated well above the required 35 psi and is also more than sufficient in size to completely fill the internal dimensions of the apparatus. Utilizing a single large airbag also mitigates the need for a central air chamber required with the use of multiple smaller inner tubes to ensure even inflation and even loading pressure. These inner tubes, as well as any necessary equipment to repair tears or punctures, is also readily available and affordable.

However, when testing the use of the inner tube as an airbag in the pullout apparatus several issues were presented. Once inflated, the surface area of the tube does not fill to match the surface area of the soil. In addition, the inflated tube takes up too much vertical space within the apparatus. This can be seen in both Figure 4-13 and Figure 4-14 where the inflated inner tube has rounded edges while also filling the entire lower portion of the soil chamber.



Figure 4-13. Inner tube when deflated.



Figure 4-14. Inner tube when inflated.

4.2.1.2 Final airbag design

The material used for construction of the final airbag was a modified *Propak* airbag that is typically used in the transport industry to secure transported goods. The bag was modified by reducing the size down from the original 4.6m by 1.2m dimensions to a size that would better fit within the soil chamber. To ensure that the bag could inflate to a square shape, a test was performed where a clamp was added to reduce the size of the airbag (Figure 4-15) and inflated using the stock valve. This produced a square shape (Figure 4-16), giving credibility to the ability of the airbag to fill a square void.



Figure 4-15. Clamped test airbag.



Figure 4-16. Inflated test airbag.

The airbag consists of an outer woven plastic layer that protects an inner plastic air bladder. The dimensions of both of these parts needed to be reduced. A standard plastic bag heat sealing device was used to reduce and seal the inner bladder and a sewing machine was used to adjust the size of the outer layer.

The final issue that needed to be addressed was the implementation of a valve for inflation of the airbag. The valve would need to be able to securely attach to the airbag but also long enough to fit through the lid of the pullout apparatus and securely attach to the airline. The use of a standard bicycle valve was considered, however, once tested, the valve was too short and delicate to use in the final design.

Therefore, a custom valve was designed using a standard M10 bolt with a 4mm hole drilled through it (Figure 4-17). This custom valve, together with two fender washers on either side of the plastic bladder, allowed for an air-tight bond around the plastic but also a rigid system for the airline to be attached to. The valve was attached prior to sealing and completing the airbag. Once fitted into the apparatus's soil chamber the completed custom airbag was capable of filling the entire void of the soil chamber (Figure 4-18).

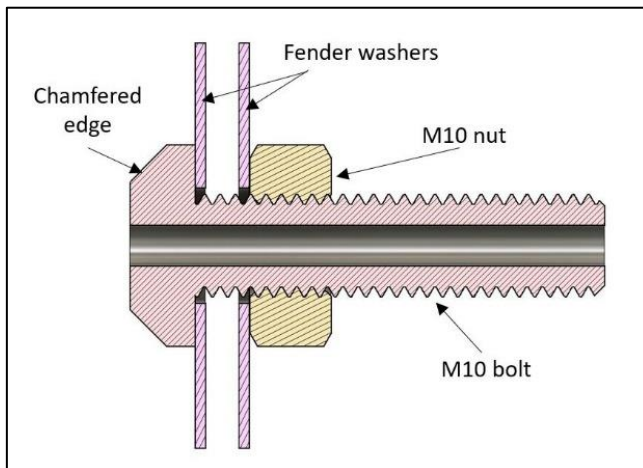


Figure 4-17. Valve design.



Figure 4-18. Final bag dimensions.

4.2.1.3 Air pressure regulation

In order to perform the pullout testing accurately, it is essential that constant air pressure is being applied within the airbag. Therefore, the use of a regulator (Figure 4-19) was implemented to adjust the inline air feed to the required pressure level. In this way, a constant feed of air would be applied even if a puncture is present in the airbag bladder. To calibrate the regulator prior to testing, two separate pressure dials (both different in make and manufacturing date) were attached to the regulator in such a way that they should theoretically read the same value. Once it was confirmed that both dials read the same value, it was clear that the regulator and pressure gauge was in working condition and could be used during pullout testing.



Figure 4-19. Air pressure regulator.

4.2.2 Hydraulic jack

4.2.2.1 Requirements

During the initial design of the pullout apparatus, the jack-mount was left open as to accommodate for any jack size and shape as the hydraulic jack that would be used was still unknown. As per the ASTM standard, a pullout rate of 1mm/min is required from the loading equipment used for pullout testing. However, all of the available loading equipment did not have the functionality of limiting the rate of displacement while performing loading. An addition is provided in the ASTM that allows for testing to be done in a stepped displacement method as an alternative to that of the constant displacement method. In order to best match the constant rate of pullout required (Figure 4-20) a stepped load path of 0.25 mm per 15 seconds (Figure 4-21) was selected for the final testing procedure. This should provide a line of best fit that has the same gradient as the initial 1 mm per 1 minute required.

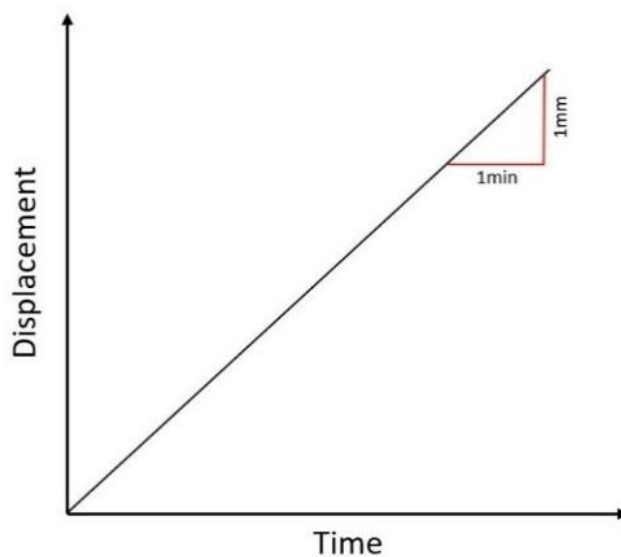


Figure 4-20. Standard rate of pullout displacement.

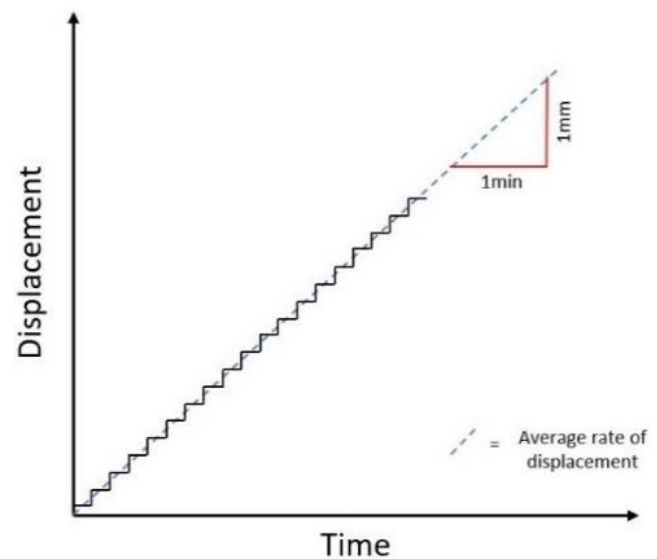


Figure 4-21. Adjusted pullout method to achieve standardized rate of pullout.

4.2.2.2 Setup configurations and testing

A local geotechnical firm was approached in order to obtain stressing equipment that could meet the requirement for testing. The equipment shown in Figure 4-22 is what was provided by the company as their stressing equipment used for all field pullout testing that they perform. The system consists of a power-pack which acts as an electrical hydraulic pump, an inline pressure gauge (used as a reference to the calibrated jack load vs pump pressure graph) and a hydraulic jack rated to 30 tonnes. However, testing the system on-site showed that the system's ability to accurately apply a pressure was non-existent. As there was no way to accurately activate the power pack to meet a desired loading pressure, it rendered the further use of that specific stressing equipment pointless.



Figure 4-22. Hydraulic jack and power pack.

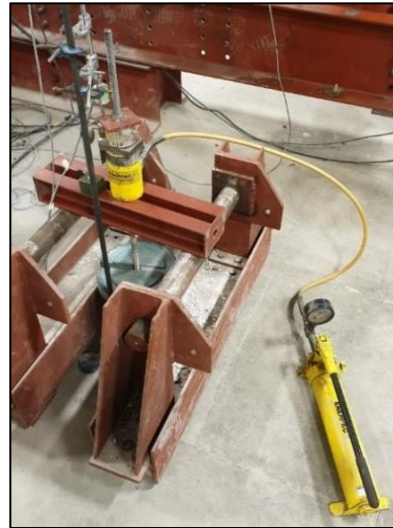


Figure 4-23. Rate of displacement test setup.

As an alternative, a single-action hollow core jack accompanied by a hand pump, both of which were available in the department's laboratory, were used for testing (Figure 4-23). The hollow core jack is rated to a maximum loading capacity of 125 kN with a stroke of 42 mm, which is adequate for the purposes of this testing as failure is expected at roughly 15 mm (Weldu, 2015). The hand pump used is no longer specified on the *Enerpac* website, yet all of their current listed products are able to apply several thousand psi of hydraulic fluid pressure which is more than sufficient to power the hydraulic jack (Figure 4-23).

To verify whether or not the hand pump could achieve the stepped displacement required, a system was set up that included the hollow core jack attached to a load cell in a vertical orientation (Figure 4-23. Rate of displacement test setup.), a threaded rod inserted through the load cell and the jack and bolted just below a weight stack beneath. Once the jack displaced a certain amount the threaded rod bolt would come into contact with the weight and suspend it.

As seen by the LVDT data plot from this test, (Figure 4-24), the hydraulic jack is displaced along a stepped displacement path and the trajectory was kept consistent throughout the pre-loading (before 1 minute), transition phase (at 1 minute) and post-loading phases (after 1 minute). The loading path, as seen by the plot in blue, shows a clear peak in loading as the weight becomes suspended.

A line of best fit was also added to define the displacement curve and shown to have a gradient of 1.0, which is exactly the required 1.0 (1 mm per 1 minute) defined by the ASTM standard. In addition, having a stepped load path of 0.25mm per 15 seconds is accurate enough to produce an R^2 value of 1. This then shows that use of a hand pump to displace the jack is sufficient in applying the required rate of displacement for testing.

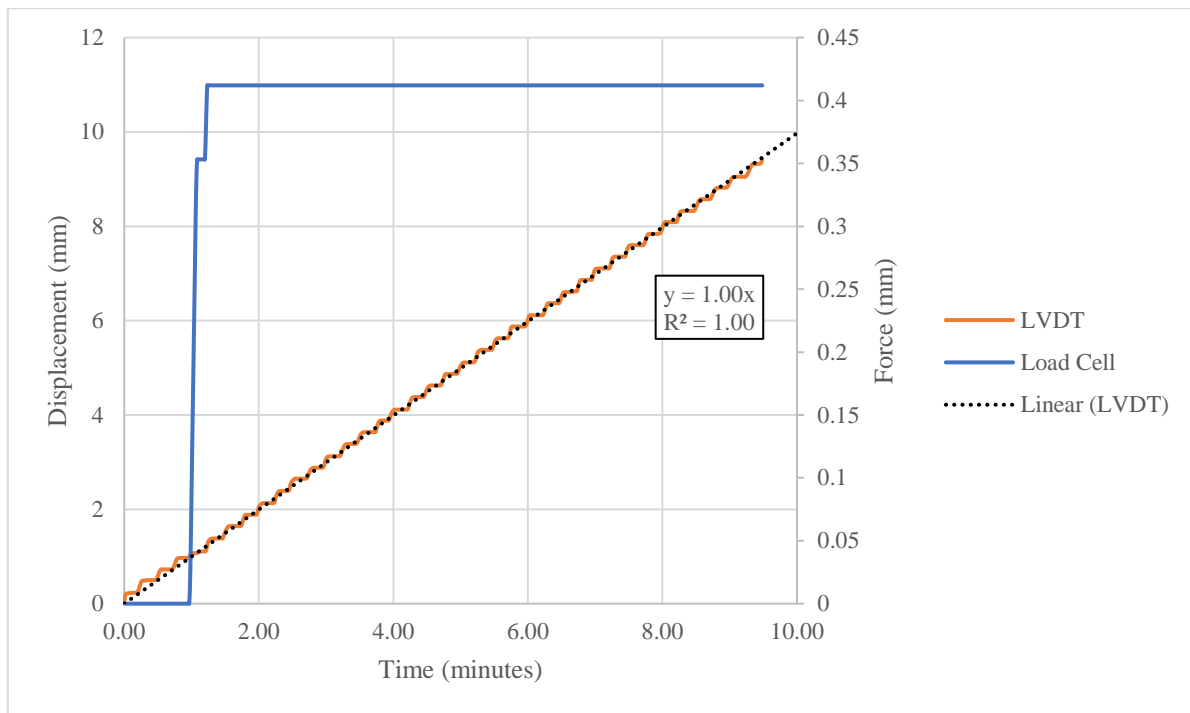


Figure 4-24. Rate of displacement testing.

4.2.2.3 Hydraulic jack housing

The final addition to the hydraulic jack is the housing used to attach it to the jack mount assembly. For the design, the use of a simple back plate (Figure 4-25) - which bolts to the jack itself – is used in connection with two threaded rods and stopper plates (Figure 4-26). This allows for the jack to be freely moved and fastened in any orientation such that the jack is always applying a load perpendicular to the steel strips orientation.



Figure 4-25. Hydraulic jack mount – front.

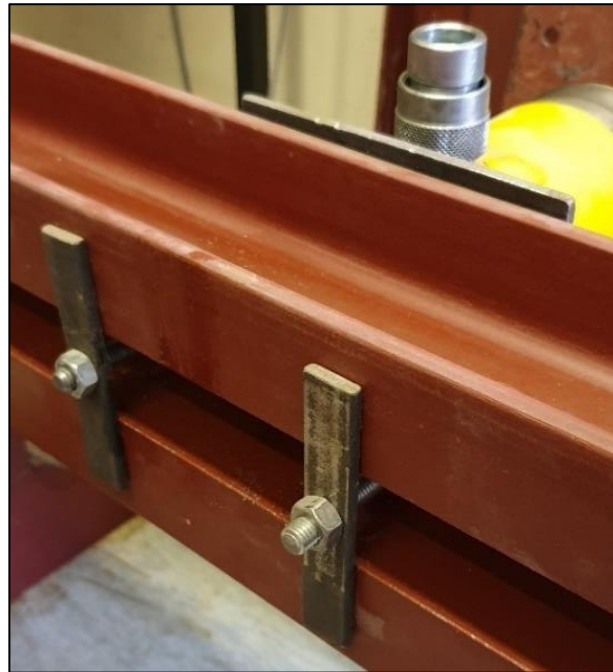


Figure 4-26. Hydraulic jack mount – back.

4.3 Data acquisition

For pullout tests to produce relevant data, a minimum of three data sources are required per test, those being two 100mm Linear Variable Differential Transformers (LVDT) attached to the steel strip as well as a load cell. The LVDTs are used to measure the displacement of the steel strips and the load cell is used to measure the load that is applied to the steel strip during displacement. As seen in Figure 4-27, the two LVDTs are placed on magnetic bases independent of the pullout apparatus in order to ensure that the reading is taken from an isolated frame of reference. Furthermore, having the LVDTs set up in this way allows the deflection of the jack mount to be calculated by measuring the difference between the two data points.

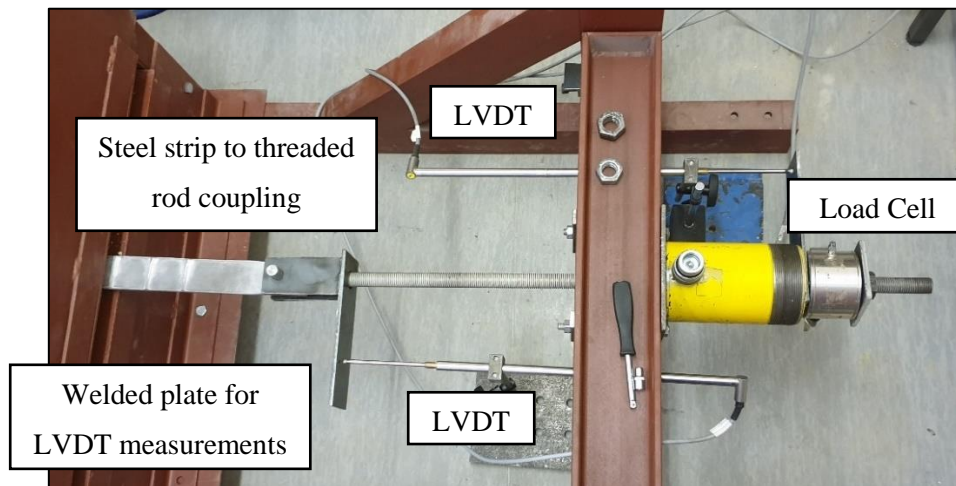


Figure 4-27. Data acquisition setup.

The load cell used is rated to 20 tonnes to ensure that the range of loading is represented by a higher percentage of the load cell's maximum loading force to enable a higher accuracy in its measurement. All data was recorded using the *Catman* software designed for digital data acquisition systems such as the one used in these tests.

4.4 Cost breakdown

The cost of constructing the pullout apparatus is summarized below (Table. 4-1). The stressing equipment, data acquisition devices, software, and machinery used for material preparation and construction have been excluded from this cost analysis. In the event that the entire system is reproduced, it is highly likely that these excluded items are already available in the department or can be rented at variable prices depending on geographical location.

All steel prices were obtained through a quote from *MacSteel* and are thus subject to change. As the channel stock is available in predefined lengths, it might require the purchasing a longer length of channel stock. Considering the cost shown below is circumstantial and only relative to the specific design of the described pullout apparatus for this project, it is subject to debate as to whether it is cost effective and should be classified as 'low-cost'. Nevertheless, when taking into consideration that having standardized geotechnical testing performed by a certified laboratory can cost in excess of R1000 per test, it is well within reason to classify the roughly R7300 cost of this apparatus to within the low-cost range.

Table 4-1. Cost breakdown of constructing pullout apparatus (excluding other equipment).

ITEM	COST PER UNIT	AMOUNT	LENGTH (MM)	TOTAL LENGTH	COST
PARALLEL FLANGE STEEL CHANNEL (S355)	R145.00	5	610	3050	
		3	710	2130	
		10	600	6000	
		5	500	2500	
		2	2200	4400	
		2	700	1400	
		2	800	1600	
					21080
STEEL PLATE 2.5M X 1.2M	R2,000.00	2			R4,000.00
BOLTS M10 X 30MM (GRADE 8.8)	R1.50	100			R150.00
NUTS M10 GALZINZED (GRADE 8.8)	R0.50	100			R50.00
				Total Cost	R7,256.60

4.5 Conclusion

Considering all the aspects that have been dealt with throughout the design and implementation of the entire pullout apparatus, the aim and all of the objectives have been met. Both the cost and construction of the entire system have been completed within an adequate amount of funds and use cases respectively. As currently constructed, the apparatus gives a clear impression that it should perform adequately during the pullout testing required to address the research topic, being the determination of pullout resistance of galvanized steel strips. However, only once the final testing has been completed within the scope of this project, can any further considerations be made to improvements on the current design.

5 Methodology

5.1 Introduction

This chapter defines the procedure for standardized pullout testing and outlines the classification of the soil samples used during these pullout tests. In addition to the use of standardized testing protocols, custom tests that are not specifically defined within the standardized testing protocols, but justified under the testing circumstances, were implemented. All testing was performed within the Stellenbosch University Geotechnical Laboratories

5.2 Aim and Objectives

The primary aim of this chapter was to perform standardized pullout testing on the available soil types while ensuring that the following objectives are met:

- Determine a test protocol which outlines the ideal testing conditions used for the standardized pullout resistance testing.
- Perform any tests necessary to allow for a comprehensive classification of the soil types being tested, including:
 - Sieve analysis
 - Direct shear testing
 - Modified AASHTO compaction tests
 - Permeability testing
- Provide feedback as to the performance of the pullout testing apparatus and all its additional features.

5.3 Soil Samples

Three soil types were selected on the basis of availability and apparent position on the permeability range (Terzaghi, 1948). The selected soils were as follows:

5.3.1 Crusher Dust

This material was the simplest to collect as it was already available within Stellenbosch University Structural Engineering Department's silos. It is an engineered fill material made from crushed greywacke and is primarily used as coarse aggregate within cement mixes. Sample collection from the silos was performed with the silo valve being fully opened. This allowed for a constant flow of the material and ensured that larger diameter soil particles were not unintentionally sieved out.

The crusher dust was also selected on the basis of its probable high permeability (as indicated by its soil particle size distribution) and its material composition being ideal for that of a backfill material within mechanically stabilized earth walls (MSE walls).

5.3.2 Cape Flats sand

This material is a wind-blown material readily found within the greater Cape Town area. The site at which the material was collected is located approximately 40 km out of Cape Town in the Mfuleni Township. The

location in Mfuleni from which the material was collected is situated approximately 200 m south of the Mfuleni Fire Station. This material was selected due to it meeting the criteria of being freely available within the greater Cape Town area but also due to its composition being that of a fine clean sand which should allow for a moderately low free draining ability.

5.3.3 Micaceous Residual Granite

This material was collected from a borrow pit in which backfill material had previously been collected for the construction of a nearby bridge abutment. It is a residual soil formed from the weathering of a granitic outcrop. This material was chosen as it had already been used as a backfill material, indicating its relevance in the current industry, as well as its origin which indicates that it should contain a high percentage of both clay minerals and larger particles made of either quartz or feldspar. The clay content determines that this material should fall within the non-free draining category. Due to research performed on the same material by Mong (2019) the residual granite was given the prefix of micaceous as it was shown to have 26% mica content through the use of X-ray powder diffraction (XRD).

5.4 Soil Classification

5.4.1 Maximum dry density and optimum moisture content

This process was performed on all three of the soil samples following the THM1's Method A7 (Committee of State Road Authorities, 1986g) standard which follows the compaction procedure to meet modified AASHTO specifications. The test was performed using an electric compaction device that lifts and drops a hammer of the correct weight for a specified number of blows per layer. The results were recorded using Microsoft Excel and sorted according to moisture content to produce the dry density versus optimum moisture content plot.

5.4.2 Soil particle size distribution

The soil particle size distribution curve was created using three separate standards: two of which were used to classify the soil fines fraction, being particles that pass through the 0.425 mm sieve; and the third coarse fraction of the material determined using the final standard where all particles larger than 0.425 mm are classified. The coarse fraction was sieved according to the THM1's Method A1 (Committee of State Road Authorities, 1986a), using a 2.36 mm sieve rather than a 2 mm sieve. This was due to unavailability of the 2 mm sieve during testing.

The fines fraction was determined by following the THM1's Method A6 and A5, with a change in sieve size distribution used in Method A5 (Committee of State Road Authorities, 1986e) to include that of 0.425 mm, 0.300 mm, 0.212 mm, 0.075 mm and the pan, essentially increasing the measured sieve size fractions. Method A6 (Committee of State Road Authorities, 1986f) was then used to determine the fraction of both clay and silts within the fines content using a hydrometer.

For each material, a soil sample was collected of the material in its normal state as well as another sample after all the pullout testing was performed. This was done to allow for the measurement of possible soil degradation through the pullout testing as the material was reused for each test.

5.4.3 Atterberg limits

A standard testing protocol following THM1's Method A2, A3 and A4 was used to determine Atterberg limits of the micaceous residual granite as the other two materials are deemed non-plastic. Method A2 was used to determine the liquid limit of the soil (Committee of State Road Authorities, 1986b). Method A3 was used to determine the Plastic Limit and Plasticity Index of the soil (Committee of State Road Authorities, 1986c), and Method A4 was used to determine the linear shrinkage of the soil (Committee of State Road Authorities, 1986d).

5.4.4 Permeability testing

Permeability testing was performed through a modified apparatus based on the testing procedure outlined by Head (1992). During the sample preparation stage, the permeameter cell used for the permeability testing was the same mould used in THM1's Method A1 to determine the maximum dry density. This mould was then used in both the constant head and falling head tests for the coarse and fine soil types respectively. The overall testing apparatus shown in Figure 5-1 consists of three standpipes of varying diameters (50.9 mm, 15.3 mm and 4.9 mm, marked as SP1, SP2 and SP3 respectively), a head standpipe with a diameter of 4.2 mm (marked as HSP) and a constant head reservoir. The ball valves are indicated by V1-V8.

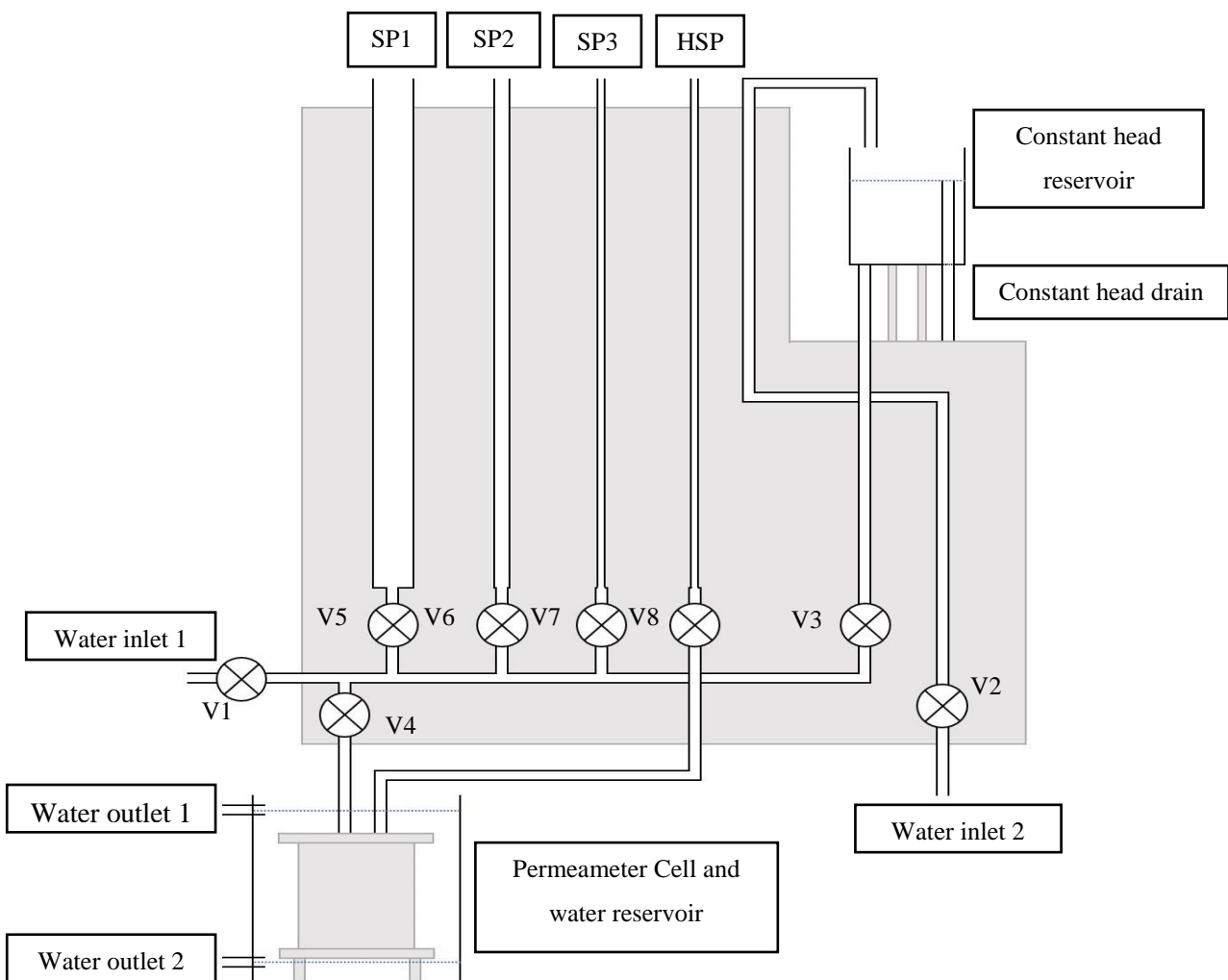


Figure 5-1. Permeability test apparatus (not to scale)

5.4.4.1 Permeameter cell preparation

For both constant and falling head permeability testing, cell preparation followed the same procedure and required the following materials and equipment (depicted in Figure 5-2):

- Top Plate
- Standard CBR plate.
 - Only required in the event that the compacted material is unable to remain in the mould when the mould is lifted.
- Base Plate
- 4x Tie rods, including
 - 4x Thin brass M10 nuts
 - 4x Thick brass M10 nuts
 - 4x Washers
- 2x Non-woven geosynthetic sheets
- 2x Wire mesh sheets
- 2x rubber gaskets
- Standard compaction mould and collar

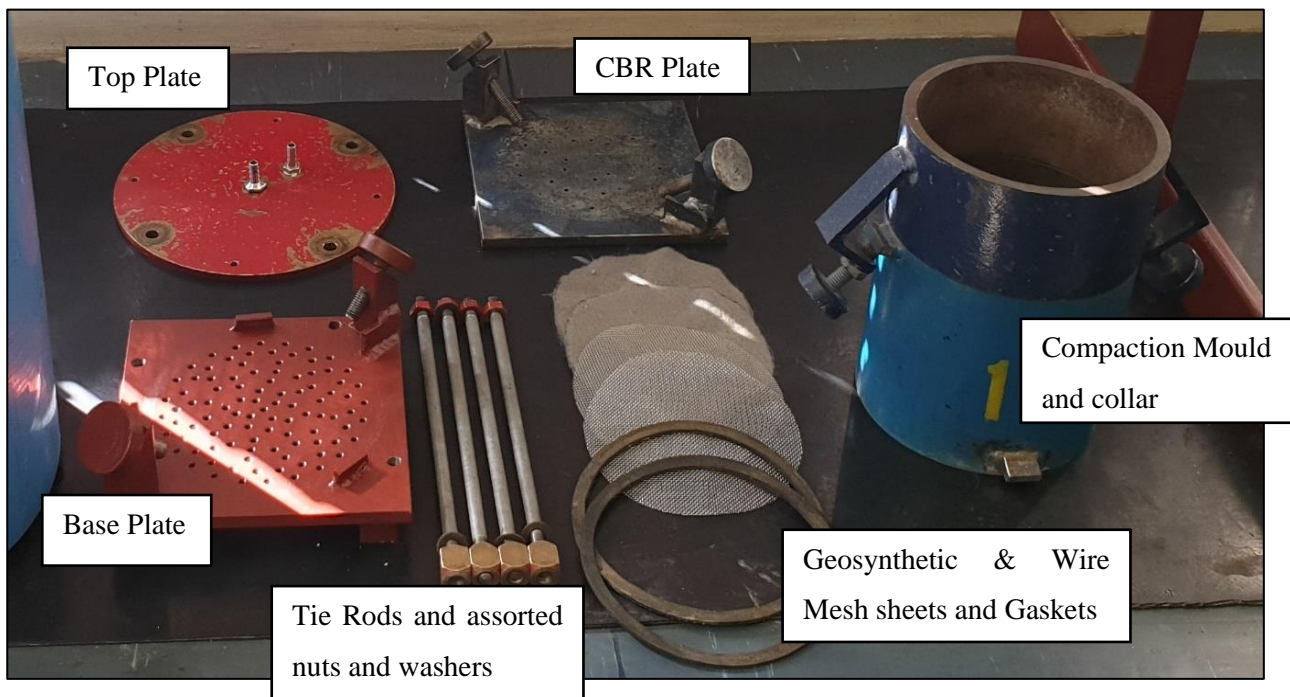


Figure 5-2. Permeameter cell assembly requirements

The cell was prepared by first applying a standard modified AASHTO compaction effort (similar to what is described in THM1's Method A1) within the soil mould and using a scraping technique to flatten the sample. This was done to ensure that the sample is always 127 mm thick and fills the mould completely, thereby reducing the likelihood of a gap forming along the soil/steel interface within the mould. The mould was then fitted with the mould collar, base plate, top plate and coarse filter material (used as completely free draining

fill to ensure linear water flow through the soil sample) and fastened using the tie rods. The completed permeameter cell is shown in Figure 5-3. The bidum cloth and wire mesh disks were used on both the top and bottom of the soil sample so that the bidum cloth was fitted between the soil and the wire mesh. This allowed for the sample to be held in place by the coarse fill during testing.

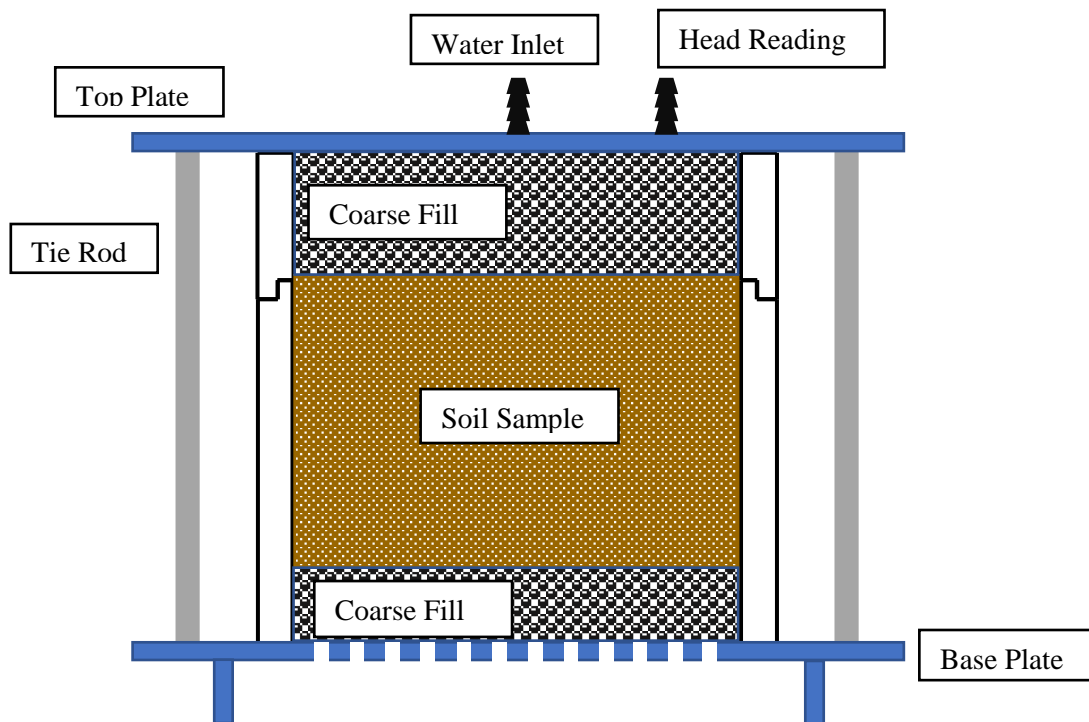


Figure 5-3. Permeameter Cell

5.4.4.2 Testing procedure

Before both the constant head and falling head tests the samples were primed for testing. In the case of the constant head test, this involved the sample having water flow through the permeameter cell and out of Water outlet 2 (Figure 5-1) for approximately 15 minutes or until water was constantly trickling from the constant head drain. For falling head tests, both the constant head reservoir and SP1 were filled with water and allowed to drain through the submerged permeameter cell (with the water level at Water outlet 2) for 24 hours.

A. Constant head

Following priming of the sample, the total volume of water that flowed out of Water outlet 1 was measured on a constant time basis. Time intervals were based on the actual flow rate of the sample at equilibrium.

The following time intervals were used:

Material	Number of readings	Time interval (minutes)
Crusher dust	5	0.5
	5	1
	1	2
Cape Flats sand	5	2
	5	5
	1	10

B. Falling head

The falling head test was performed on the micaceous residual granite by filling SP3 to a predetermined height and a set of two 50 mm intervals were added below the water level. The time that elapsed until the water level reached each interval was recorded. This process was repeated by filling the water level back up to the initial height and recording the same readings.

5.4.5 Direct shear testing

Direct shear testing was performed according to ASTM Standard D3080 (2014) within a 100 mm shear box (the components of which can be seen in Figure 5-4) to obtain each soil's angle of internal friction (ϕ) and cohesion (c). The samples were tested at 50, 100 and 150 kPa to match the vertical stresses used within the pullout testing (described in Section 5.5), excluding the 0 kPa test.

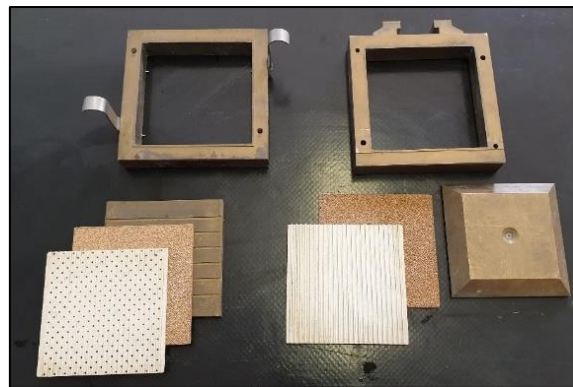


Figure 5-4. 100 mm Shear box components

All tests were performed on the moist compacted material (to 93% modified AASHTO compaction) at a rate of displacement of 0.005 mm/min within a dry shear box. This allowed for the total stress parameters to be obtained for each soil. In the case of the crusher dust, the fraction larger than 3.35 mm was sieved out to ensure that the maximum grain size meets the criteria set by the ASTM Standard D3080 (2014).

The majority of the samples were prepared using the same technique of mixing the desired material at a dry mass and water content required to obtain a minimum compaction of the 93% modified AASHTO compaction effort at the optimum moisture content. The sample was compacted within the shear box using a steel tamper (Figure 5-5) in 3 separate layers ensuring that the layers do not fall on the shear plane (Figure 5-6).



Figure 5-5. Shear box sample preparation



Figure 5-6. Shear box layer compaction height

The only samples that deviated from the above-mentioned sample preparation and testing procedure are those of the sieved crusher dust test. These tests were performed at a rate of 0.25 mm/min and compacted within the shear box using a wooden insert used to apply an even vertical stress through pressing by hand while the entire shear box assembly was vibrated using a vibrating sieve base.

Three tests were done per sample to create a failure envelope on a shear stress – normal stress plot. The total stress strength parameters were obtained for each material type in both the pre- and post-pullout testing soil conditions. As mentioned before, the shear test was performed in a dry shear box with the material in a moist compacted state (to the 93% modified AASHTO compaction). This was done to mimic the soil conditions within a backfill just after construction.

5.5 Pullout testing

Pullout tests were performed following the standard testing procedure as defined by the ASTM Standard D6706 (2013) with a slight modification to sample preparation with regards to a predefined moisture content and its compaction within the soil chamber. Both procedures are described within the following sections.

5.5.1 Steel Strip

The focus of the project was based on the pullout resistance of a galvanized steel strip within a backfill material. The strips used were manufactured by *Reinforced Earth* with overall dimensions being 3 m in length, 5 mm thick and 50 mm wide.

The 3 m strip was cut down to a length of 1.5 m (Figure 5-7) to ensure constant 1.0 m embedment of the strip within the soil chamber but also to have a section protruding to connect to the hydraulic jack. The strips have a bolted connection point on both the tip and tail of the strip located on an enlarged section (Figure 5-8) where the strip is reduced in width while the thickness is increased.

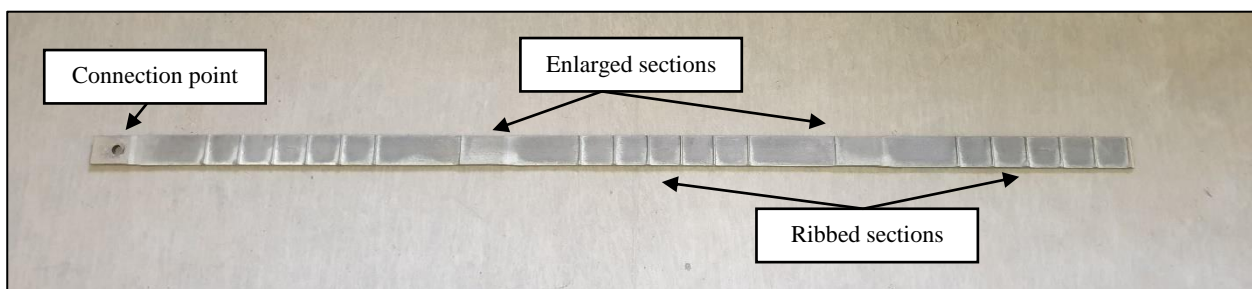


Figure 5-7. Steel strip used for testing – dimensions



Figure 5-8. Enlarged image of steel strip features

5.5.2 Sample preparation

For each of the three testing materials, the same sample preparation was followed. Using the results from the optimum moisture content and maximum dry density testing completed in Section 5.4.1, each of the materials were sectioned into 25 kg bags of dry material and mixed using a commercial grade cement mixer (Figure 5-9). The material was added with the required water and mixed for a sufficient amount of time to ensure adequate mixing. Once mixed, the moist material was transferred back into the respective sample bags and zip-tied shut to ensure that the moisture content was maintained. The material for each soil sample was mixed the day prior to pullout testing to minimize the amount of time the material was stored within the sample bags.



Figure 5-9. Pullout testing sample preparation

5.5.3 Pullout resistance testing

A total of eight tests were performed on each soil material, with varying applied vertical stresses as well as replicates for each test at a given vertical stress. The samples were tested at 0 kPa, 50 kPa, 100 kPa and 150 kPa (in that order), with one set of repeat tests performed in the same order. This was done to ensure that any possible soil degradation would be spread over the course of all the testing rather than only affecting the later tests. A summary of testing conditions is given in Table 5-1.

Table 5-1. Summary of pullout testing conditions

Material	Respective test number	Number of times material has been reused	Applied vertical stress (kPa)	Moisture content to which testing material was mixed (%)	93% Modified AASHTO Density (kN/m ³)	Sum of applied vertical stress and soils self-weight (kN/m ²)
Crusher Dust	1	0	0	6.5	18.4	4.0
	2	1	50	6.5	18.4	54.0
	3	2	100	6.5	18.4	104.0
	4	3	150	6.5	18.4	154.0
	5	4	0	6.5	18.4	4.0
	6	5	50	6.5	18.4	54.0
	7	6	100	6.5	18.4	104.0
	8	7	150	6.5	18.4	154.0
Cape Flats sand	9	0	0	15.8	14.6	3.1
	10	1	50	15.8	14.6	3.1
	11	2	100	15.8	14.6	53.1
	12	3	150	15.8	14.6	53.1
	13	4	0	15.8	14.6	103.1
	14	5	50	15.8	14.6	103.1
	15	6	100	15.8	14.6	153.1
	16	7	150	15.8	14.6	153.1
Micaceous residual granite	17	0	0	8.5	18.4	4.0
	18	1	50	8.5	18.4	4.0
	19	2	100	8.5	18.4	54.0
	20	3	150	8.5	18.4	54.0
	21	4	0	8.5	18.4	104.0
	22	5	50	8.5	18.4	104.0
	23	6	100	8.5	18.4	154.0
	24	7	150	8.5	18.4	154.0

For each of the eight tests, the entire soil chamber was cleaned of all compacted material and prepared again according to the following steps:

1. The soil chamber was lined with HDPE plastic to reduce side wall friction (Figure 5-10).
2. The soil was compacted to 93% modified AASHTO compaction in layers to a predetermined soil height (Figure 5-11) ensuring that the steel strip is inserted at the correct height as to not cause interference with the load transfer sleeve.
 - Compaction was achieved using a steel tamper with a foot area of 16.5 cm by 15.2 cm.
 - The steel strip was inserted to the same depth of embedment and aligned with the same face pointed up for each test performed.
3. Once the soil chamber was filled and compacted flat (Figure 5-12), HDPE plastic was placed over the soil surface (Figure 5-13).
4. The airbag was inserted (Figure 5-14) and lined with a sheet of HDPE plastic (Figure 5-15). This was done to remove friction between the airbag and the surrounding material while inflating.

5. The lid was then attached and bolted down with the airbag valve protruding through the lid (Figure 5-16).
6. The air regulator was then attached to the airbag (Figure 5-16).
7. The steel strip was attached to the hydraulic jack at the pinned connection (Figure 5-16).
8. The required vertical stress was applied, ensuring that the air pressure is stable and not dropping.
9. The pullout test was performed.
10. The applied vertical stress was removed, and the lid detached from the pullout apparatus.
11. All compacted material was removed from the pullout apparatus soil chamber and stored in large sample bags.
12. Steps 1 to 12 were repeated for the following test.



Figure 5-10. Soil chamber lined with HDPE plastic



Figure 5-11. Soil heights used for compaction



Figure 5-12. Compacted soil within the soil chamber



Figure 5-13. HDPE lining on soil surface



Figure 5-14. Airbag within the soil chamber



Figure 5-15. HDPE plastic lining around airbag to reduce friction

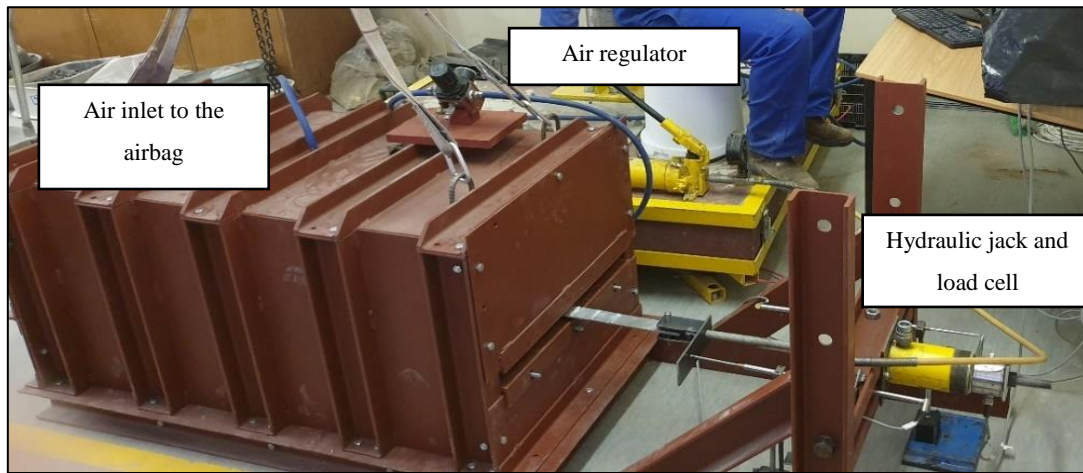


Figure 5-16. Soil chamber with bolted lid and air pressure regulator attached

With regards to the re-compaction of the soil chamber, care was taken to ensure that the previous test's soil that was located around the steel strip was not compacted around the steel strip again for the following test. This ensured that a uniform ware was placed on all material throughout testing.

6 Results

6.1 Introduction

The following section is used to present the results obtained from the testing procedures outlined in Chapter 5. The results will be presented in the same order in which the respective testing protocol was outlined. Where applicable, a summary of the results is given as well as the raw results obtained for the respective test. For all testing in which soil samples were taken in a pre-test and post-test state with regards to pullout testing, a small sample was taken from each of the sample bags containing the post-test material and combined into a collective sample. This was done to produce a representative sample of the entire soil mass in its post-pullout testing state.

6.2 Soil Classification

6.2.1 Maximum dry density and optimum moisture content

For each of the three samples, a maximum dry density was determined for the respective optimum moisture content according to the modified AASHTO compaction effort. The test was performed over a range of moisture contents in order to best quantify the optimum moisture content that related to the maximum dry density.

The crusher dust presented a maximum dry density of 2016 kg/m^3 at a corresponding optimum moisture content of 6.5% (Figure 6-1). Compared to the crusher dust, the micaceous residual granite presented a similar maximum dry density of 2018 kg/m^3 at a higher optimum moisture content of 8.5% (Figure 6-2).

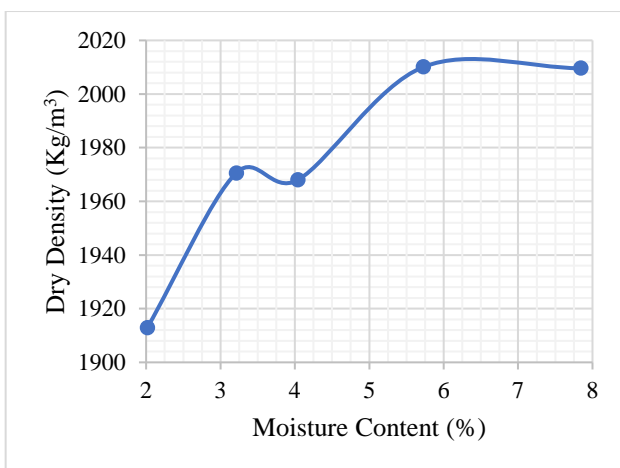


Figure 6-1. Dry density curve of the crusher dust

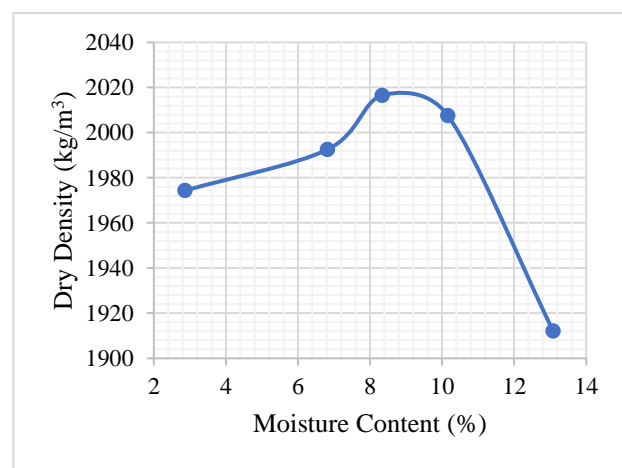


Figure 6-2. Dry density curve of micaceous residual granite

The Cape Flats sand was measured to be the least dense material as its maximum dry density was that of 1598 kg/m^3 at an optimum moisture content of 15.8% (Figure 6-3). This density corresponds to previous literature done on the Cape Flats sand (Schoeman, 2018).

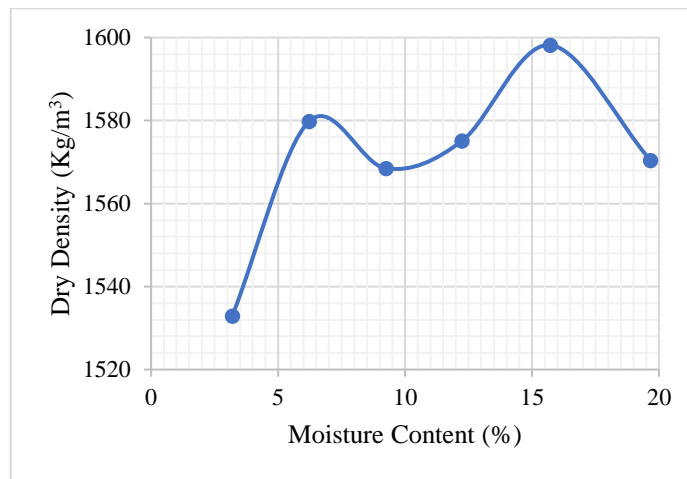


Figure 6-3. Dry density curve of Cape Flats sand

The soil classification will be discussed in further sections. However, considering soil classification according to the unified soil classification system (ASTM Standard D248, 2006), the maximum dry densities obtained fall well within the realm of what the material consisted of. According to Byrne and Berry (2008) in *A Guide to Practical Geotechnical Engineering*, both the crusher dust and the micaceous residual granite classify as very dense due to the maximum dry density. The Cape Flats sand, however, is on the boundary from loose to medium dense.

6.2.2 Soil particle size distribution

Considering that each material type was reused for each pullout test, the soil particle size distribution was produced in both the pre- and post-pullout testing state. The pre-pullout state is considered the point where the soil has only been mixed to the desired moisture content, and post-pullout testing state where all eight tests have been performed on the given material. This was done to determine if any soil degradation occurred between the beginning and the end of the pullout testing. The particle size distribution is given below where each material is plotted on the same axis for both pre- and post-pullout testing. The soil classification was derived from obtaining the soil's coefficient of uniformity (C_u) and coefficient of curvature (C_z).

It is clear for both the crusher dust and the Cape Flats sand that no soil degradation occurred, as both particle size distribution curves fall perfectly over each other. The residual micaceous granite showed the greatest change in the particle size distribution; however, this could simply be due to the breakdown of the larger quartz clusters (those which are highly fractured) into smaller size particles. The issue of breaking down clustered material is addressed by the THM1's Method A1 (Committee of State Road Authorities, 1986a). The technique provided by the standard is that of soaking the material overnight. It is apparent that this did not provide the required mechanical effort needed to break the particles down, a force which was sufficiently provided by the compaction tamper used during the pullout tests.

6.2.2.1 Crusher dust

The crusher dust is classified as a uniform graded material with a C_u and C_z value of 0.13 and 1.81 respectively. Using the USCS classification chart (ASTM Standard D248, 2006), the crusher dust can be classified as GP (poorly graded gravel).

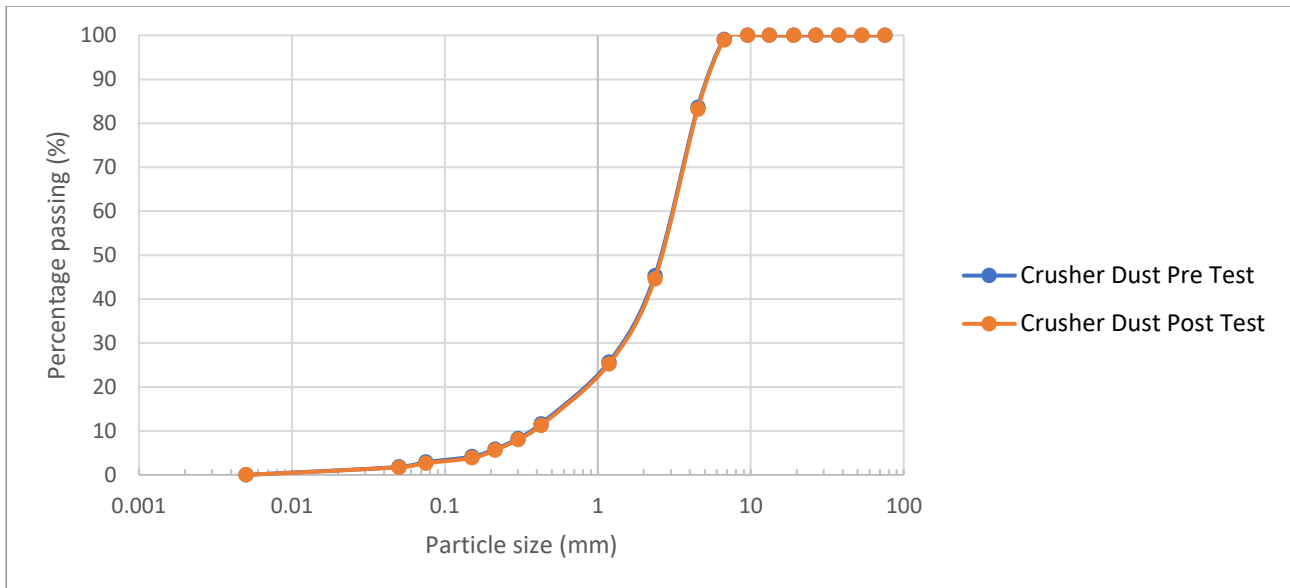


Figure 6-4. Particle size distribution of crusher dust in both pre- and post-pullout testing conditions

6.2.2.2 Cape Flats sand

The Cape Flats sand is classified as a uniform graded material with a C_u and C_z value of 0.36 and 1.03 respectively. Using the USCS classification chart (ASTM Standard D248, 2006), the Cape Flats sand can be classified as SP (poorly graded sand).

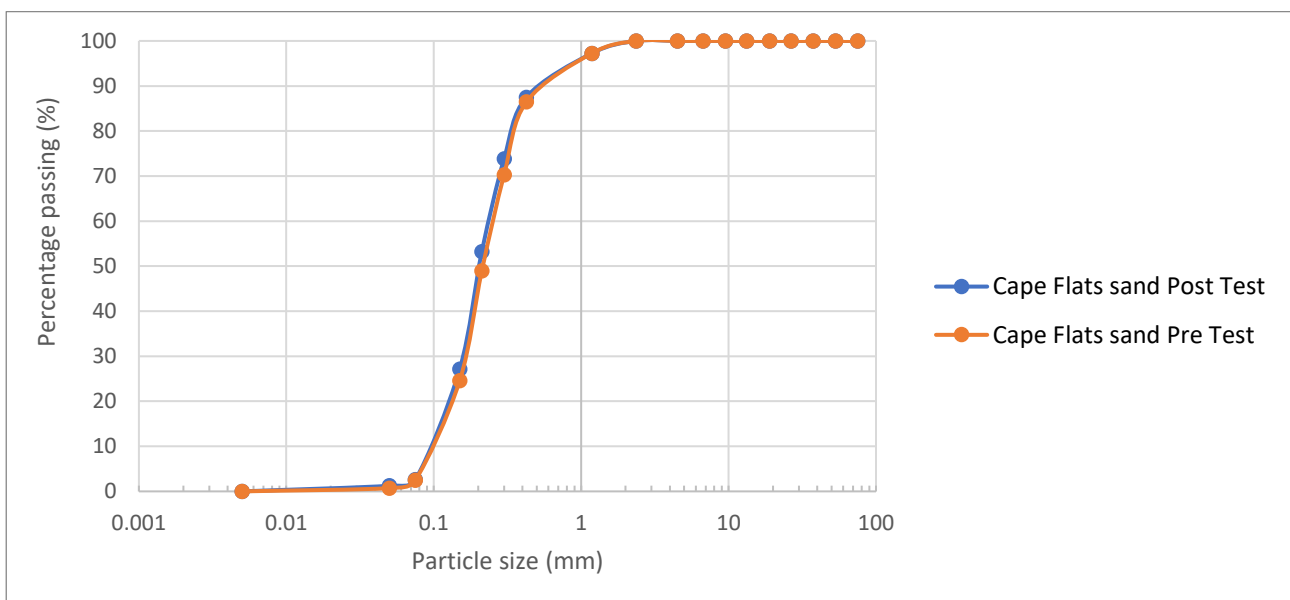


Figure 6-5. Particle size distribution of Cape Flats sand in both pre- and post-pullout testing conditions

6.2.2.3 Micaceous residual granite

The micaceous residual granite has a value for C_u and C_z for both the pre- and post-pullout testing sample. For the pre-pullout testing sample, the C_u and C_z were calculated to be 0.05 and 1.25 respectively, with the post-pullout testing having a C_u and C_z value of 0.4 and 0.81 respectively. According to the USCS classification chart (ASTM Standard D248, 2006), both the pre and post-pullout testing samples can be classified as a joint symbol, SP-SM (poorly graded silty sand). This classification was also based on the results for the Atterberg limits determined in Section 5.2.3.

As stated at the beginning of this section, the standard required the material which is going to be sieved to sit overnight in a water bath to remove all poorly joined or clustered material. However, after soaking overnight, there were still fairly large and highly fractured quartz grains which had not been broken up. Those which represent the fraction between 90% and 100% passing pre-test sample are the quartz clusters which only broke down through means of soil compaction during pullout testing. This accounts for the sudden drop in particle size which represents the 90% to 100% fraction.

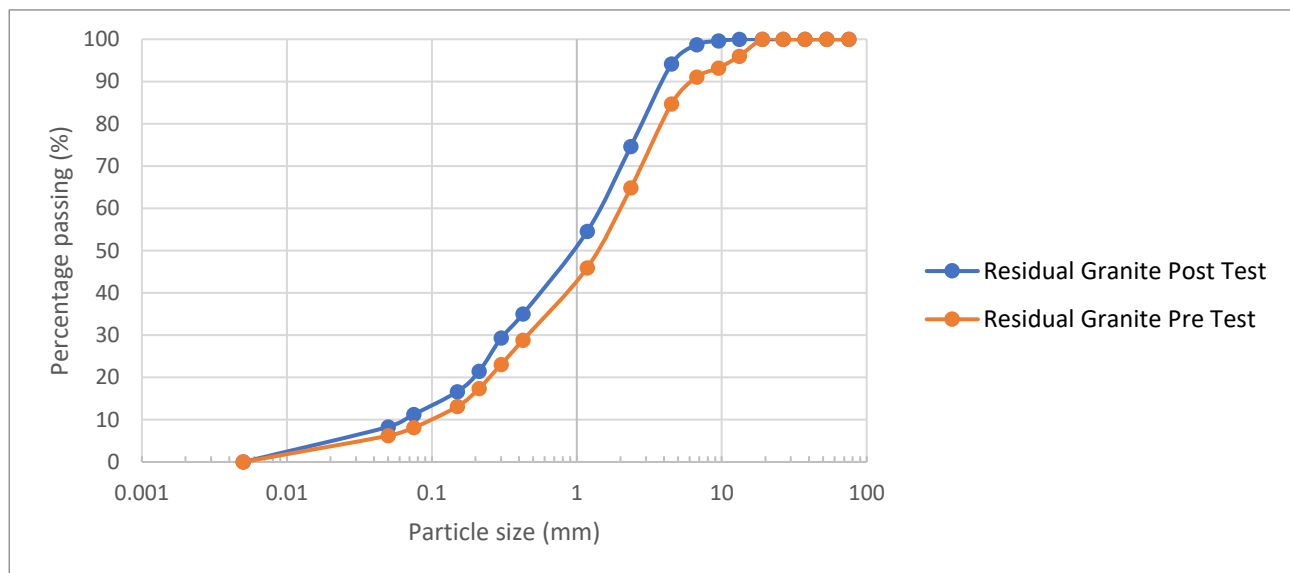


Figure 6-6. Particle size distribution of micaceous residual granite in both pre- and post-pullout testing conditions

6.2.3 Atterberg limits

The Atterberg limits were determined through testing which was only performed on the micaceous residual granite as both the crusher dust and Cape Flats sand are both non-plastic materials. The results for the micaceous residual granite can be found in Table 6-1. The small plasticity index combined with the liquid limit places this material just below the A-line of the Unified Plasticity Chart (ASTM Standard D248, 2006).

Table 6-1. Atterberg limits of micaceous residual granite

Linear shrinkage	2.7%
Liquid limit	33.9%
Plastic limit	28.3%
Plasticity index	5.7

6.2.4 Permeability testing

For the permeability testing, the following values were obtained for the soils compacted to maximum dry density at optimum moisture content according to the modified AASHTO compaction effort. This showed a clear range of permeability values with the crusher dust having the overall highest permeability of 1.2×10^{-4} m/s, which is approximately 4 times greater than the Cape Flats sand's permeability of only 3.3×10^{-5} m/s. Both the crusher dust and the Cape Flats sand can be classified as having good drainage according to Terzaghi (1948). The micaceous residual granite has the lowest permeability of 7.8×10^{-6} m/s, which allows it to be described as poor draining material according to Terzaghi (1948).

Table 6-2. Summary of material permeability

Soil Type	Permeability (m/s)	Dry Density (kg/m ³)	Permeability classification (Terzaghi, 1948)
Crusher Dust	1.2×10^{-4}	2016	Good drainage comprised of clean sand and gravel blends
Cape Flats sand	3.3×10^{-5}	1596	Good drainage comprised of fine sands
Mica	7.8×10^{-6}	2016	Poor drainage comprised of sand silt and clay blends

6.2.5 Direct shear testing

The direct shear box tests were performed within a dry shear box on moist compacted material to simulate the conditions within a backfill. Similar to the testing procedure done with particle size distribution, the materials were sampled and tested pre-pullout testing and post-pullout testing. This was done in addition to the sieving of pre-pullout testing crusher dust material in order to remove the particle fraction greater than that of 3.35 mm, this was done to ensure the shearing would be performed in accordance to ASTM Standard D3080 (2014). A summary of the materials' shear properties is given in Table 6-3 and will be followed with the raw data.

Table 6-3. Summary of shear strength parameters for all soil materials

Material description		Phi (ϕ)	Cohesion
Crusher dust	Pretest (full particle size distribution)	41.1	21.4
	Posttest (full particle size distribution)	41.6	22.6
	Pretest (<3.35mm sieved)	37.9	24.7
	Posttest (<3.35mm sieved)	41.2	14.4
Cape Flats sand	Pretest	40.4	8.9
	Posttest	39.8	5.3
Micaceous residual granite	Pretest	37.2	35.8
	Posttest	37.7	33.2

Although there are slight deviations from the pre-test and post-test strength parameters given in Table 6-3, once cross-referenced with the corresponding figures it is clear to see that, for each sample, the strength parameters were unaffected during pullout testing. Considering the crusher dust and Cape Flats sand are cohesionless materials, the cohesion values can possibly be attributed to particle pore water suction or due to

high degrees of interlocking at the lower vertical stress, which would in turn shift the trendline in such a way that an apparent cohesion is measured.

The raw data showing the failure envelopes for the crusher dust (in both the original soil distribution, shown in Figure 6-7, and in the sieved soil condition, shown in Figure 6-8), Cape Flats sand (Figure 6-9) and micaceous residual granite (Figure 6-10) is shown as follows:

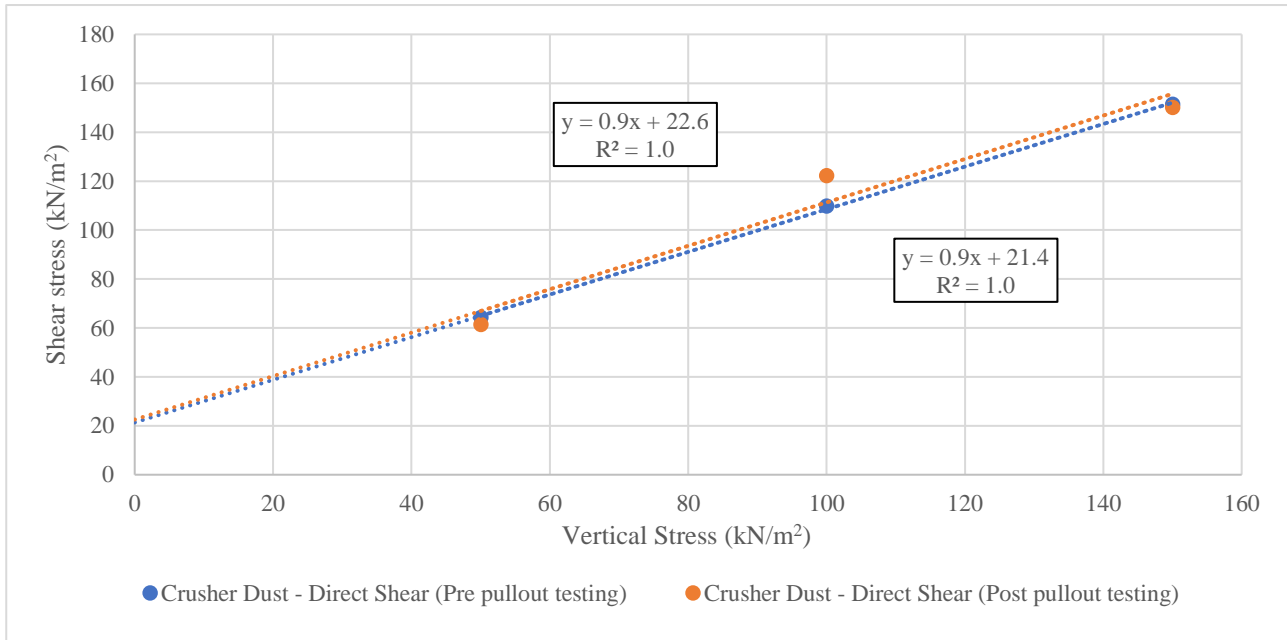


Figure 6-7. Failure envelope of the crusher dust in both pre- and post-pullout testing conditions

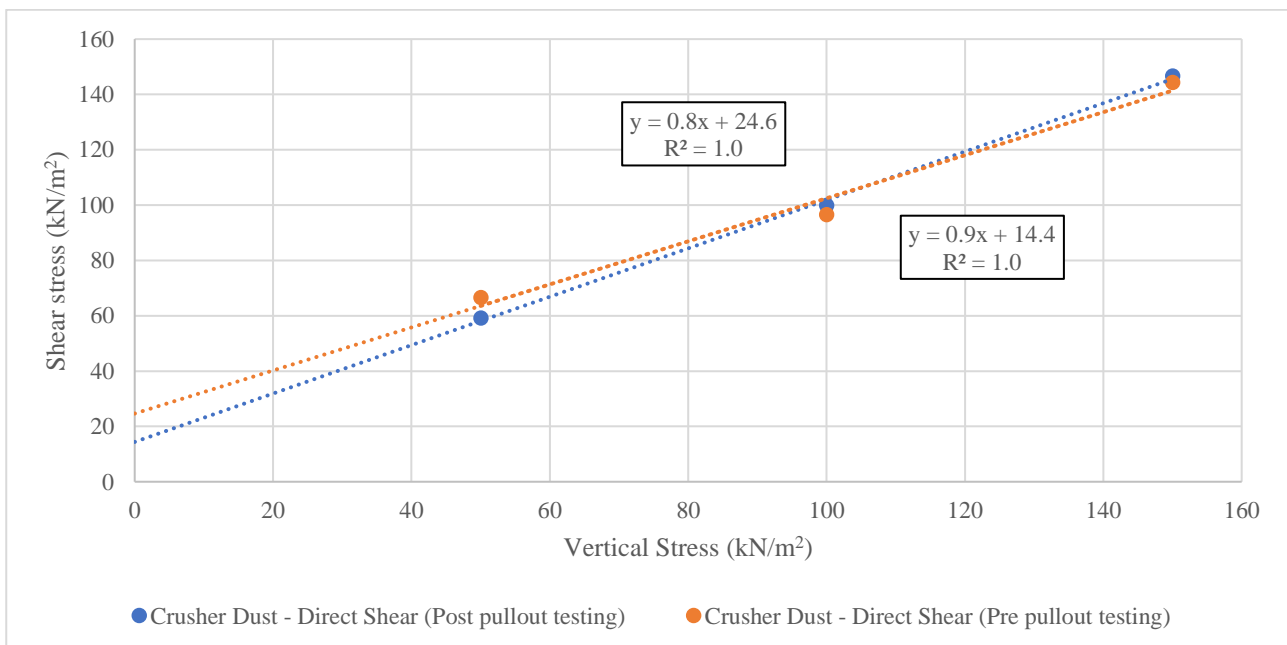


Figure 6-8. Failure envelope of the sieved crusher dust in both pre- and post-pullout testing conditions

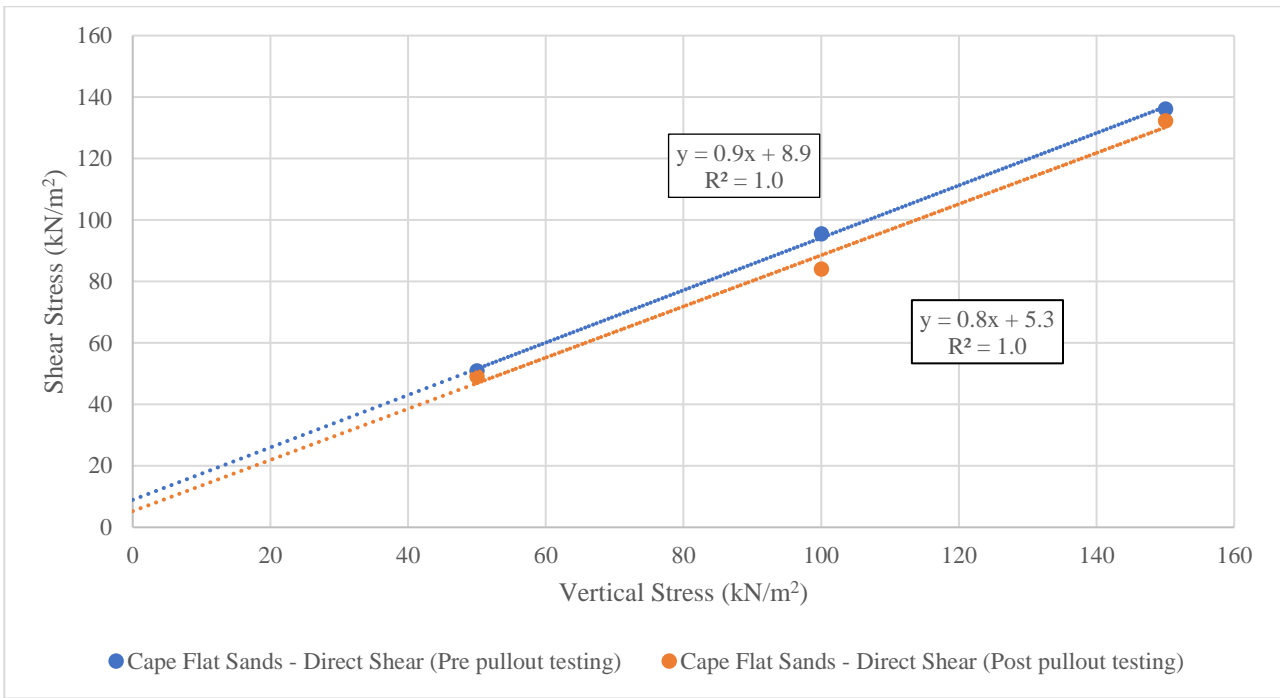


Figure 6-9. Failure envelope of the Cape Flats sand in both pre- and post-pullout testing conditions

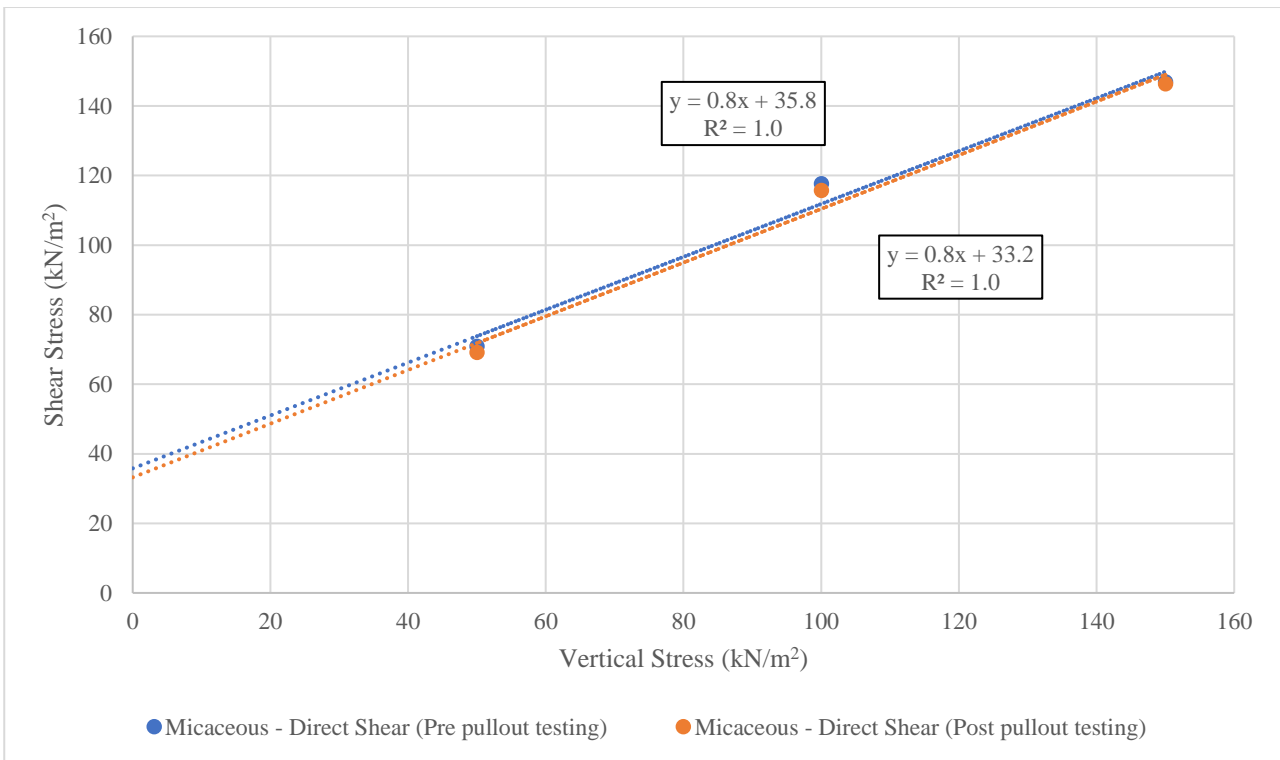


Figure 6-10. Failure envelope of the micaceous residual granite in both pre- and post-pullout testing conditions

6.3 Pullout testing

6.3.1 Pullout resistance testing

The following data represents the eight pullout resistance tests performed on each respective soil. The graphs all plot pullout resistance over time (or pullout resistance over displacement as the displacement was kept constant throughout testing). It should be noted that the constant micro peaks and troughs are caused by the hydraulic jack displacement being achieved through a stepped manner of 0.25 mm / 15 seconds (as described in Section 4.2.2). The x-axis is given in terms of time as the method used to displace the hydraulic jack was based on the relevant time interval between displacements. Individual pullout test graphs are included in Appendix A.

6.3.1.1 Crusher dust

A clear increase in pullout resistance was observed as the vertical stress was increased. Each test performed at a given vertical stress provided a clear grouping with the replicate test performed at the same vertical stress. The second replicate test performed at the same vertical stress consistently produced a slightly lower value. Considering that this is consistently observed between all tests at a given vertical stress, it could indicate that the moisture lost during each test could have allowed for a loss of compaction in the layers containing the steel strip and thus reduced the resistance to pullout. This will be further elaborated on in Section 7.3.

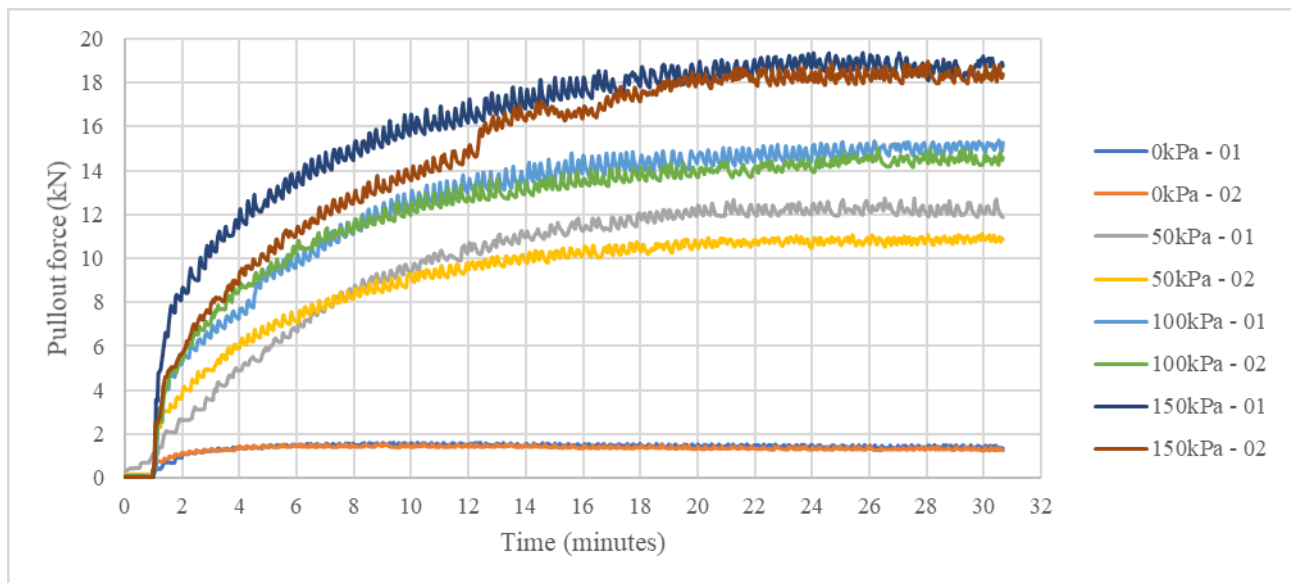


Figure 6-11. Pullout resistance over time - Crusher dust

6.3.1.2 Cape Flats sand

Much like the crusher dust, every replicate test performed at the same vertical stress plotted lower than that of the first test. This could be attributed to the same mechanism of moisture loss mentioned above. The 50kPa – 02 test was the only test (out of all 24 tests) which exhibited a highly irregular trend. This could be attributed to poor compaction efforts. The anomaly of the 50kPa – 02 test is further addressed in Section 7.3.2.

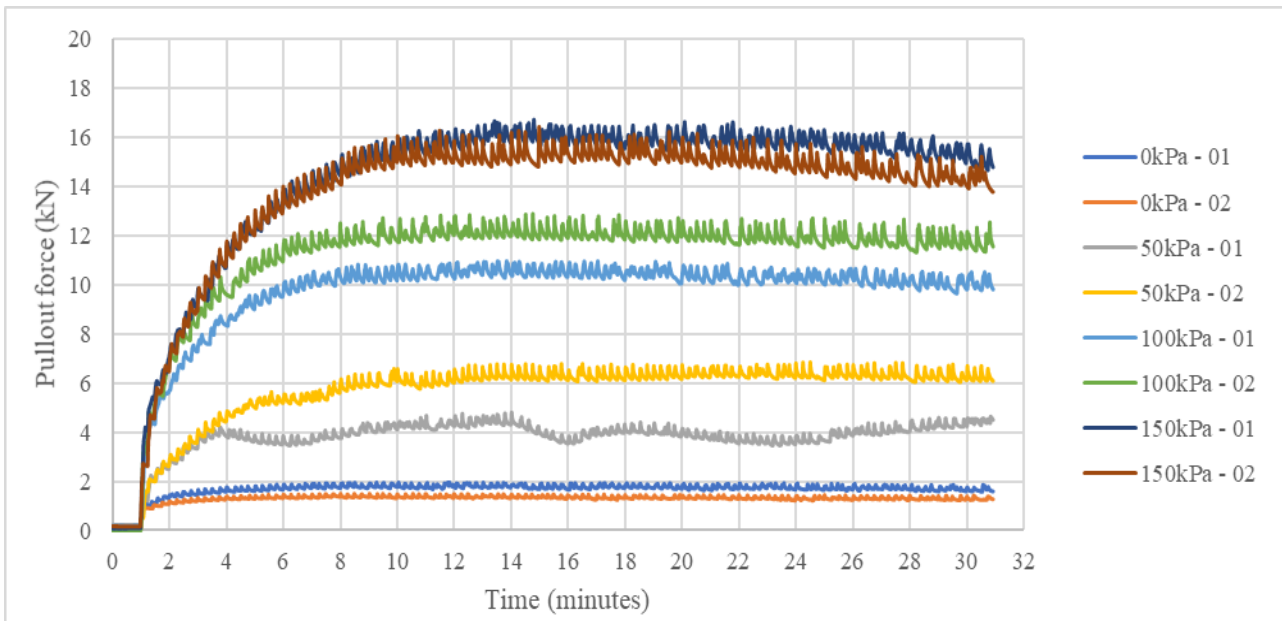


Figure 6-12. Pullout resistance over time - Cape Flats sand

6.3.1.3 Micaceous residual granite

The micaceous residual granite clearly had the lowest pullout resistance of all the soil types tested. It did, however, have the highest pullout resistance for the 0 kPa tests. The replicate tests for a given vertical stress lack the same clear separation that the other materials expressed as all tests present a spread-out range of pullout resistances.

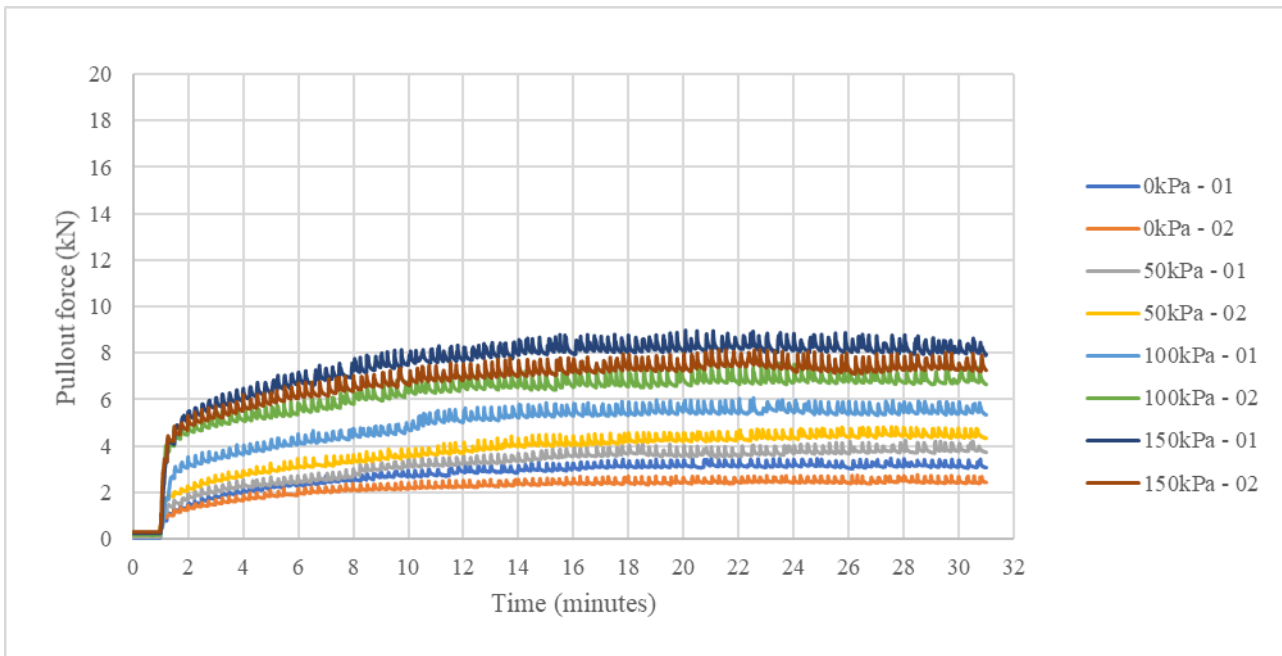


Figure 6-13. Pullout resistance over time - Micaceous residual granite

6.3.2 Displacement during pullout testing

For each of the pullout tests performed, two LVDT's were used to capture the relevant displacement data. As discussed in Section 0, the first LVDT (indicated as (a) for a given test) was set up to measure the displacement directly on the steel strip and the second was set up to measure displacement at the location of the load cell (indicated as (b) for a given test).

The following displacement data is presented in a way that separates the data obtained for each of the LDVTs. This allows for the data collected from the LVDT connected to the steel strip to act as verification of the rate of pullout displacement. As the plot is given in displacement (mm) per minute the gradient which the trend should fit to is that of 1.00, as the standard requires 1 mm per 1 minute. The data collected by the LVDT connected to the load cell provides an indication as to the deflection experienced by the hydraulic jack mount. The higher the vertical stress during a given test and subsequent pullout resistance, the greater the deflection will be of the hydraulic jack mount, thereby increasing the spread of all the trends with respect to each other.

6.3.2.1 Crusher dust

As seen by the trend line in Figure 6-14, the overall rate of displacement met the requirements. A clear anomaly can be seen by the initial slope of the trend for the 50 kPa plots in Figure 6-14. The reason for this was an operating error during the initial displacement rate which was successfully corrected after the first 2 minutes of testing. This is confirmed by the gradient still falling within 97% of the standard's requirements. The flat trend of displacement shown by the 50 kPa – 01(b) plot was due to operating error where insufficient preload was given for the LVDT, allowing the LVDT to reach maximum stroke and thus no longer able to measure displacement (Figure 6-15). The vertical spread of the trends gives an indication that the hydraulic jack mount deflected roughly 2.5 mm during testing (Figure 6-15).

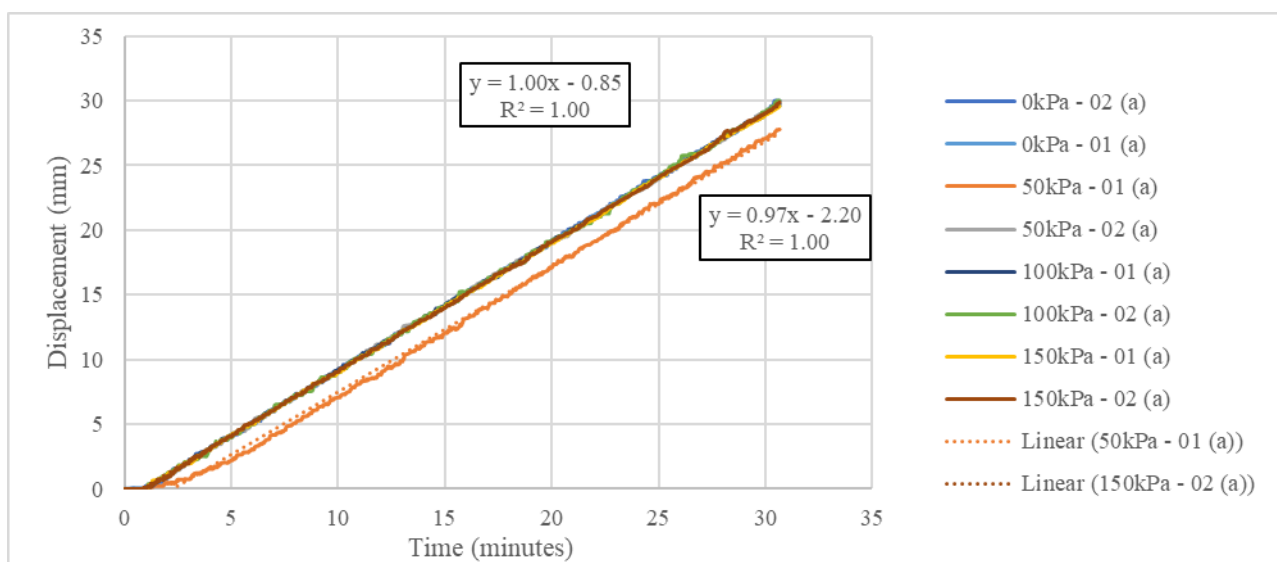


Figure 6-14. Rate of displacement confirmation for crusher dust pullout testing

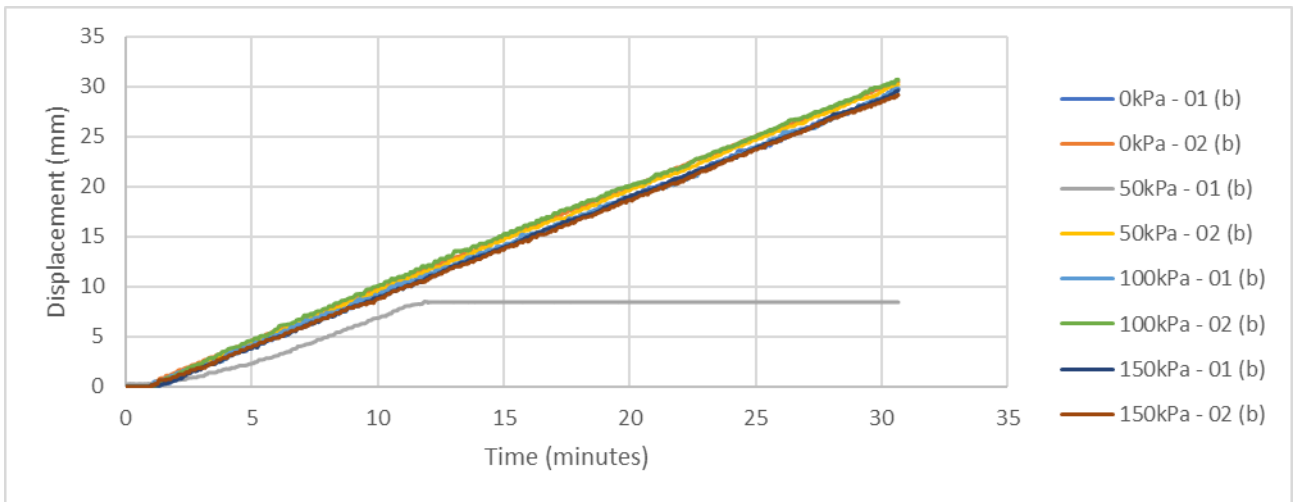


Figure 6-15. Displacement results indicating hydraulic jack mount deflection for the crusher dust tests

6.3.2.2 Cape Flats sand

The displacement data for the Cape Flats sand shows that the rate of displacement meets the 1 mm per minute requirement (Figure 6-16). It is also clear that the smaller spread of LVDT readings of the Cape Flats sand correlates to the lesser pullout capacity (Figure 6-17). For the Cape Flats sands, the relative deflection of the hydraulic jack mount is approximately 2 mm.

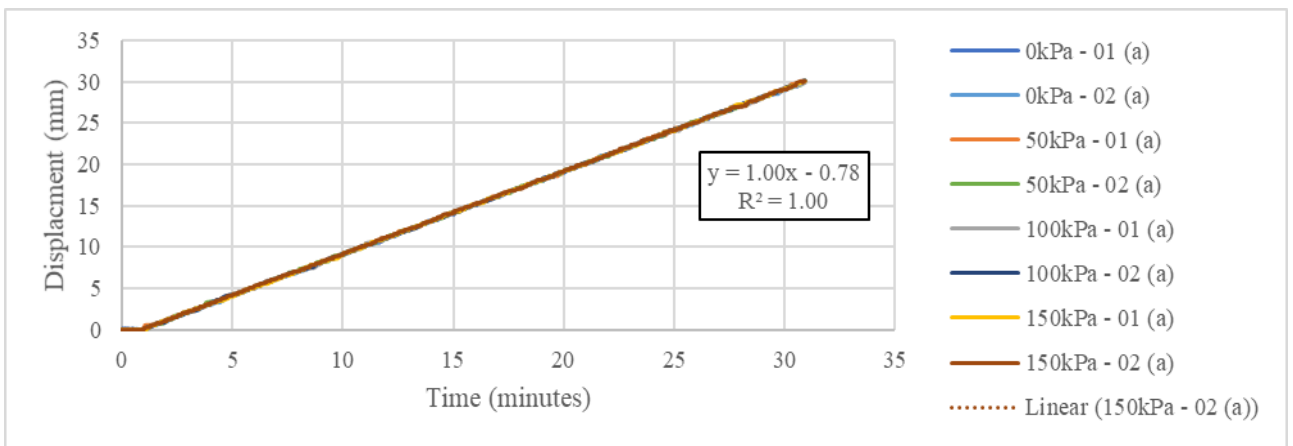


Figure 6-16. Rate of displacement confirmation for Cape Flats sand pullout testing

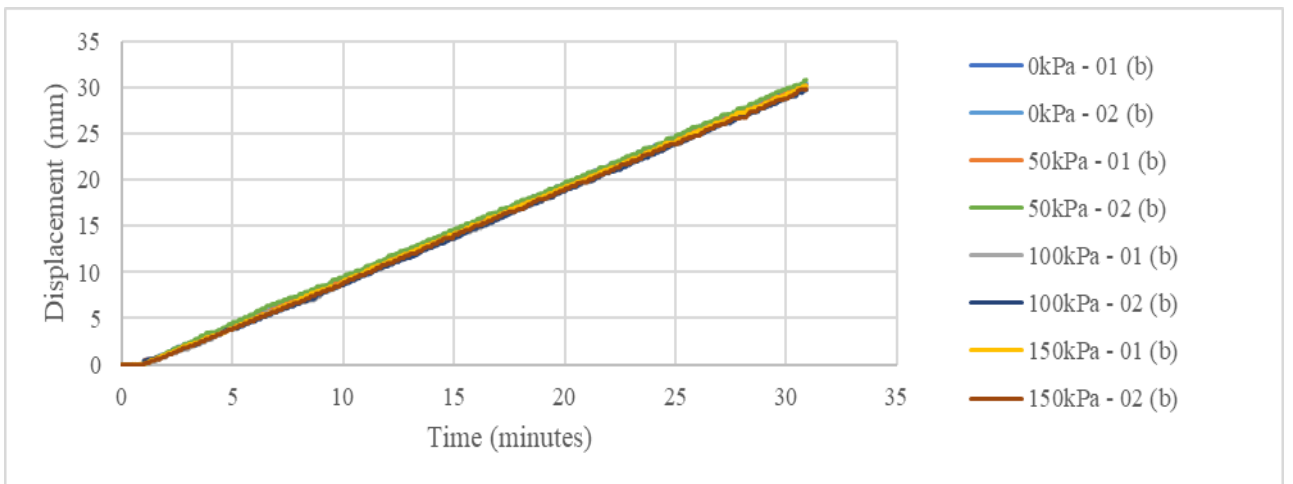


Figure 6-17. Displacement results indicating hydraulic jack mount deflection for the Cape Flats sand tests

6.3.2.3 Micaceous residual granite

Once again, the gradient of the displacement trendline shows that the required rate of displacement was met and kept consistent throughout the entire range of tests (Figure 6-18). As expected, the spread of the displacements shown in Figure 6-19 is nearly identical to that of the positive displacement. This is simply due to the micaceous residual granite having the lowest pullout resistance of all materials tested.

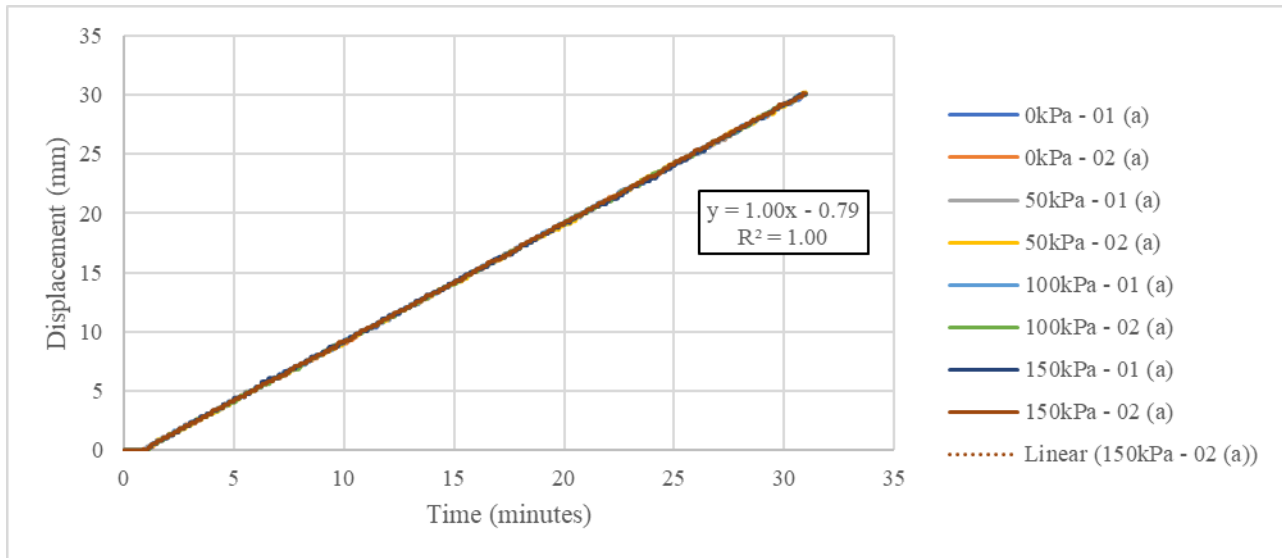


Figure 6-18. Displacement data for micaceous residual granite pullout testing

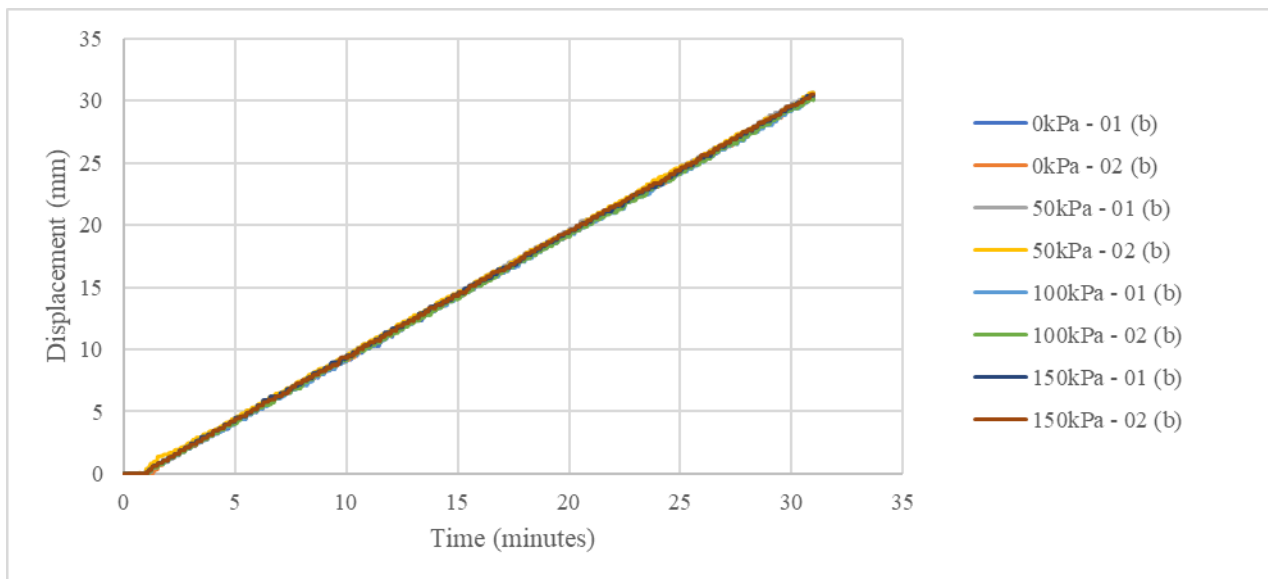


Figure 6-19. Displacement results indicating hydraulic jack mount deflection for the micaceous residual granite tests

7 Discussion

7.1 Introduction

This chapter is based on further analysis of the results obtained in Chapter 6. The aim of this chapter is to analyze the data provided in Chapter 6 in a way that substantiates the success or failure to meet the primary aims and objectives of this project.

7.2 Soil classifications

Prior to testing of pullout resistance, each soil type was classified through a range of standardized tests. This was done to ensure that adequate backfill conditions were simulated during pullout testing (93% Modified AASHTO compaction effort) as well as to confirm that the materials met the aims of this project with regards to the soil's inherent permeability. Additional tests such as the soil particle size distribution and soil strength parameters were performed to ensure that these materials fall within the expected range provided by *Reinforced Earth* and other national standards such as SANS 207 (2011) and AASHTO (2007).

7.2.1 Soil compaction

The maximum dry density obtained for each of the three materials fell within the expected values for the material types (Das, 2010). The poorly graded Cape Flats sand presented a double peak with a maximum dry density of 1598 kg/m³, while both the crusher dust and micaceous residual granite presented much higher maximum dry densities of 2016 kg/m³ and 2018 kg/m³ respectively. Considering the nature of the crusher dust is that of a crushed greywacke which has undergone no chemical weathering, the dry density obtained is well within the expected range as the density of an intact greywacke is generally between 2500 kg/m³ and 3000 kg/m³ (Schön, 2011). The poorly graded silty sand classification of the micaceous residual granite showed that this sample was collected from a relatively deep position in the residual granite soil horizon where completed weathering has not yet occurred. This is based on the fines content (approximately 10%) which would be considerably higher for samples collected closer to the 'surface' of the residual granite soil horizon as it would show higher degrees of weathering than materials located deeper down in the soil horizon.

7.2.2 Soil permeability

One of the primary aims of this project was to obtain South African soils which would represent a spectrum of soil permeability values in a compacted state. The compacted state in which these materials were tested met the standardized 93% modified AASHTO compaction effort used in constructing backfills (SANS 207, 2011). The soil permeability values (k) obtained for the three test materials fell over a range that allows for clear differentiation of their drainage potential. The crusher dust had a k value of 1.2×10^{-4} m/s which is approximately four times more permeable than that of the Cape Flats sand, having a k value of 3.3×10^{-5} m/s. The crusher dust and Cape Flats sand are therefore ideal representatives of the good drainage ranges for a clean and fine sand respectively as described by Terzaghi (1948).

The k value of $7.8 \times 10^{-6} \text{m/s}$ for the micaceous residual granite fell within the nearly poor drainage (non-free draining) range as described by Terzaghi (1948). This also matched their soil description of this range being a silty sand or clay blend (Head & Epps, 2011).

7.2.3 Shear strength parameters

Determining the shear strength of a granular material becomes an issue when a large portion of a soil sample's particle size falls out of the size limitations as stipulated by ASTM (D3080, 2014). Although AASHTO (2007) does provide a clause which states that the shear strength of a material should only be calculated on the fraction of that material that passes the 2.0 mm sieve, this is still not representative of the whole soil being used within the backfill. This particularly becomes problematic when two or more soils with different particle size distributions are being compared. For example, in the case of the crusher dust approximately 40% of its overall particle size distribution will be removed by sieving, whereas a material such as the Cape Flats sand requires no sieving to meet the required size fractions. A summary of issues that arise from shear strength tests when trying to classify all material under the same conditions are given in Table 7-1.

Table 7-1. Issues derived for shear strength tests

Shear strength test conditions	Issues with test condition	Reference
Saturated conditions	Although this best suits cohesive materials such as the micaceous residual granite, the granular crusher dust and Cape Flats sand would never be in a saturated condition assuming the correct construction of the MSE wall.	SANS 207 (2011), AASHTO (2007), Head & Epps (2011)
Perform the tests in a larger direct shear apparatus to mitigate the maximum particle size that can be tested.	The larger the shear box, the lesser the angle of internal friction for a given soil type. This will still include issues arising from the above-mentioned conditions.	Wang & Gutierrez (2010), Cerato & Lutenegeger (2006)

For this reason, the tests were performed in a manner to determine the shear strength of a backfill immediately after construction. This required the direct shear tests to be performed on moist compacted material (compacted to the required 93% compaction effort). All tests were performed in an unsaturated condition to ensure that the sample remains at the same moisture content of compaction at a shear rate of 0.005 mm/min. Due to the presence of negative pore water pressures in the unsaturated samples, the measured values are that of total stress parameters and not effective stress, and any cohesion values obtained from the shear tests can be attributed to the effect of suction between soil particles. Considering the test conditions, the results determined for these materials may be slightly higher than the soil's actual values.

As described in Chapter 6, there was no change in shear strength parameters for the materials in the pre-pullout testing state and the post-pullout testing state. This allowed the results to be further simplified into a single shear strength and cohesion value for each soil type (Table 7-2).

Table 7-2. Shear strength parameters of testing materials

Material description	Phi (ϕ)	Cohesion
Crusher Dust	Full particle size distribution	21
	Material containing <3.35mm	14

Cape Flats sand	40	6
Micaceous residual granite	37	36

The cohesion values of 21 kN/m² measured for the crusher dust in its full particle size distribution could be attributed to a high degree of interlocking at the lower vertical stress test, as well as its particle size distribution breaking a boundary condition for maximum particle size allowed within the sample. The sieved particle size distribution of the crusher dust presented a slightly lower shear strength (41° compared to 42°) and a significantly lower cohesion of 14 kN/m² compared to the unsieved value of 21 kN/m². This then allows for the cohesion to be attributed to a combination of apparent cohesion due to suction between soil particles and interlocking of particles at low vertical stresses. The micaceous residual granite had the largest cohesion of all three soils, which is to be expected due to its fines content which comprises of a clay-like mineralogy. However, the 36 kN/m² cohesion measured for the micaceous residual granite could be attributed to both mineralogy and suction between soil particles.

7.3 Pullout resistance testing

7.3.1 Condensing pullout resistance over time graphs

All the pullout tests that were conducted followed the same procedure which aimed at reproducing the condition of backfill materials directly after construction. This procedure therefore did not allow for consolidation time prior to applying the pullout force. The time taken for failure to occur is derived from the pullout force versus time curve. Once the curve for a given test reached a plateau, thereby indicating that the residual strength had been reached, the displacement was noted and indicated as the point of failure.

Considering the tests were performed using the incremental hydraulic jack displacement method, the overall pullout force curve comprised of locally occurring peaks and troughs. These peaks and troughs are associated with the peak in force due to the incremental displacement of the hydraulic jack and the subsequent dissipation of force, respectively. Therefore, the highest point on the overall pullout force trend line was taken as both the local peak value as well as the local trough value. Both the local peak and trough are shown in Figure 7-1 located on the top and bottom for the orange trend line. This allows for an average value to be calculated using the local peak and trough values.

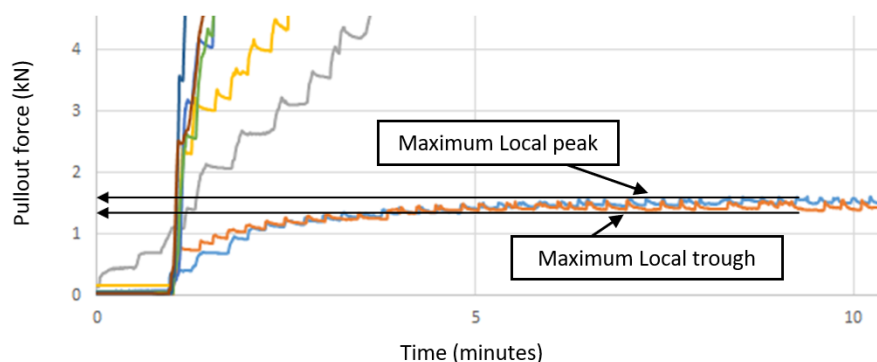


Figure 7-1. Determination of an average pullout resistance for a given pullout resistance versus time plot

7.3.2 Analysis of pullout resistance data

All three materials used for pullout testing adhere to the required backfill material specifications outlined in Section 2.5. Both the crusher dust and Cape Flats sand are classified as being a free draining non-plastic material (Lee, 1978), while the plasticity of the micaceous residual granite falls below the threshold set by AASHTO (2007). This, however, provides reason for concern as the pullout resistance of the micaceous residual granite performed poorly compared to both the crusher dust and Cape Flats sand. The pullout resistance (kN/m^2) was calculated by adjusting the pullout force (kN) by the area of the steel strip embedded in the soil chamber. One of the tests performed on the Cape Flats sand at an applied vertical stress of 50 kPa displayed a clear deviation from all the other tests performed. For this reason, the values for that test are considered inaccurate and have not been factored in during analysis of the data. The sum of vertical stresses is obtained from the addition of the applied vertical stress and the self-weight of the soil above the steel strip within the pullout apparatus soil chamber. A summary of all the pullout test results is provided in Table 7-3.

Table 7-3. Summary of pullout resistance results including calculated F_m^* values

Soil description	Average peak pullout force (kN)	Average peak pullout resistance (kN/m^2)	Applied vertical stress (kN/m^2)	Sum of vertical stresses (kN/m^2)	Displacement at failure (mm)
Crusher dust	1.5	15.0	0.00	4.0	3.00
	1.5	15.0	0.00	4.0	3.00
	11.2	112.0	50.00	54.0	N/A
	12.3	122.5	50.00	54.0	19.00
	14.6	146.0	100.00	104.0	13.00
	15.1	151.0	100.00	104.0	13.00
	18.3	183.0	150.00	154.0	21.00
	18.9	189.0	150.00	154.0	21.00
Cape Flats sand	1.8	17.5	0.00	3.1	5.00
	1.4	13.5	0.00	3.1	5.00
	N/A	N/A	50.00	N/A	N/A
	6.5	64.5	50.00	53.1	3.00
	10.6	106.0	100.00	103.1	7.00
	12.4	123.5	100.00	103.1	7.00
	15.4	154.0	150.00	153.1	9.00
	16.2	162.0	150.00	153.1	9.00
Micaceous residual granite	2.6	25.5	0.00	4.0	13.00
	3.3	33.0	0.00	4.0	13.00
	4.0	39.5	50.00	54.0	13.00
	4.5	45.0	50.00	54.0	13.00
	5.7	56.5	100.00	104.0	13.00
	7.0	70.0	100.00	104.0	13.00
	7.6	76.0	150.00	154.0	13.00
	8.6	85.5	150.00	154.0	13.00

The comparison between the sum of vertical stresses and the average pullout resistance gives a clear indication as to a material's ability to perform as a backfill material compared to the other materials tested under the same conditions (Figure 7-2). As expected, with an increase in vertical stress the pullout resistance of each material increased (Vidal, 1969). The gradient of the trendlines for each respective soil gives an indication as to how

much the increased vertical stress affects the increased pullout resistance. Out of the three soils tested, the micaceous residual granite soil performs the worst as its peak pullout resistance at an applied vertical stress of 150 kN/m² only slightly outperforms that of the Cape Flats sand at an applied vertical stress of 50 kN/m².

An interesting comparison can be made between the Cape Flats sand and the crusher dust, as the gradient of the Cape Flats sand is nearly identical to that of the crusher dust. However, the pullout resistance expressed by the crusher dust is greater than that of the Cape Flats sands. This might be due to higher localized normal forces exerted on the steel strip by the coarser grained crusher dust, as the higher the normal force the higher the frictional resistance the steel strip will exhibit. As the Cape Flats sands is a finer grained material, the contact area is greater than that of the crusher dust, so there is a lower yet more uniform distribution of normal forces exerted over the length of the steel strip.

A large deviation from the trendline is observed for the crusher dust at an applied vertical stress of 50 kPa, which could give an indication to the above expected performance of the crusher dust. This shows that even for a small applied vertical stress the crusher dust is still able to provide a large amount of pullout resistance. An additional test should be performed at 25 kPa applied vertical stress to further define the trend of the crusher dust's performance.

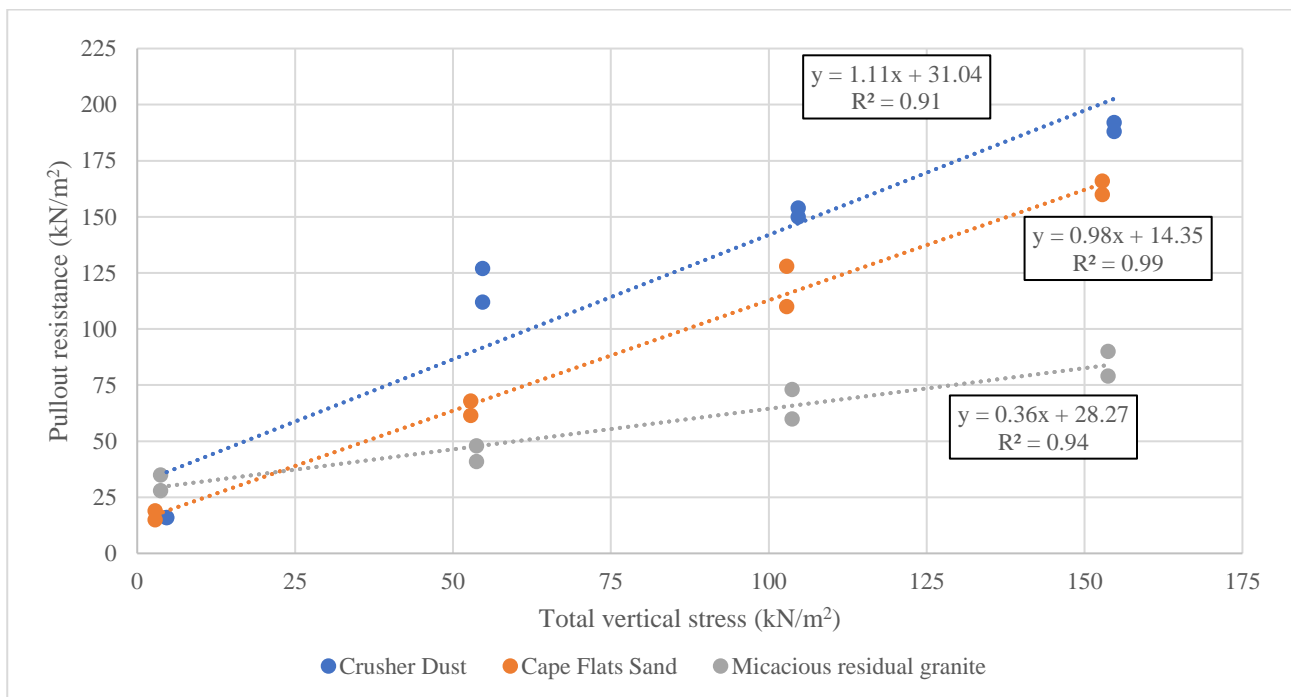


Figure 7-2. Average peak pullout resistance measured for each soil type

Although frictional resistance is the dominant mechanism which dictates pullout resistance of steel strips, for plastic materials, there might be a shift to passive resistance being dominant at low vertical stresses. This explains the relatively high pullout resistance for the micaceous residual granite at the applied vertical stress of 4 kPa. This could be attributed to the natural cohesion of the micaceous material which leads to a soil stiffness that accounts for a higher passive resistance to that of the cohesionless Cape Flats sands and crusher dust.

7.3.3 Moisture content

A possible cause for a drop in pullout resistance in the second replicate of each test performed could be due to a lack of moisture within the compacted soil layer containing the steel strip (Figure 7-3). This was a noticeable issue with the crusher dust in particular as it showed a loss in moisture content from the optimum 6.5% to approximately 5% moisture content. A similar moisture content loss was observed in the Cape Flats sand, which dropped from an optimum moisture content of 15.8% to that of 14% (Figure 7-3).

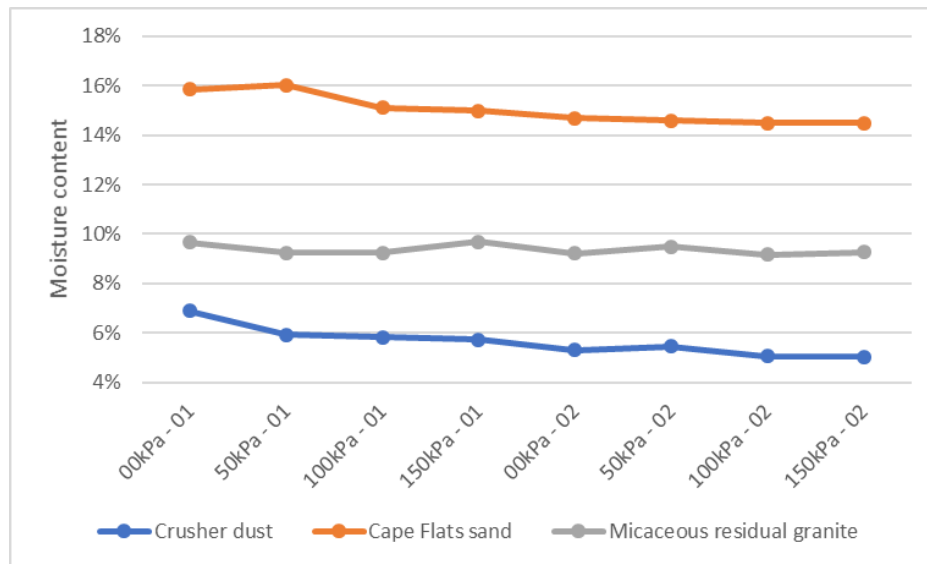


Figure 7-3. Moisture content of embedment layer during pullout testing.

Analogous to a sponge, a granular material can hold a given amount of water but once compressed, the water is pressed from the voids in the soil. The loss of moisture content can thus be attributed to the loading of the soils during testing and expulsion of water from the soil structure. Although this did not affect the ability for compaction to take place using the hand tamper, there may have been a reduction in the degree of immediate consolidation and thus a lesser degree of compaction under loading.

7.3.4 Link to rate of shearing

The displacement measured at failure allows for a point of interest concerning a material's maximum rate of shear as defined by ASTM Standard D3080 (2014). The standard allows the consolidation characteristics of a material to give an indication as to the maximum rate of shear, however, they also assume a point at which shear failure occurs being that of 10 mm. Although a soil-on-soil shear test is not a direct comparison to the shearing which occurs in soil-steel shearing, it is interesting that all the pullout tests showed a point of failure close to that of the estimated 10 mm (Table 7-3).

7.3.5 Anomalies in pullout resistance trends

During pullout testing the air pressure was a variable that was always kept constant. However, during some tests on the crusher dust a small drop in pressure did occur, as seen at the 12 minute mark during the 150 kPa test (Figure 6-11). Although the trend of the curve still matched the replicate test at the same given vertical stress, an interesting anomaly occurs once the air pressure is returned to the required value. After the air

pressure was corrected, an immediate increase in pullout force was noticed. This is a good indicator that there is an immediate transfer of effective stress from the overburden to the steel strip.

7.3.6 Pullout resistance factor comparison

As described within Section 0, a typical comparison made in literature is the comparison between the measured pullout resistance factor (F_m^*) of a given soil reinforcement (determined through pullout testing) and the estimated pullout factor, F_e^* , defined by AASHTO (2007). This method is often cited as a valid estimation of pullout resistance for a given soil type (Jayawickrama et al., 2013), an opinion that is supported by Reinforced Earth Company (1995). Using the pullout forces obtained during the laboratory pullout tests, the F_m^* can be calculated using Equation 2.15.

$$F_m^* = \frac{P_r}{\alpha \sigma'_v L_e C w} \quad \text{Equation 2.15 from Section 0}$$

For each of the calculated F_m^* values there is a corresponding vertical stress associated with it. This vertical stress can then be converted into a simulated wall height using the tested soil's compacted density. The calculated F_m^* can therefore be compared to the estimated pullout resistance factor F_e^* at the same loading conditions (relative wall height). As described in Section 0, the F_e^* is obtained by constructing a resistance factor versus depth plot with two depth conditions. The depth conditions used to determine the F_e^* value are given below:

Plotted from surface level to 6 m depth: $F_e^* = 1.2 + \text{Log}(Cu) \leq 2.0$ Equation 2.13

Plot from 6 m depth and below: $F_e^* = \tan\phi$ Equation 2.14

As each soil type has a different density, the corresponding wall height for each of the pullout tests will be different which requires an individual plot to be constructed for each of the soil types. In combination to the construction of the standard plot, an additional plot is given which represents the upper limit defined by Equation 2.13. A summary of the required soil properties needed to construct the F_e^* plot for all three material types is given in Table 7-4.

Table 7-4. Values required to determine F_e^*

	Crusher Dust	Cape Flats Sand	Micaceous residual granite
Angle of internal friction (ϕ)	41	40	37
Coefficient of uniformity (Cu)	0.13	0.36	0.2
$\tan(\phi)$	0.87	0.84	0.75
Log Cu	0.31	0.76	0.50
93% Modified AASHTO Density (kN/m ³)	18.4	14.6	18.4

The plot comparing the measured pullout resistance factor to the estimated factors using the above mentioned methods for the crusher dust, Cape Flats sand and micaceous residual granite are given in Figure 7-4, Figure 7-5 and Figure 7-6 respectively.

As expected, the crusher dust and Cape Flats sand had F_m^* values which all plotted well above the boundary for the estimated value F_e^* . This was also true when comparing those same F_m^* to that of the upper limit expressed by Equation 2.13. The only exception was the test performed on the Cape Flats sand at a relative depth of 3.5 m, which only slightly underperformed compared to the upper limit. The opposite is true for the micaceous residual granite as for any wall greater than 4 m in height would present calculated values being less than those of the estimated one. Using the upper limit of Equation 2.13 as a boundary only exaggerates the issue as any wall greater than that of 1.5 m in height would overestimate the pullout resistance factor.

Although the measured F_m^* values for the micaceous residual granite only slightly plot below the estimated boundary, the effects thereof are still considerable. For comparison, using the measured F_m^* values for vertical stresses which exceed the 6 m wall height condition, a related internal angle of friction can be calculated using Equation 2.14. Considering the F_m^* value plots as 0.5 for heights above the 6 m condition, the corresponding angle of internal friction is that of 26.5° . This estimated angle of internal friction is well below the minimum requirements given by AASHTO (2007) which defines the minimum value to be 34° .

These results ultimately agreed with the statement made by Swiger (1978) in the closing notes of the Symposium for Reinforced Earth where he stated that designs based on free draining non-plastic backfills are conservative and that the use of poorly draining materials should be further investigated prior to proceeding with the design.

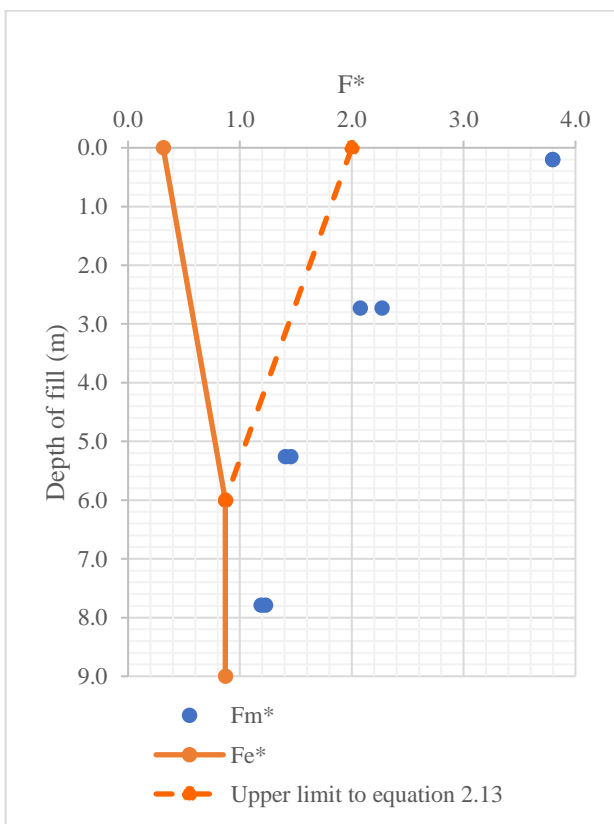


Figure 7-4. Pullout resistance factor comparison for the crusher dust

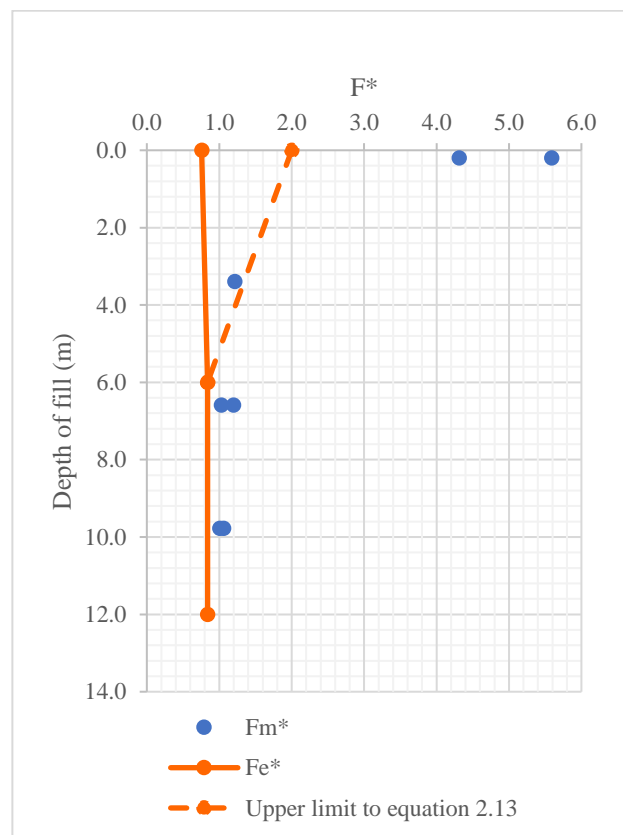


Figure 7-5. Pullout resistance factor comparison for the Cape Flats sand

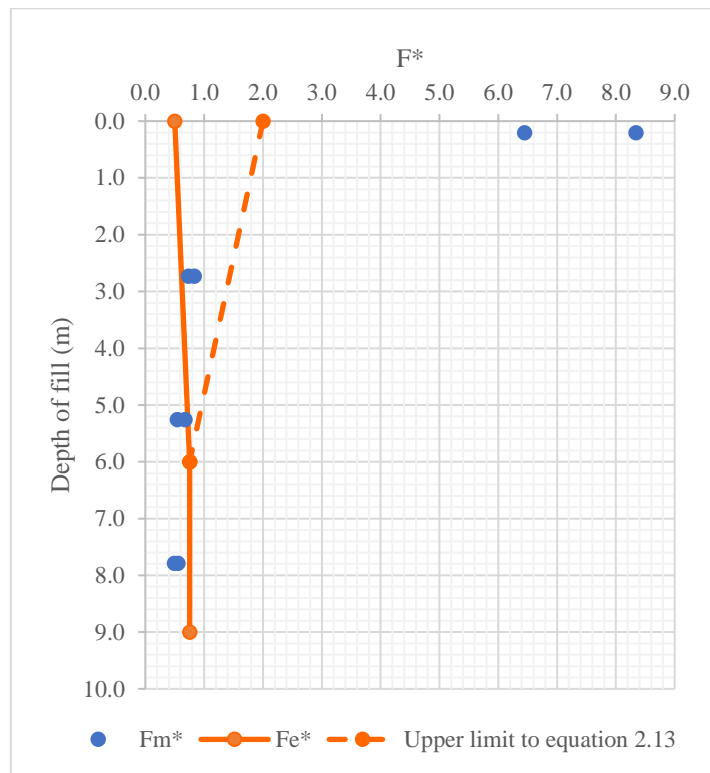


Figure 7-6. Pullout resistance factor comparison for the micaceous residual granite

7.3.7 Estimated factor of safety

Using the pullout resistance obtained from the pullout tests and the calculated pullout resistance derived from the estimated pullout resistance factor F_e^* (calculated using Equation 2.12), a factor of safety can be determined with relation to the wall height. The factor of safety is calculated using Equation 7.1.

$$\text{Factor of Safety} = \frac{P_r (\text{Measured})}{P_r (\text{Derived})} \quad (7.1)$$

Combining the data given in Table 7-3 as well as the results obtained from Figure 7-4 to Figure 7-6, a summary of pullout resistance factors and their corresponding pullout forces is given in Table 7-5. For sake of simplicity, the average between replicates for each test at a given vertical stress was taken.

Table 7-5. Factor of Safety for each material type with respect to wall height

Soil Classification	Average pullout resistance (kN)	Average F_m^*	Average F_e^*	Height of wall (m)	Derived pullout resistance (kN)	Factor of safety
Crusher Dust	1.6	3.8	0.3	0.2	0.1	12.7
	12.0	2.2	0.5	2.7	2.7	4.3
	15.2	1.4	0.8	5.3	8.3	1.8
	19.0	1.2	0.9	7.8	13.9	1.3
Cape Flats sand	1.7	5.0	0.9	0.2	0.3	5.5
	6.8	1.2	0.9	3.4	2.4	1.3
	11.9	1.1	0.9	6.6	9.3	1.2
Micaceous residual granite	16.3	1.1	0.9	9.8	13.8	1.1
	3.2	7.5	0.5	0.2	0.2	14.8
	4.5	0.7	0.6	2.7	3.2	1.3
	6.7	0.6	0.8	5.3	8.3	0.8
	8.5	0.5	0.8	7.8	12.3	0.7

In plotting the factor of safety with relation to wall height, it becomes apparent that both the crusher dust and the Cape Flats sand tend towards a factor of safety just larger than 1. The factor of safety for the micaceous residual granite however trends towards a value lesser than 1. This factor of safety does not represent the overall structure's safety but rather the factor of safety regarding each individual steel strip's pullout resistance.

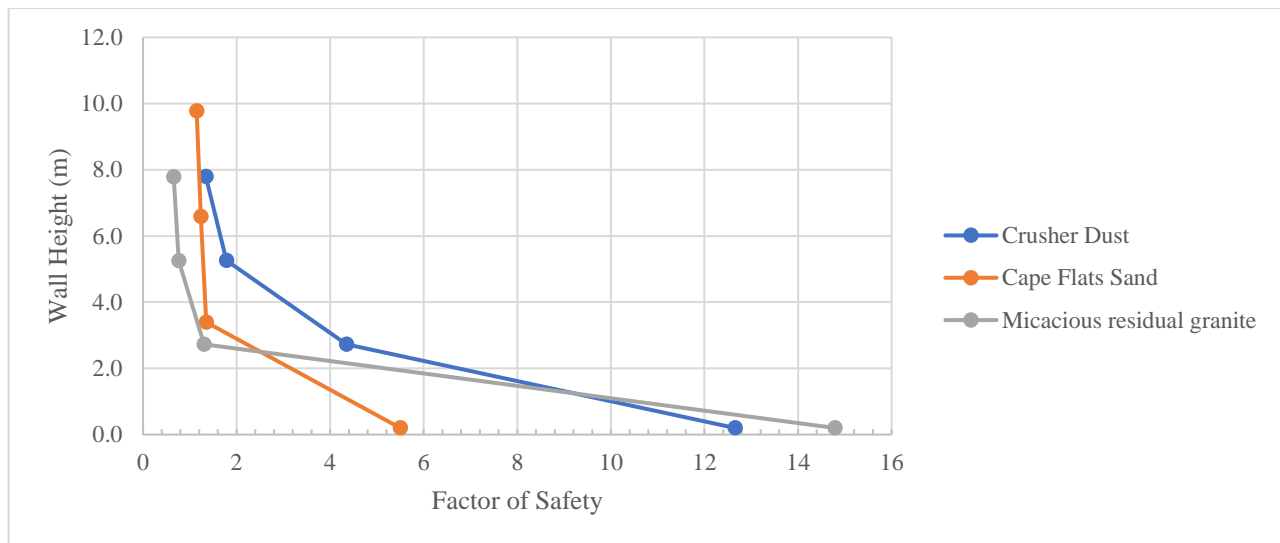


Figure 7-7. Factor of safety versus wall height

This shows that for a given MSE wall which utilized ribbed steel strips as the soil reinforcement would overperform if the crusher dust or Cape Flats sand was used as a backfill material. The same level of performance could be obtained using the micaceous residual granite if the amount of steel strips used was doubled. That way even though the estimated pullout resistance is greater than what is measured, by adding more soil reinforcements, the overall pullout resistance would increase.

7.3.8 Importance of laboratory pullout testing

The results discussed within this section clearly show that only through the use of laboratory pullout resistance tests can a soil's actual performance be determined prior to construction. Considering that all three of the materials tested within this study met the minimum backfill standards outlined in Section 2.5, the large variation in pullout resistance only further emphasizes the need for laboratory pullout tests. By defining a material's actual pullout resistance, it can be categorized as being better suited for either large or small MSE wall constructions. Materials with high pullout resistances are best suited for large MSE wall constructions while small MSE wall constructions are exposed to a lesser degree of vertical loading due to self-weight, and therefore not subject to large bond strength stresses.

8 Final Conclusions and Research Recommendations

The primary aim of this study was to perform pullout tests on South African soils with the primary selection criteria being the soil's free draining ability. In order to do this, a pullout apparatus was designed, constructed and used to conduct a total of 24 pullout tests on South African soils. The following conclusions and recommendations can be made for the pullout apparatus design and the testing performed using this apparatus.

8.1 Pullout apparatus

The final aim outlined in Chapter 3 was defined as a review of the performance of the pullout apparatus during testing. The pullout apparatus performed as expected and allowed for the collection of consistent and accurate results. The following improvements can be made to the pullout apparatus:

- The addition of bracing to the side panels in between the vertical load-carrying beams. This will not only increase the strength of the side walls, but also straighten out the side panels as they currently have a natural tendency to bend parallel to the direction of load carrying members.
- The addition of reinforcements that prevent the side walls from bowing outwards during soil compaction. This is an issue due to the side panels being attached by bolts that are all situated on a straight line, meaning that the soil has the ability to bow the side walls out with respect to the base. The deflection is not enough to affect compaction efforts but is enough to cause alignment issues with the bolted connection points of the lid.

Although the initial design study was aimed at producing an apparatus that could be used for various types of testing as well as be able to completely disassemble for storage, it is strongly advised that the design should be altered to remove most of these additional features. The ability to disassemble the apparatus completely for storage is needed due to the current space limitations within the laboratory but once a designated area is provided for the apparatus, the permanent attachment of the side walls should be considered. This would include the replacement of temporary bolted connections with permanent welded joints.

8.2 Pullout testing and soil classification

The aims and objectives set out in Chapter 4 have satisfactorily been met. The methodology employed provided sufficient data on soil classification to ensure accurate pullout testing was performed.

The following conclusions can be made regarding the pullout performance of the tested materials:

- Free draining granular materials clearly outperformed the cohesive non-free draining materials.
- Laboratory pullout resistance testing prior to MSE wall construction is essential in determining actual pullout resistance performance for a given soil type.
- Granular free-draining materials are better suited for large MSE walls.
- Any deviation from the standard fast-construction techniques used to build MSE walls using free draining materials will only lead to further issues. For example, if a slower rate of construction is

required to prevent a build-up of pore water pressure, once loaded, the soil reinforcements themselves might cause a localized peak in pore water pressure after a pullout force is applied.

Further research topics would include the following:

- The same methods could be applied to quantify a larger range of soil types common in South Africa.
- Construct two soils with matching particle size distributions and overall mineralogy. The one material should have a non-plastic fines content while the other should have a plastic fines content. This would hopefully produce two soils with similar compaction curves and strength parameters but two differing permeabilities. Pullout testing could be performed on these soils to determine if free draining ability by itself is enough to affect pullout resistance.
- Pullout testing which includes consolidation time for cohesive materials. This should include pore water pressure gauges to measure localized porewater pressure created by the displacement of a steel strip.
- Quantify shear strength changes in backfill materials before and after the addition of a hydraulic gradient. This aims to see if a backfill loses or gains strength once fines have been washed out of the soil mass through the life of construction.
- Construct a reference table of material type and ideal soil reinforcement. This would include various soil reinforcement and common soil types found in South Africa.

9 Bibliography

- AASHTO. (2007). Section 7 Earth Retaining Systems. In *AASHTO LRFD Bridge Design Construction specifications* (2nd ed.). Washington, DC: American Association of State Highway and Transportation Officials.
- ASTM Standard D248. (2006). Standard Practice for Classification of Soils for Engineering Purposes (Unified Soil Classification System). *ASTM Standard Guide, D5521-05*, 1–5. <https://doi.org/10.1520/D2487-11>.
- ASTM Standard D3080. (2014). Standard Test Method for Direct Shear Test of Soils Under Consolidated Drained Conditions. In *ASTM International* (pp. 1–9). <https://doi.org/10.1520/D3080>
- ASTM Standard D6706. (2013). Standard Test Method for Measuring Geosynthetic Pullout Resistance in Soil. In *ASTM International* (Vol. 01, pp. 1–8).
- Autodesk. (2018). *Autodesk Fusion 360*. Retrieved from <https://www.autodesk.com/products/fusion-360/>
- Berg, R., Christopher, B., & Samtani, N. (2009). Design and construction of mechanically stabilized earth walls and reinforced soil slopes—Volume I. *Federal High Way Administration (FHWA)*, I(November). <https://doi.org/FHWA-NHI-10-024> & [FHWA-NHI-10-025](https://doi.org/FHWA-NHI-10-025)
- Byrne, G., & Berry, A. D. (2008). A Guide to Practical Geotechnical Engineering. In *Franki* (Vol. 75). Johannesburg, South Africa: Franki.
- Cerato, A. B., & Lutenecker, A. J. (2006). Specimen size and scale effects of direct shear box tests of sands. *Geotechnical Testing Journal*, 29(6), 507–516. <https://doi.org/10.1520/GTJ100312>
- Committee of State Road Authorities. (1986a). Method A1: The wet preparation and sieve analysis of gravel, sand and soil samples. In *Technical Methods for Highways*. Pretoria, South Africa: Department of Transport.
- Committee of State Road Authorities. (1986b). Method A2: The determination of the liquid limit of soils by means of the flow curve method. In *Technical Methods for Highways*. Pretoria, South Africa: Department of Transport.
- Committee of State Road Authorities. (1986c). Method A3: The determination of the plastic limit and plasticity index of soils. In *Technical Methods for Highways*. Pretoria, South Africa: Department of Transport.
- Committee of State Road Authorities. (1986d). Method A4: The determination of the linear shrinkage of soils. In *Highway Research Record*. Pretoria, South Africa: Department of Transport.
- Committee of State Road Authorities. (1986e). Method A5: The determination of the percentage of material, in a soil sample, passing a 0,075mm sieve. In *Technical Methods for Highways*. Pretoria, South Africa: Department of Transport.

- Committee of State Road Authorities. (1986f). Method A6: The determination of the grain size distribution in soils by means of a hydrometer. In *Technical Methods for Highways*. Pretoria, South Africa: Department of Transport.
- Committee of State Road Authorities. (1986g). Method A7: The determination of the maximum dry density and optimum moisture content of gravel, soil and sand. In *Technical Methods for Highways*. Pretoria, South Africa: Department of Transport.
- Craig, R. F., & Knappett, J. (2004). *Craig's Soil Mechanics* (8th ed.). Abingdon, Oxon.: Spon Press.
- Das, B. M. (2010). *Principles of Geotechnical Engineering* (7th ed.; H. Gowans, Ed.). Cengage Learning.
- Esmaili, D., Hatami, K., & Miller, G. A. (2014). Influence of matric suction on geotextile reinforcement-marginal soil interface strength. *Geotextiles and Geomembranes*, 42(2), 139–153.
- Freeze, R. A., & Cherry, J. A. (1979). *Groundwater*. Englewood Cliffs, New Jersey: Prentice-Hall.
- Hausmann, M., & Lee, I. (1976). *Strength Characteristics of Reinforced Soil*. School of Civil Engineering, University of New South Wales Kensington, N.S.W.
- Hazen, A. (1930). "Water Supply" in *American Civil Engineers Handbook*. New York, N.Y.: Wiley.
- Head, K. H. (1992). *Manual of Soil Laboratory Testing* (2nd ed.). London, England: Pentech.
- Head, K. H., & Epps, R. J. (2011). *Manual of Soil Laboratory Testing* (Third Edit). Scotland, UK: Whittles Publishing.
- Ingold, T. S. (1982). *Reinforced earth*. London, England: Telford.
- Jayawickrama, P. W., Lawson, W. D., Wood, T. A., & Surles, J. G. (2013). Pullout resistance factors for inextensible mechanically stabilized earth reinforcements in sandy backfill. *Transportation Research Record*, (2363), 21–29.
- Jayawickrama, Priyantha, Lawson, W., Wood, T., Surles, J., & Senanayake, A. (2012). Effect of skewing and splaying on pullout capacity of steel reinforcements in mechanically stabilized earth structures. *Transportation Research Record*, (2310), 81–89.
- Jayawickrama, PW, Lawson, W., Wood, T., & Surles, J. (2015). *Pullout Resistance Factors for Steel MSE Reinforcements Embedded in Gravelly Back fill*. 141(2), 1–10. [https://doi.org/10.1061/\(ASCE\)GT.1943-5606.0001192](https://doi.org/10.1061/(ASCE)GT.1943-5606.0001192).
- Jones, C. (1978). The York Method of Reinforced Earth Construction. *Proceedings of Symposium on Earth Reinforcement*, American Society of Civil Engineers. New York, United States.
- Jones, C. (1985). *Earth Reinforcement and Soil Structures*. London, England: Butterworths.
- Lee, H., & Bobet, A. (2005). Laboratory Evaluation of Pullout Capacity of Reinforced Silty Sands in Drained and Undrained Conditions. *Geotechnical Testing Journal*, 28(4), 370–379.

<https://doi.org/10.1520/GTJ12011>

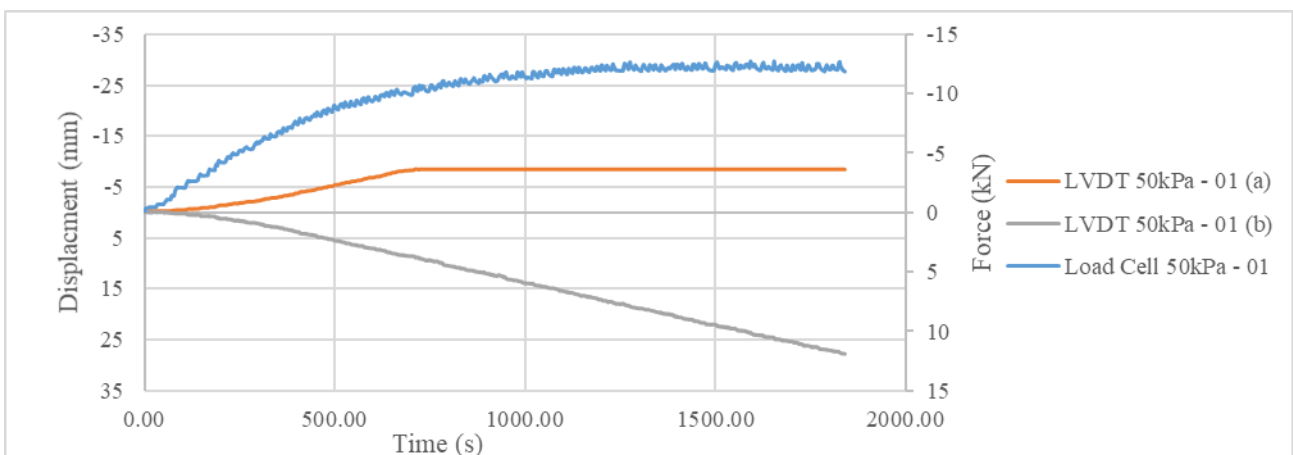
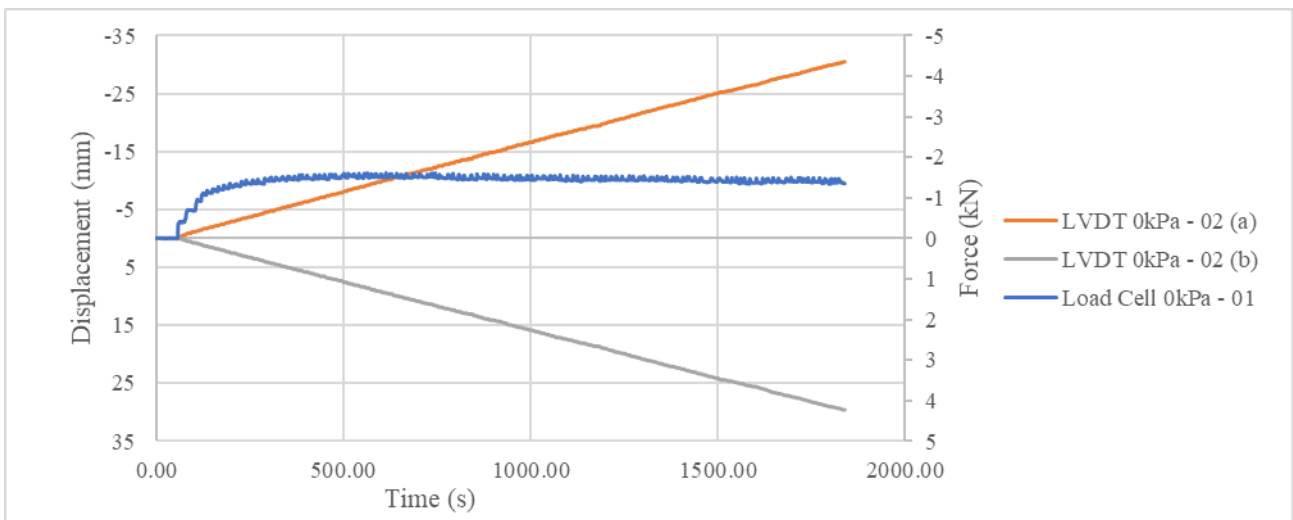
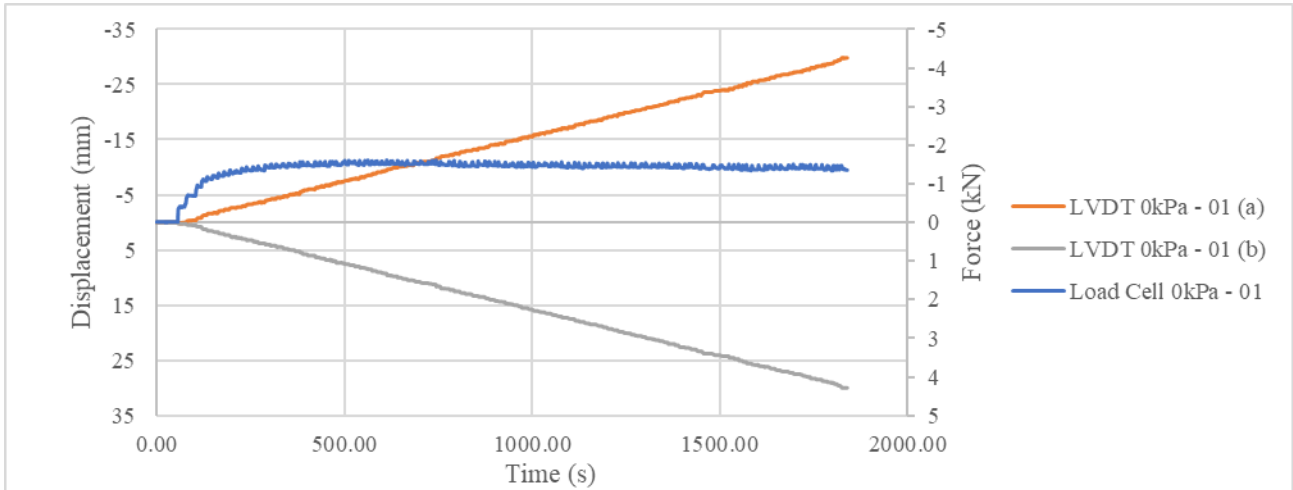
- Lee, K. L. (1978). Mechanisms, Analysis and Design of Reinforced Earth. *Proceedings of Symposium on Earth Reinforcement*, American Society of Civil Engineers. New York, United States.
- McKittrick, D. (1978). Design, Construction, Technology and Performance of Reinforced Earth. *Proceedings of Symposium on Earth Reinforcement*, American Society of Civil Engineers. New York, United States.
- Mong, D. (2019). *An investigation of the influence of mica group minerals on the engineering properties of a soil*, Final Year Research Project, Stellenbosch University. Stellenbosch, South Africa.
- Narain, J. (1978). Reinforced Earth. *Proceedings of the Seventh IGS Annual Lecture, 26th Annual General Session*. Calcutta, India.
- Reinforced Earth Company. (1995). Apparent coefficient of friction, f^* to be used in the design of reinforced earth structures. *Technical Bulletin MSE-6*.
- SANS 207. (2011). The design and construction of reinforced soils and fills. In *SANS 207 : 2011 SOUTH AFRICAN NATIONAL STANDARD*. SABS Standards Division.
- Schlosser, F., & Elias, V. (1978). Friction in Reinforced Earth. *Proceedings of Symposium on Earth Reinforcement*, American Society of Civil Engineers. New York, United States.
- Schoeman, J. J. (2018). *The Liquefaction potential of soils on the Cape Flats established by means of empirical correlation*, (MEng) Stellenbosch University. Stellenbosch, South Africa.
- Schön, J. (2011). *Physical Properties of Rocks - A Workbook*. Oxford: Elsevier.
- Smith, A. C. S. (2010). Reinforced Earth ® structures for headwalls to crushing plants in Africa. Retrieved April 25, 2019, from Reinforced Earth: Technical Papers website: <https://www.recosa.co.za/technicaldrawings.php>
- Smith, A. C. S., & Vadron, T. (1993). Durability of Reinforced Earth reinforcing strips in Southern Africa. *SAICE Journal*, 23(2), 23-27.
- Strahler, A. W., Walters, J. J., & Stuedlein, A. W. (2016). Frictional resistance of closely spaced steel reinforcement strips used in MSE walls. *Journal of Geotechnical and Geoenvironmental Engineering*, 142(8), 04016030. [https://doi.org/10.1061/\(ASCE\)GT.1943-5606.0001492](https://doi.org/10.1061/(ASCE)GT.1943-5606.0001492)
- Swiger, W. (1978). Closing Notes for the Symposium on Earth Reinforcement. *Proceedings of Symposium on Earth Reinforcement*, American Society of Civil Engineers. New York, United States.
- Taghavi, S. H. S., & Mosallanezhad, M. (2017). Experimental analysis of large-scale pullout tests conducted on polyester anchored geogrid reinforcement systems. *Canadian Geotechnical Journal*, 54, 621–630.
- Terzaghi, K. (1948). *Soil Mechanics in Engineering Practice*. New York: J. Wiley.

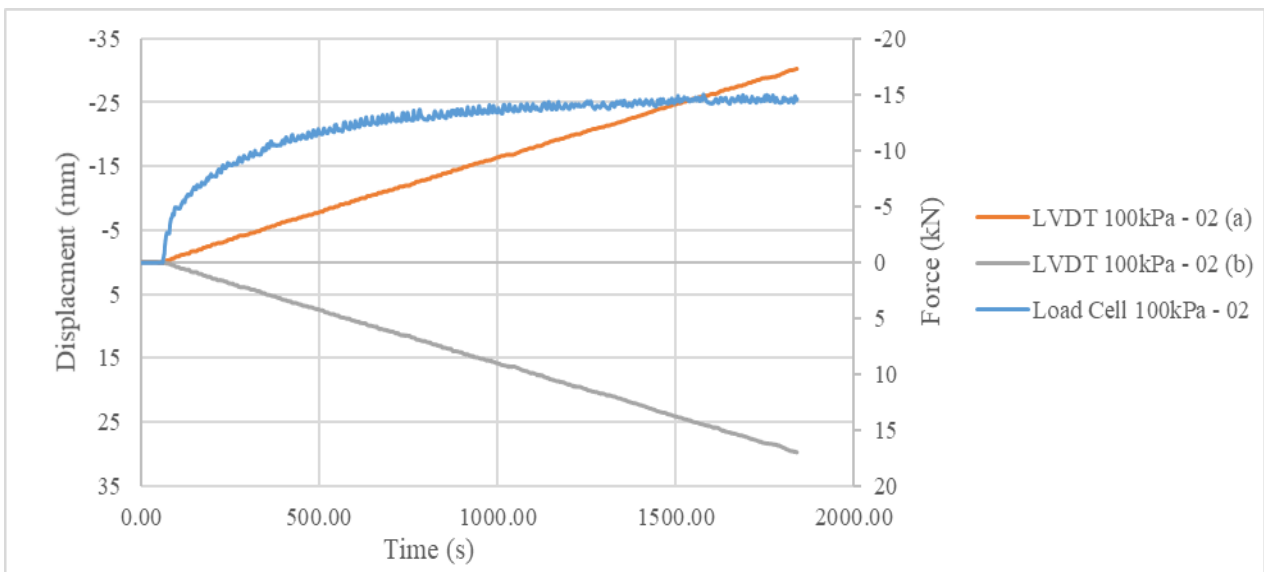
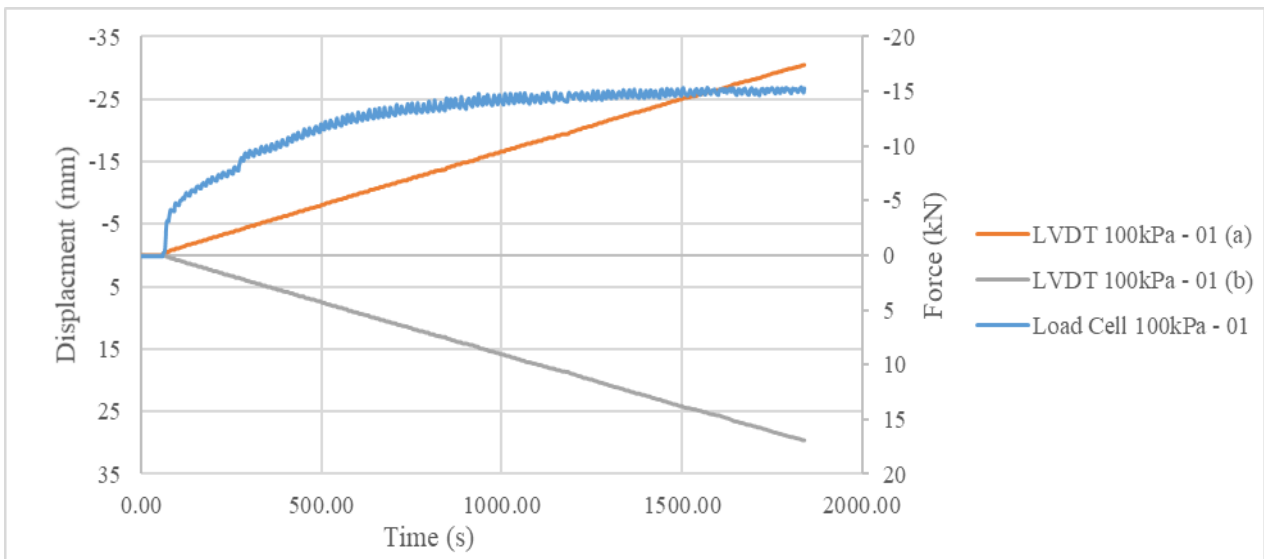
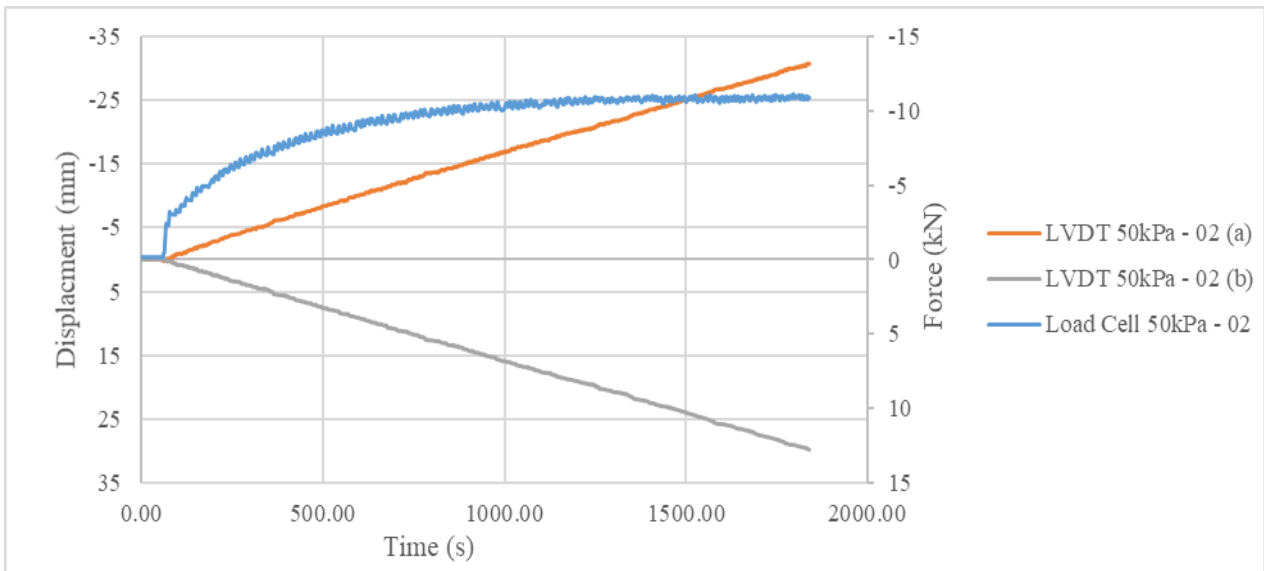
- Vidal, H. (1969). The Principle of Reinforced Earth. In *Highway Research Record* (pp. 1–16). Retrieved from <http://onlinepubs.trb.org/Onlinepubs/hrr/1969/282/282-001.pdf>
- Wang, J., & Gutierrez, M. (2010). Discrete element simulations of direct shear specimen scale effects. *Geotechnique*, *60*(5), 395–409. <https://doi.org/10.1680/geot.2010.60.5.395>
- Wang, Z., Jacobs, F., & Ziegler, M. (2016). Experimental and DEM investigation of geogrid-soil interaction under pullout loads. *Geotextiles and Geomembranes*, *44*(3), 230–246. <https://doi.org/10.1016/j.geotexmem.2015.11.001>
- Weldu, M. T. (2015). *Pullout Resistance of MSE Wall Steel Strip Reinforcement in Uniform Aggregate*, (MSc) University of Kansas. Kansas, United States.

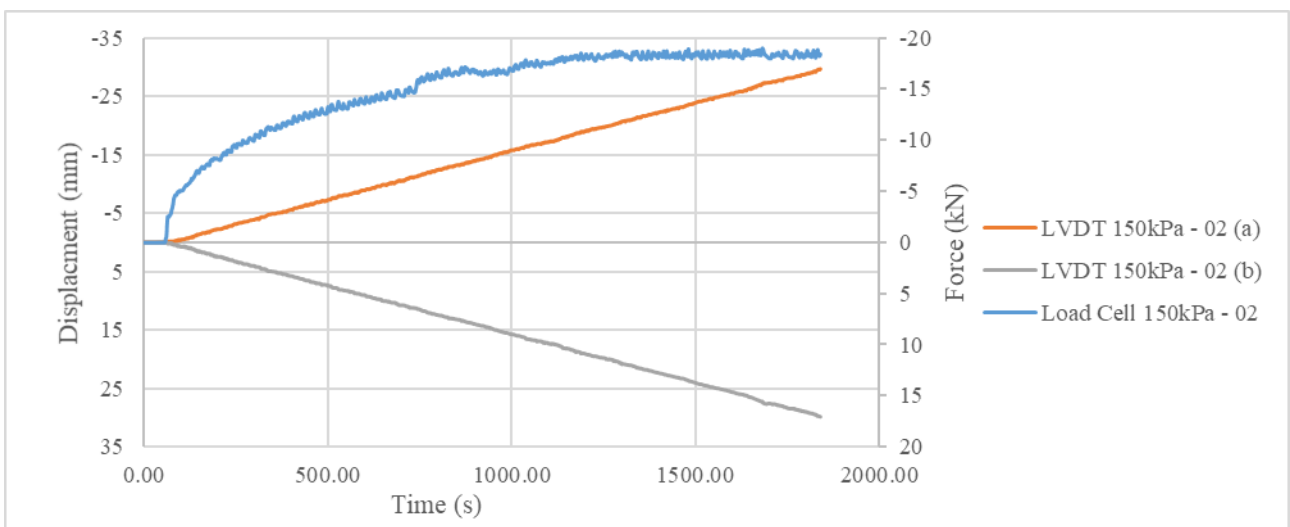
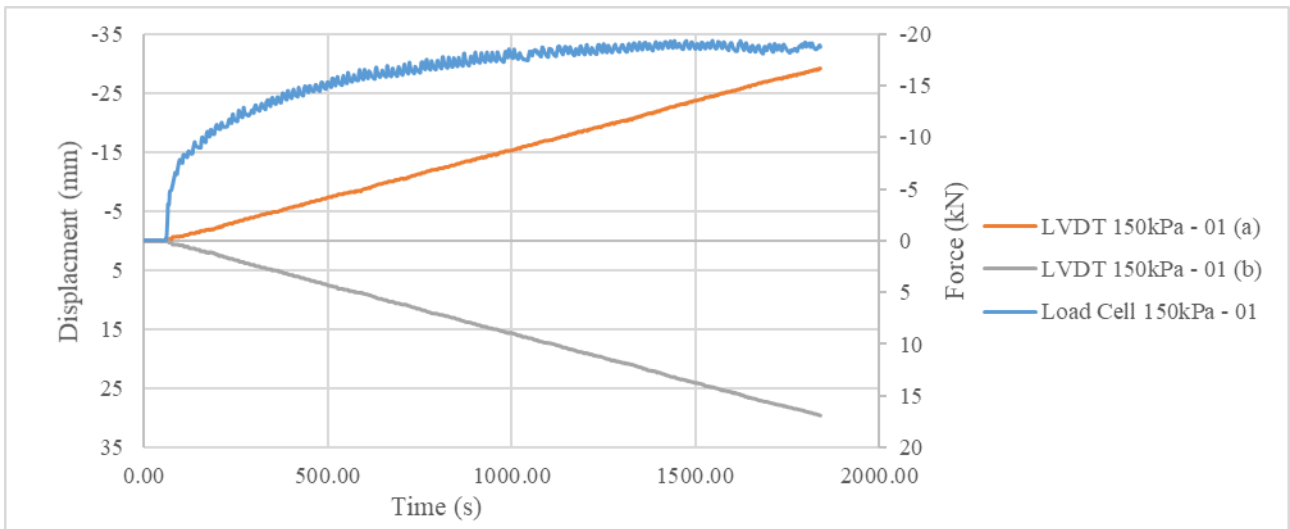
Appendix A. Individual pullout test data

The following figures are presented in a way that both the LVDT readings are plotted on the primary y-axis and the corresponding pullout resistance on the secondary y-axis. Each figure consists of the pullout resistance for a test at a given vertical stress.

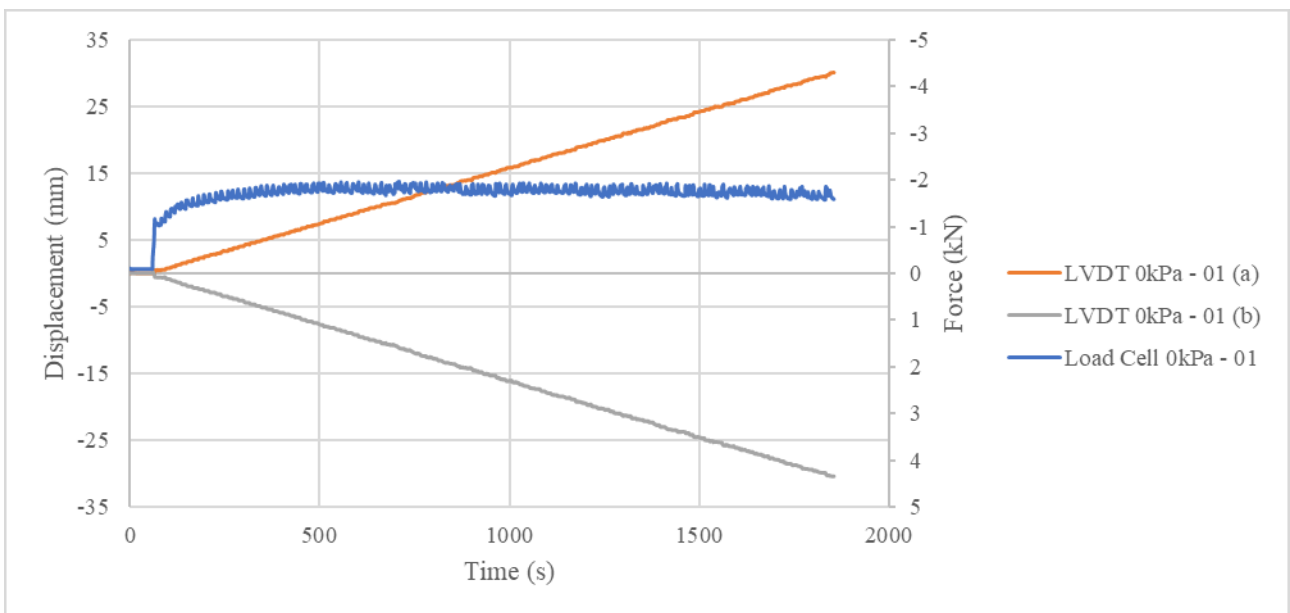
- Crusher dust

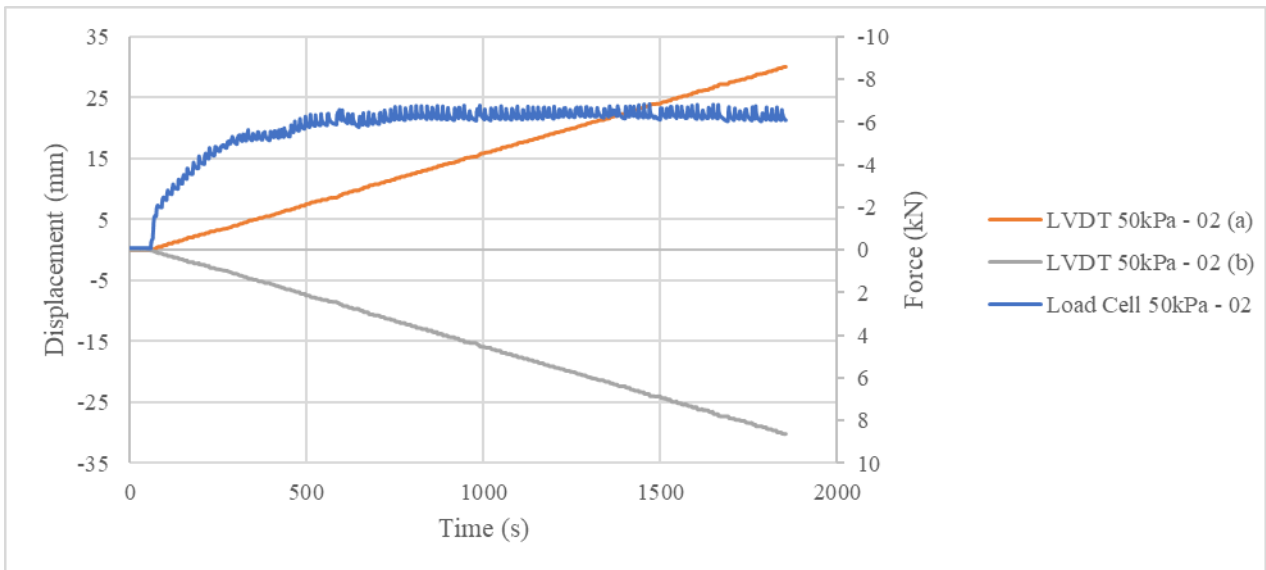
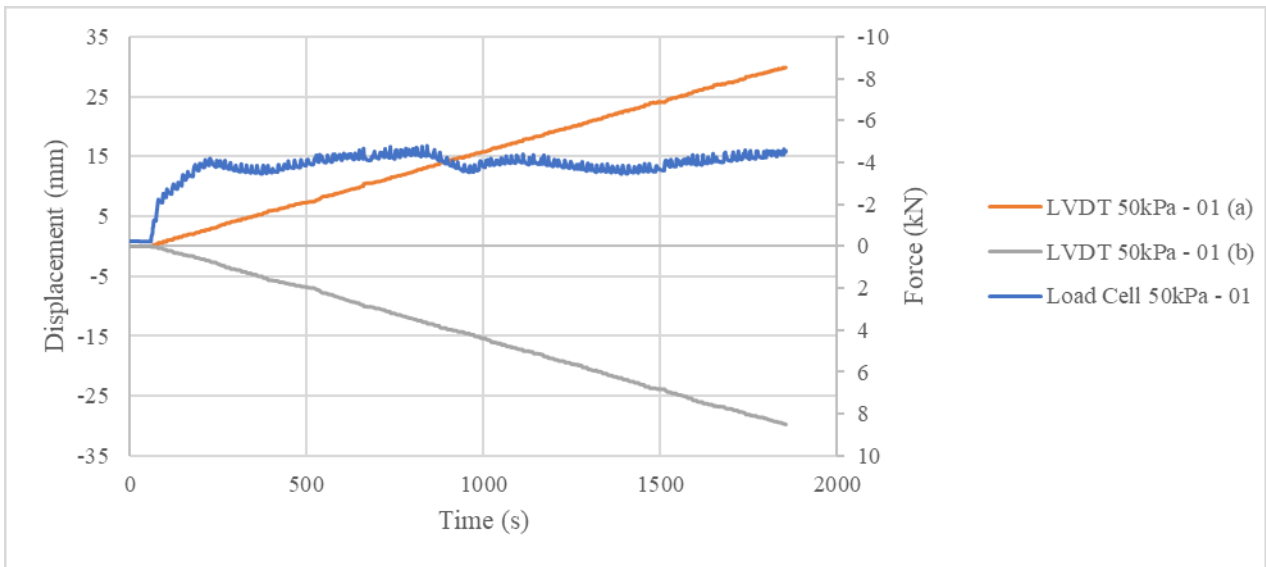
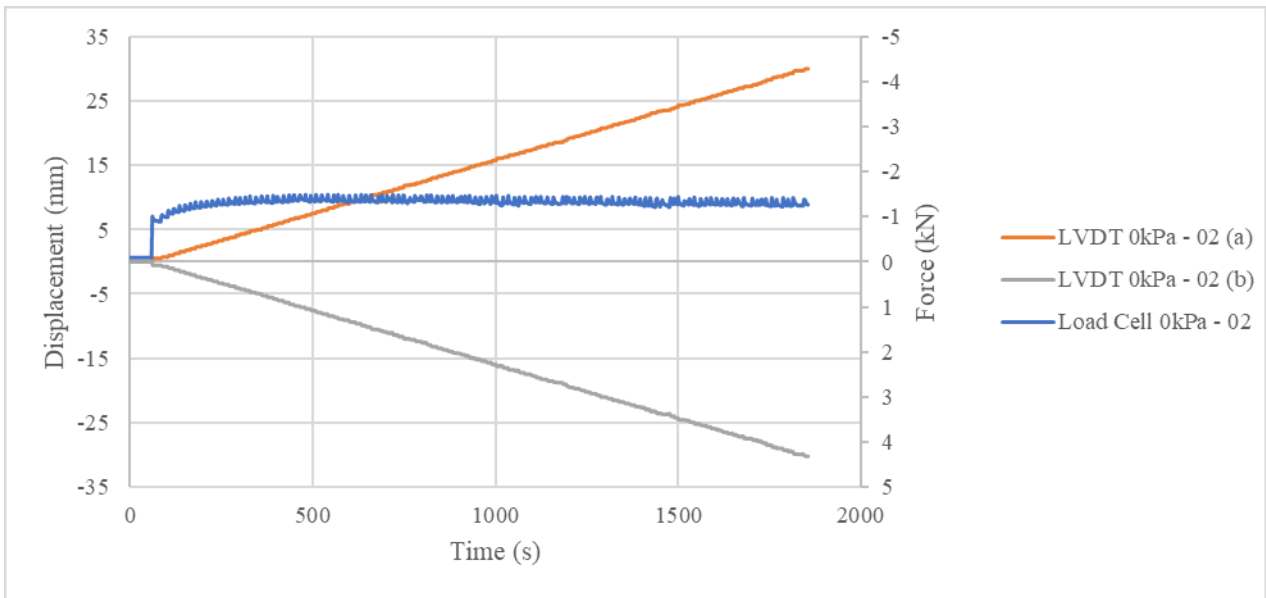


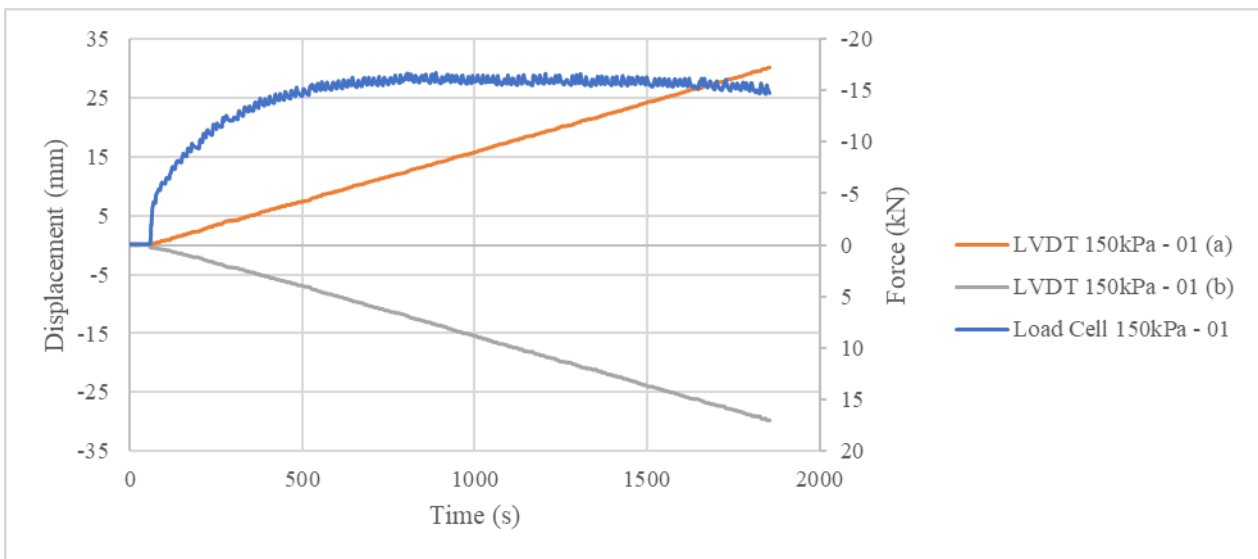
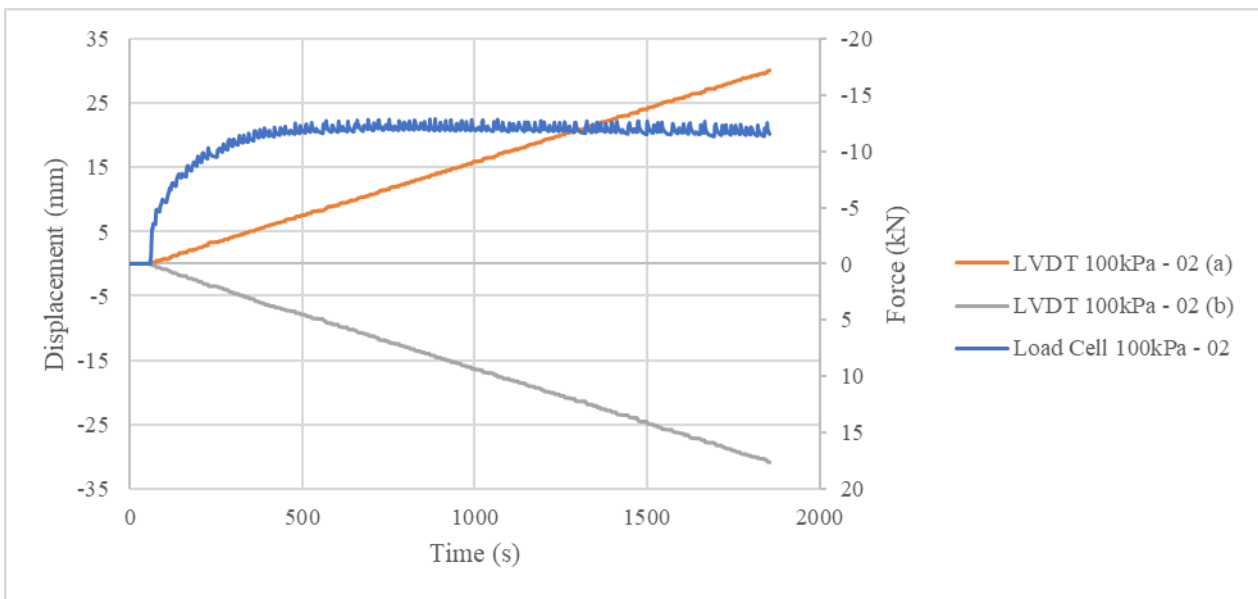
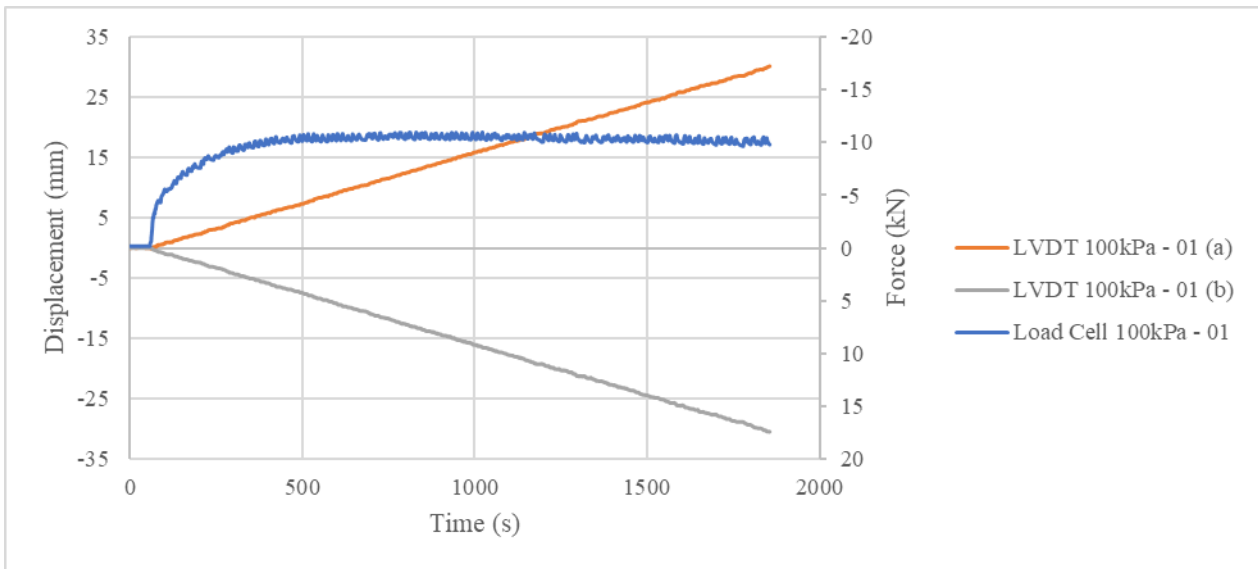


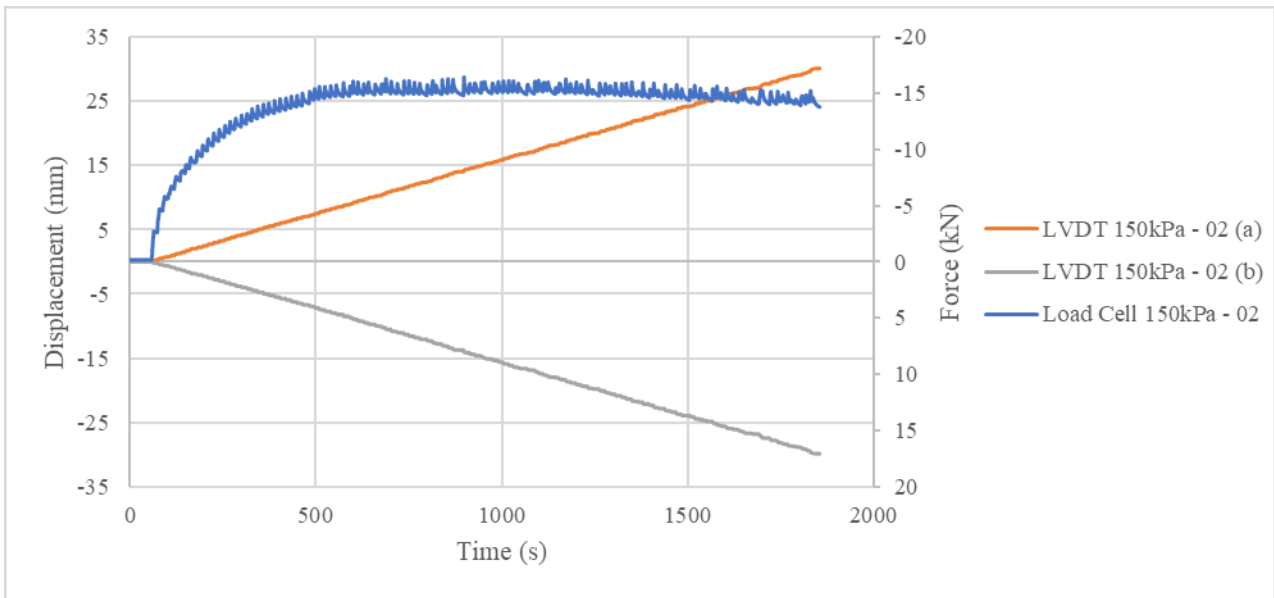


- Cape Flats sand

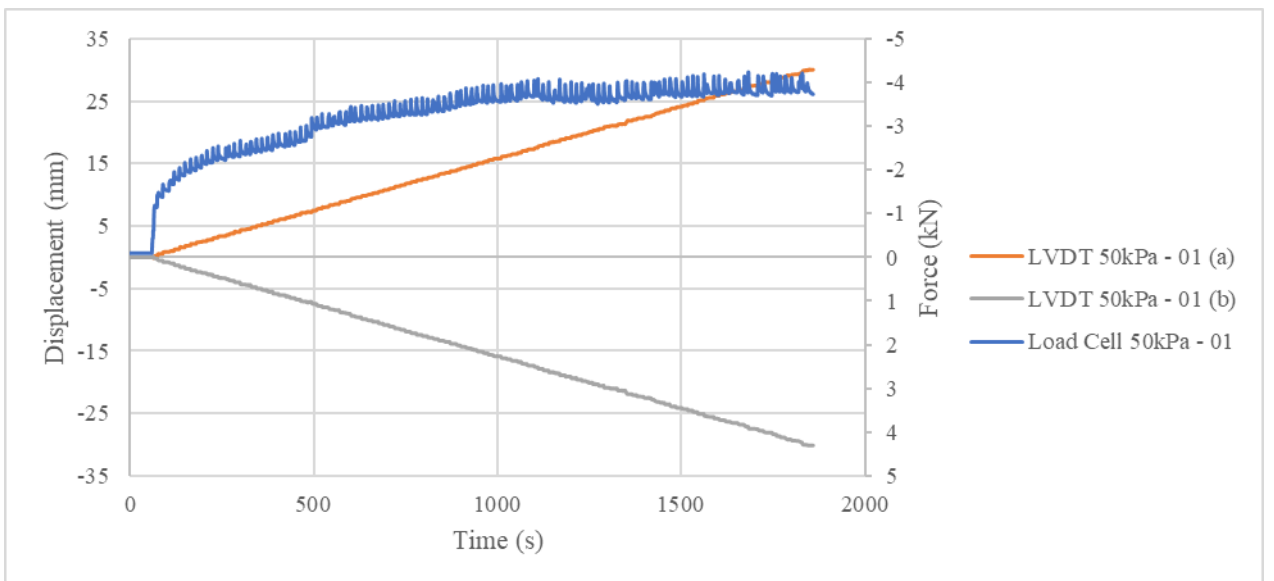
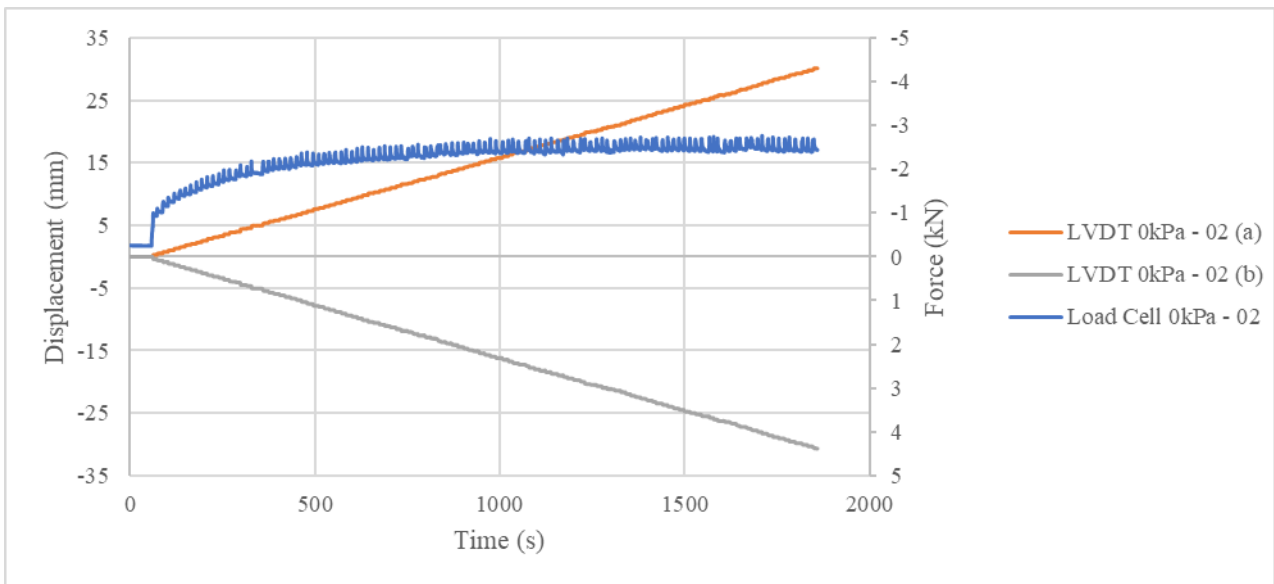


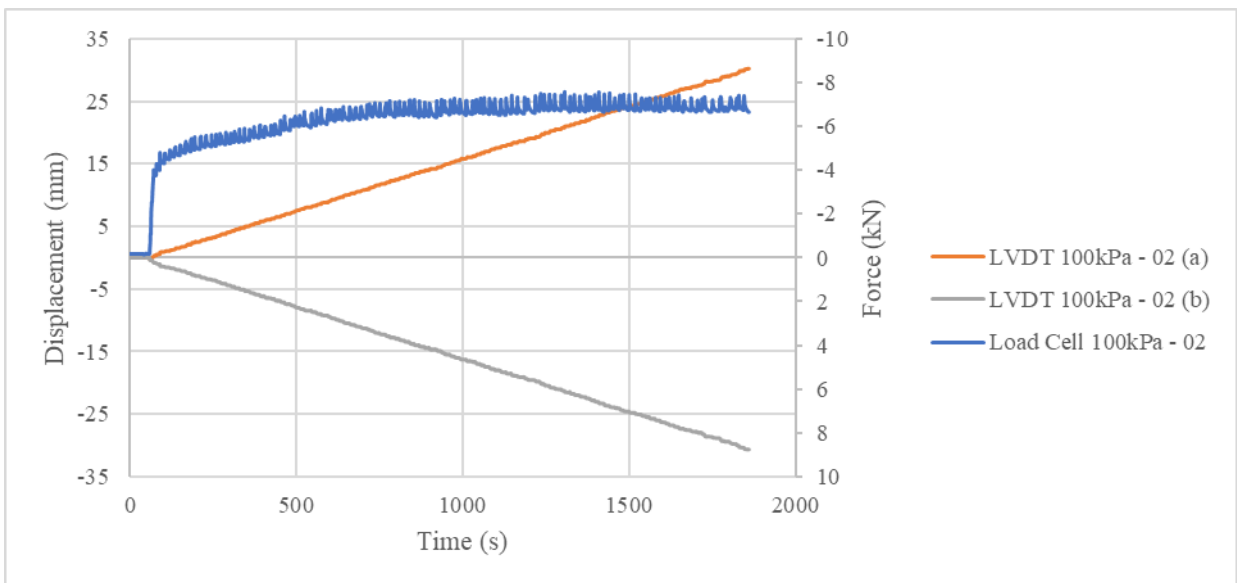
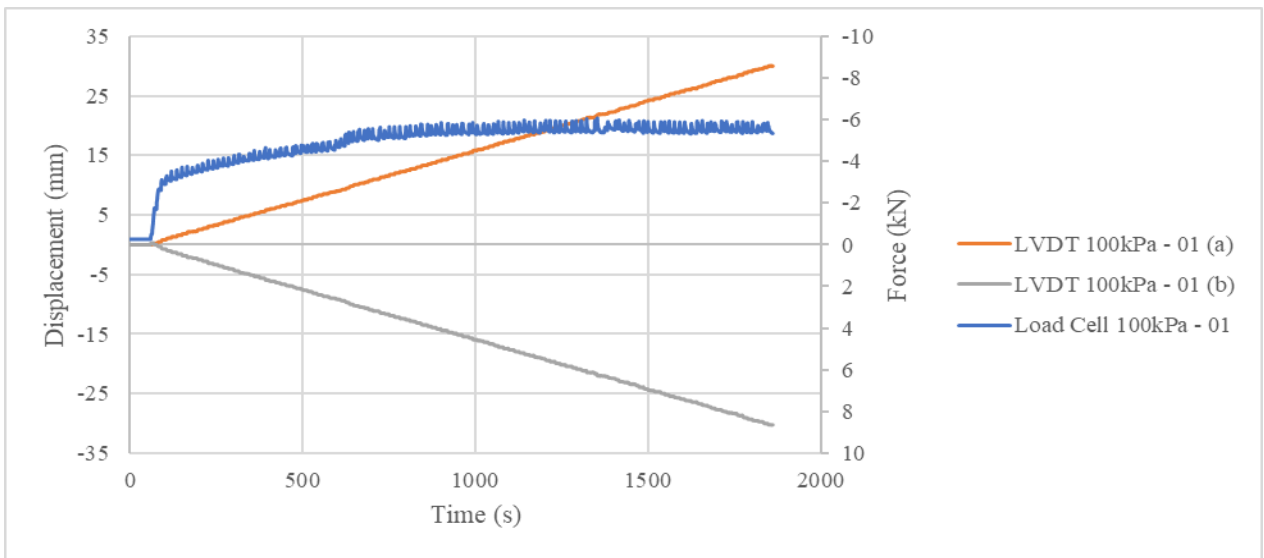
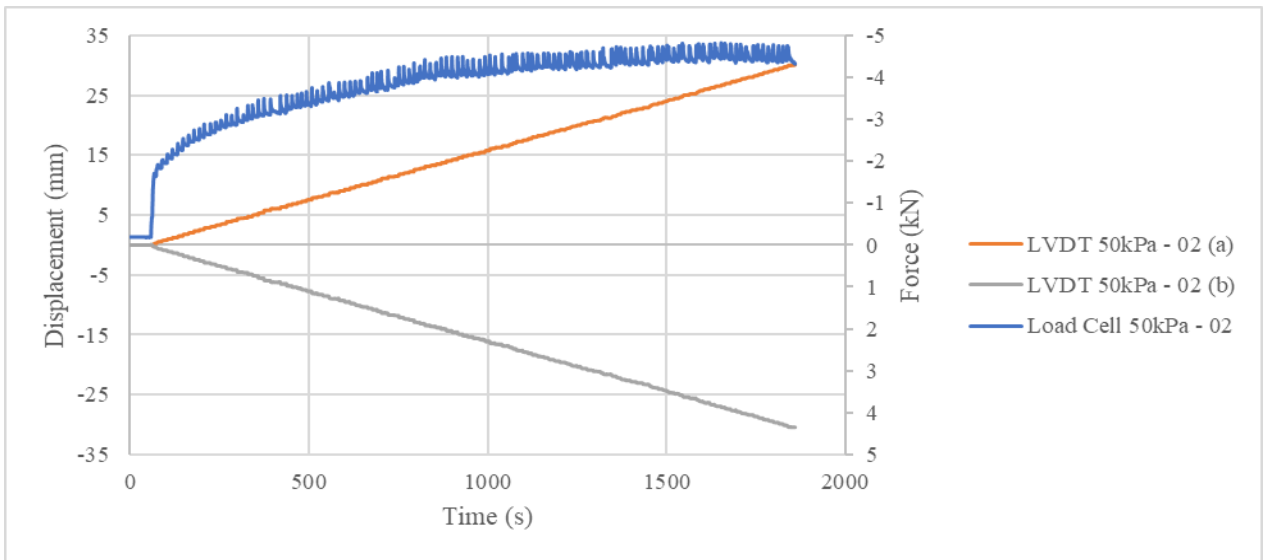


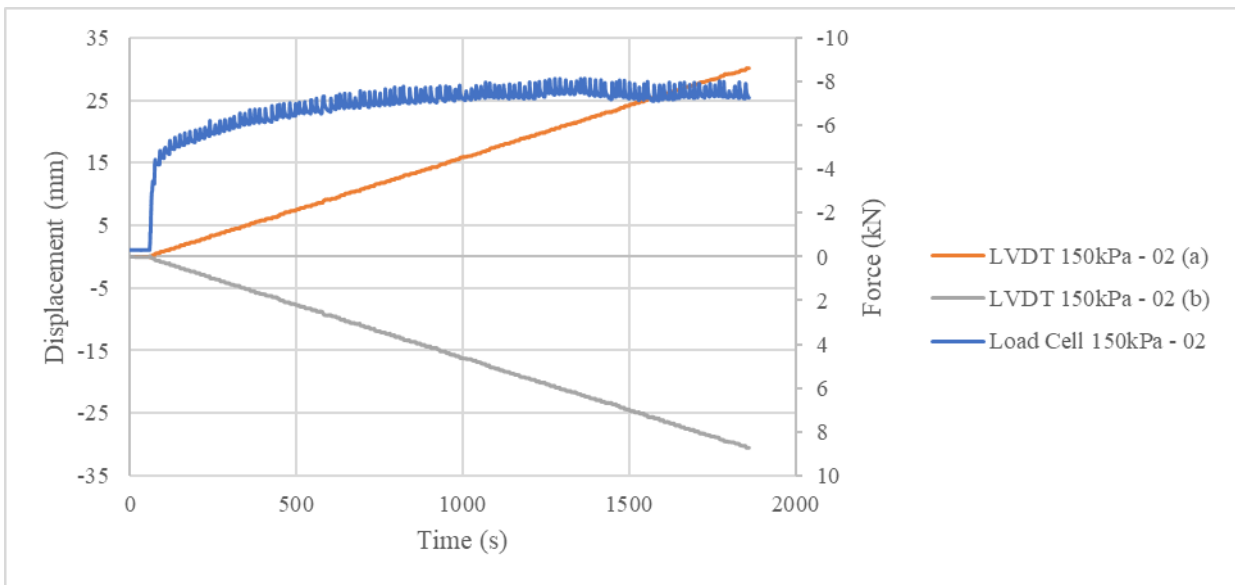
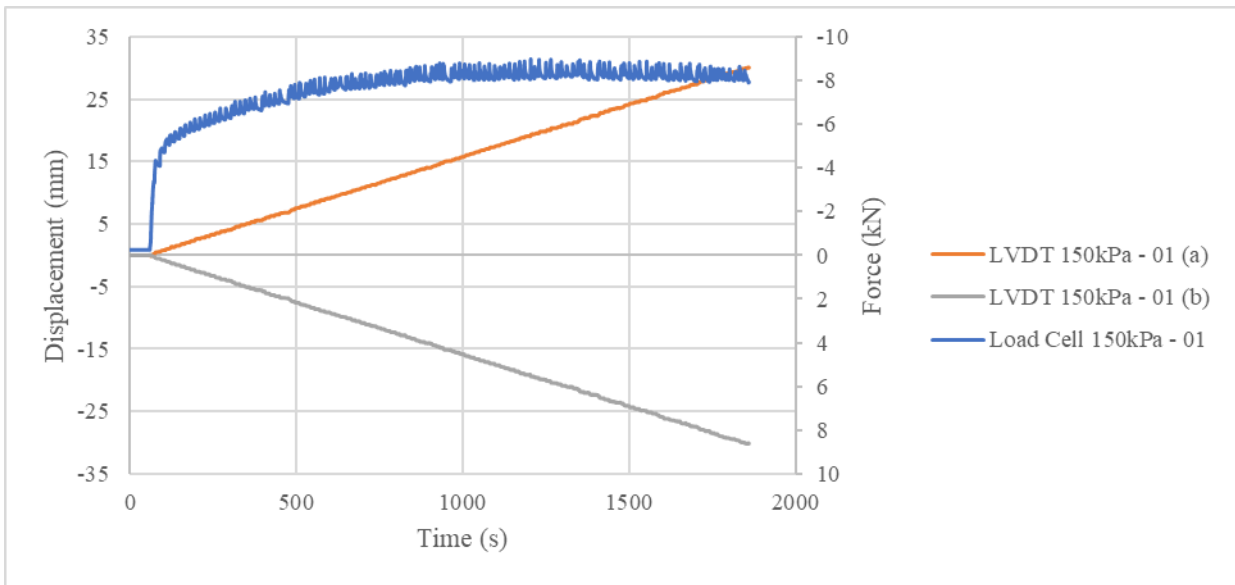




- Micaceous residual granite







Appendix B. Pullout apparatus assembly guide



UNIVERSITEIT
STELLENBOSCH
UNIVERSITY

Geotechnical Engineering



Pullout Box Apparatus Assembly Guide

2019

1 Introduction

This document serves as a guide of how to assemble the pullout apparatus in the horizontal orientation. Where necessary, extra information will be mentioned as required for any additional steps which should be taken in order to perform vertical pullout testing. The apparatus design currently allows for both horizontal and vertical testing, which excludes the airbag required to apply a vertical stress.

Safe working loads

The following safe working loads have only been tested for loading conditions where the box is assembled in the horizontal orientation. Therefore, amendments need to be made to this document to record any further testing that analyzes the safe working loads for other loading orientations.

Loading Type	Load	Comments
Airbag expansion applying overburden pressure	300 kPa	Loading was tested at 500 kPa and a deflection was calculated that is considered safe and should not produce any permanent deformation of the apparatus itself. It is however becoming dangerous as the loading on the bolts should be taken into consideration.
Hydraulic jack applying pullout force	50 kN	This is analyzed when having the jack mounted at position 1 on the base beams and position 3 of the upright jack supports.

Please make sure that all bolts used in the construction are of grade 8.8 or higher. If this is not adhered to, the possibility of failure is highly likely.

Setup procedure

Step 1: Initial spacing room requirements

Begin by placing the base beams in the orientation shown in Figure B-1. The total footing size of the box is 2.2 m in length and 0.71 m in width. Ensure that there will be sufficient space surrounding the box for comfortable movement. Make sure that the long beams have their bolting holes on the top of the beams.



Figure B-1. Base construction

Each short cross member is marked with a welded dot which corresponds to one of the long channel sections to ensure that each cross member is inserted in the correct orientation and in the correct position.

The alignment works by following the ‘dots match dots’ alignment. As seen Figure B-2 the members will always have the dots placed next to each other.

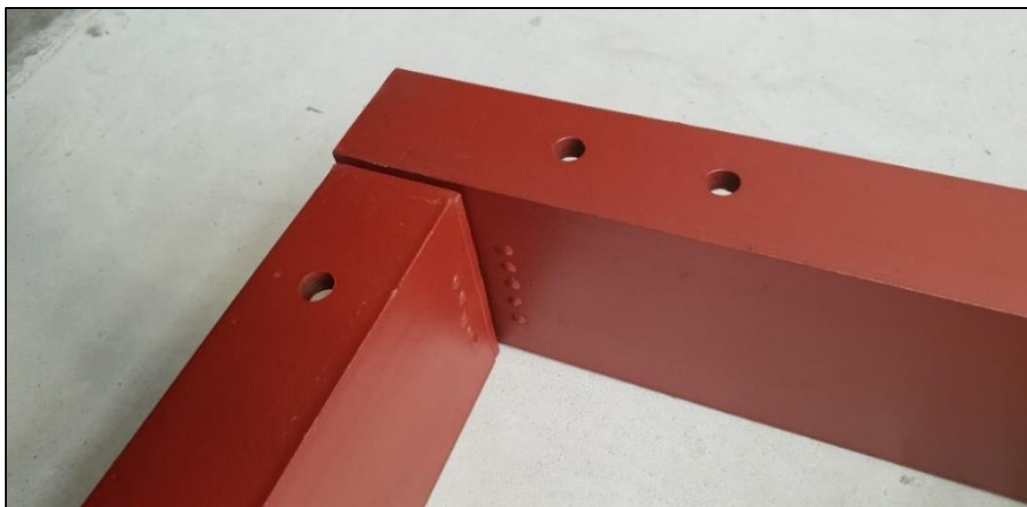


Figure B-2. Dot alignment method

Step 2: Base plate alignment

Prior to tightening the bolts of the base construction, make sure that the base plate is correctly aligned with the marked 'A' and 'B' on the plate. Also ensure that the bolt holes on the plate are aligned with those along the top section of the long channel beams. The plate is then laid on top of the base construction as seen in Figure B-3.

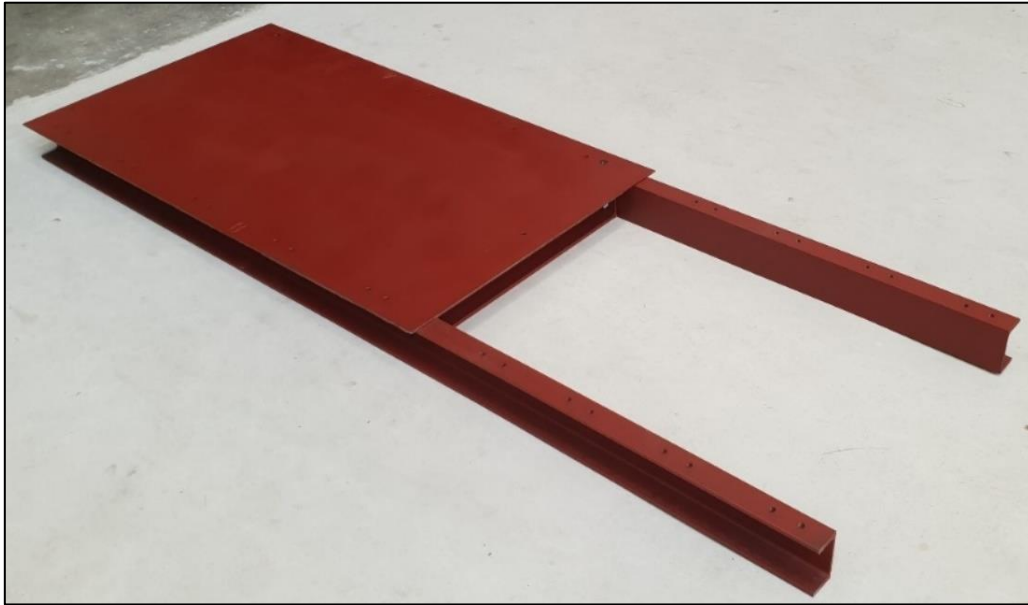


Figure B-3. Base plate positioning

The 'A' and 'B' marks are welded throughout the box where alignment is necessary. The plates' alignment should match as seen in Figure B-4 and Figure B-5 to the corresponding marking on the long channels



Figure B-4. Plate 'A' Alignment

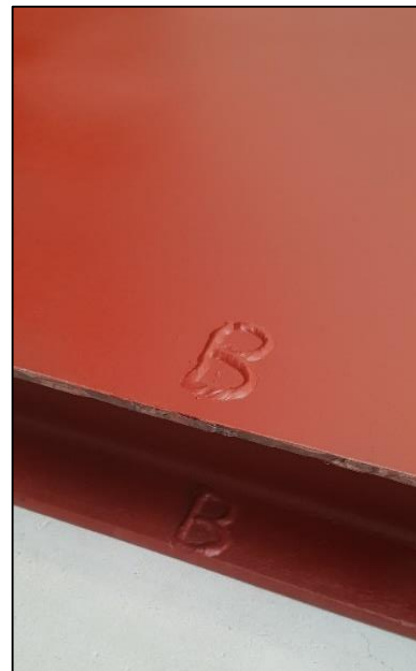


Figure B-5. Plate 'B' Alignment

Step 3: Attaching the side panels

Both of the side panels should be attached securely before continuing to the following steps. At this stage, the alignments should follow the alignment depicted in Figure B-6.

Just as in step 2, the side panels are both marked with respective 'A' or 'B' markings to ensure that the bolt holes align correctly.

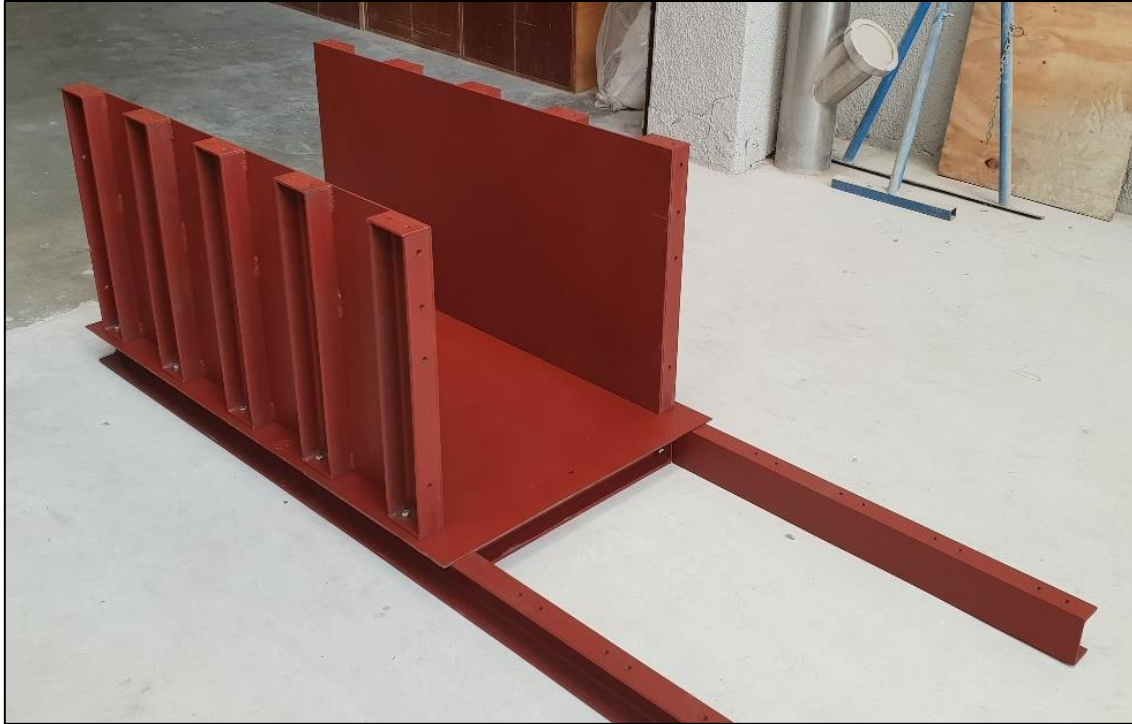


Figure B-6. Side panel assembly



Figure B-7. 'A' Alignment



Figure B-8. 'B' Alignment

Step 4: Lower Face and Back Plate

For this step, the box will be in a state to which the first zone of soil can be added. For the use case of horizontal pullouts, the soil needs to be compacted to the heights of these panels as it will allow the soil reinforcement to be pulled out in alignment with one of the hydraulic jack positions.



Figure B-9. Lower back panel alignment



Figure B-10. Lower front panel alignment

The Back panel is split into two sections. For all horizontal pullout testing, the back panel should be installed in two separate pieces as to facilitate better soil compaction to the correct depth (Figure B-9). If the pullout apparatus is being constructed for use in the vertical orientation, then the entire back plate should be installed (as seen Figure B-13

For horizontal pullout testing, the lower front panel can be installed as shown in (Figure B-10). Similar to the back panel, if the assembly of the apparatus is for the use of vertical pullout testing, the front plate (Figure B-10 and Figure B-14) should not be installed at this stage as it would inhibit insertion of the soil required for pullout testing

Step 5: Load transfer sleeve

This step is only required if the apparatus will be used to pull geotextiles/geosynthetics as the load transfer sleeve is only deemed necessary according to ASTM (ASTM Standard D6706, 2013).

Once the soil has been compacted to the correct height, the lower load transfer sleeve can be installed as seen in Figure B-13.



Figure B-11. Lower load transfer sleeve

The lower load transfer sleeve (LTS) is fitted with three slotted fixtures (Figure B-12) which allow the LTS to be fitted in such a way that it will always be in contact with the soil within the soil chamber.



Figure B-12. Load transfer sleeve slotted fixture

Step 6: Upper back plate

The upper back plate (Figure B-13) should first be attached by the three connecting bolt holes to the lower back plate, followed by the middle bolting points which are located just below the lip of the angle iron. This is the point where caution should be taken to ensure the apparatus is being assembled as square and inline as possible, otherwise attaching the lid might become problematic.



Figure B-13. Upper back plate

Step 5: Upper front plate



Figure B-14. Upper front plate

The upper front plate also contains the upper section of the load transfer sleeve. The panel (Figure B-14) should then be attached and made sure that the pullout material does not make contact with the upper or lower load transfer sleeve.

At this point, the apparatus should resemble that of Figure B-15. This will act as the final chamber for the test soil to be inserted and compacted to the desired density. A minimum of 60 mm should be left for the airbag to be inserted above the soil material to provide adequate space prior to attachment of the lid.



Figure B-15. Completed soil chamber

Step 7: Attaching the lid

The desired airbag should be inserted into the soil chamber prior to the lid being attached. The holes can be made where necessary for airbag fill pipes to be fed through. Any additional holes should be amended to this document.

If the apparatus is being assembled to be used in the vertical orientation, the lid should be attached as normal (Figure B-16) and then the entire apparatus can be lifted and placed in the vertical orientation. In other words, the back side of the apparatus should be orientated to form the bottom of the soil chamber in the vertical position.



Figure B-16. Completed soil chamber

The lid will once again be aligned according to the 'A' and 'B' markings on the box. The final soil chamber assembly should resemble Figure B-17 and Figure B-18.



Figure B-17. Final 'A' alignment

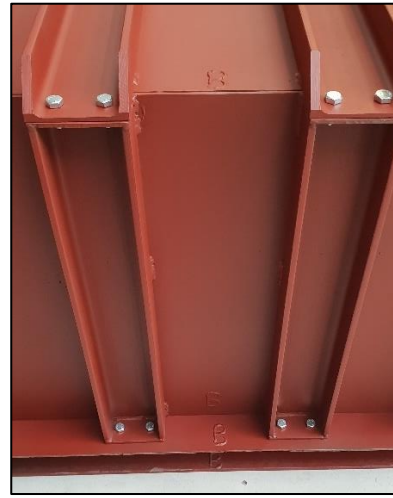


Figure B-18. Final 'B' alignment

Step 8: Jack support assembly

This is highly dependent on the setup that best suits the needs of the user performing the tests. The uprights of the jack support have a set of three mounting locations, as seen in Figure B-19. The base support also contains a set of four mounting positions, as seen in Figure B-20.

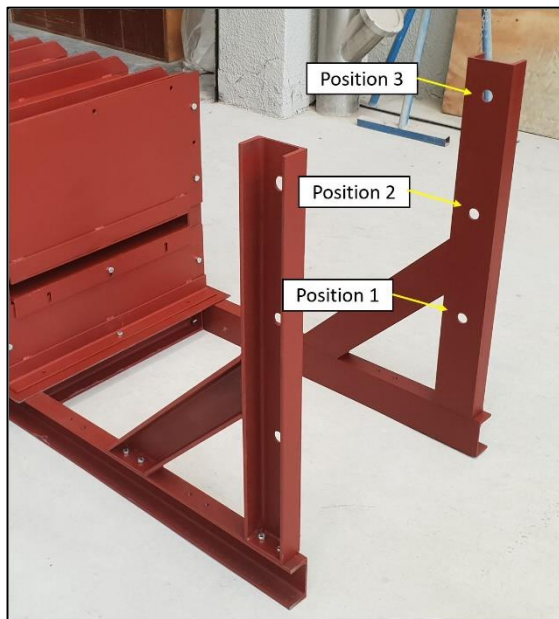


Figure B-19. Upright support positions

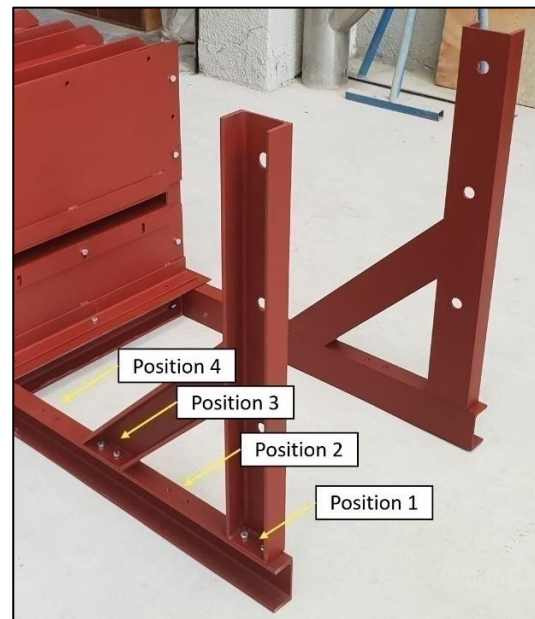


Figure B-20. Base mounting positions

This allows for a total of 12 different positions that the hydraulic jack can be attached in (the position of which is ultimately determined by the user and the purpose of testing).

Additional Information

The jack supports were designed to be interchangeable in order to ensure that the required bracing for high jack loading conditions is achieved in all possible jack support locations. Figure B-21 to Figure B-24 depicts the four positions the jack can be mounted in.



Figure B-21. Jack position 1



Figure B-22. Jack position 2



Figure B-23. Jack position 4



Figure B-24. Jack position 3

Appendix C. Finite Element Analysis

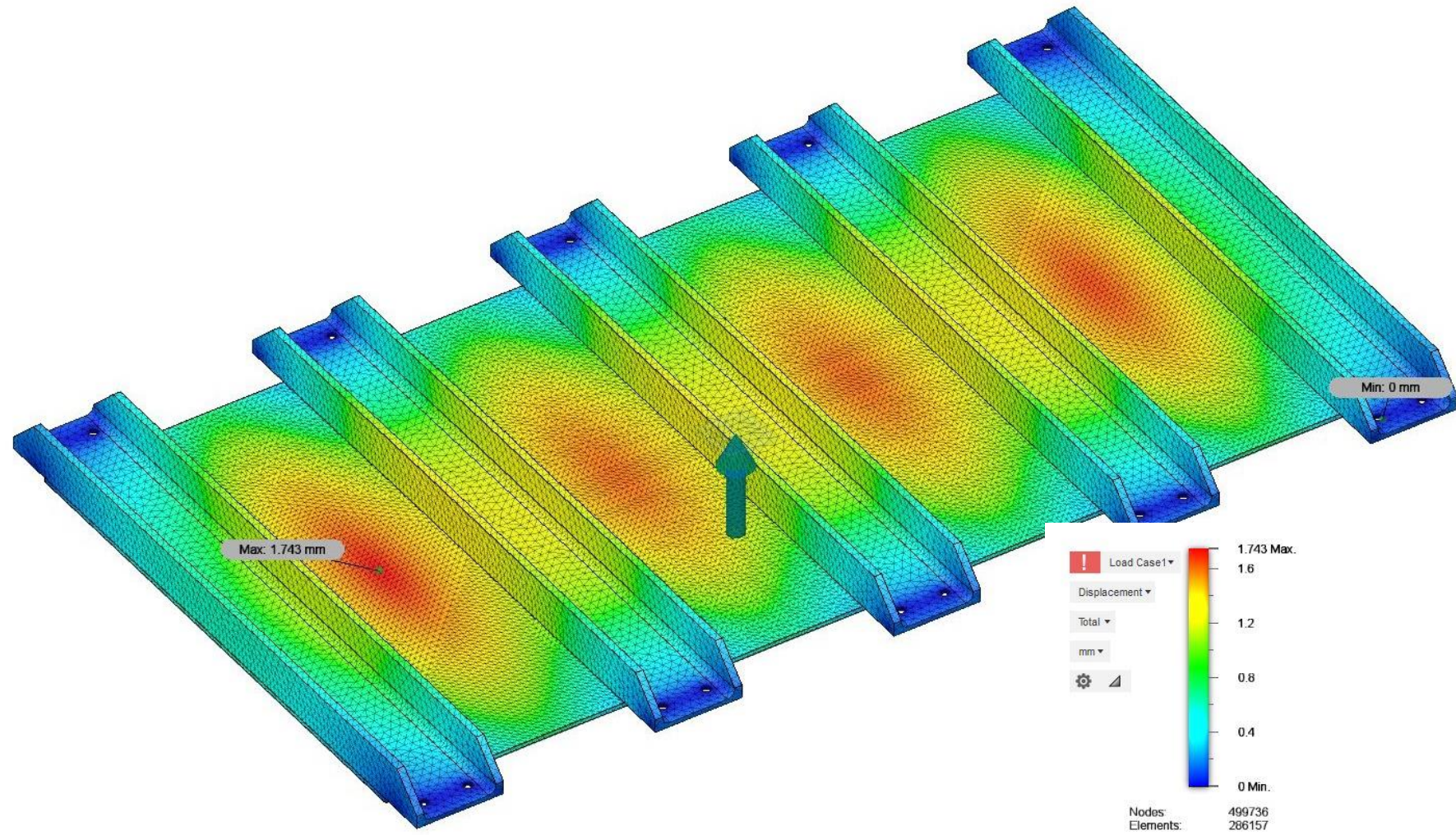


Figure C-1. Finite Element Analysis of pullout box lid at 300 kPa. Deflection was observed to be 1.8 mm.

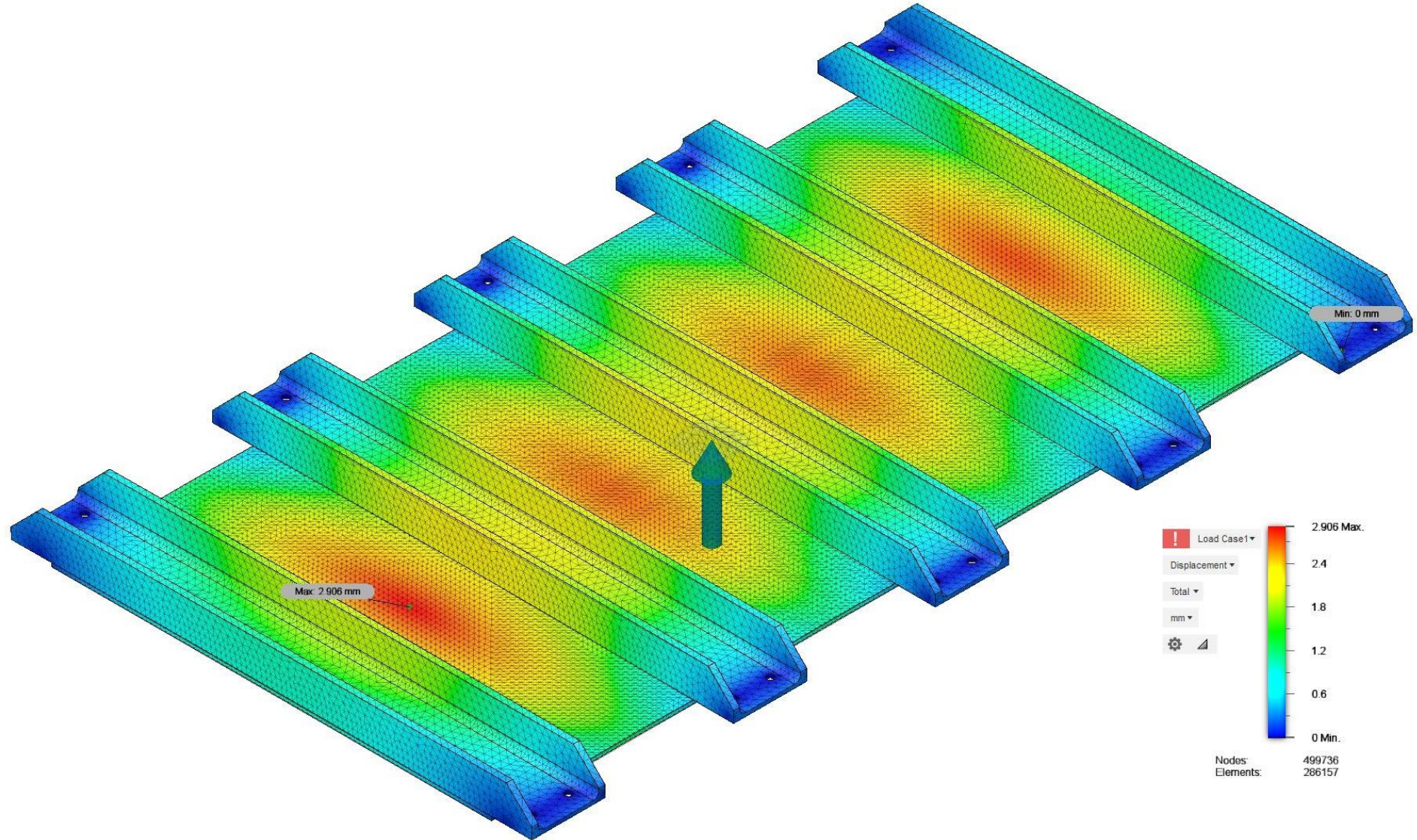


Figure C-2. Finite Element Analysis of pullout box lid at 500 kPa. Deflection was observed to be 2.9 mm.

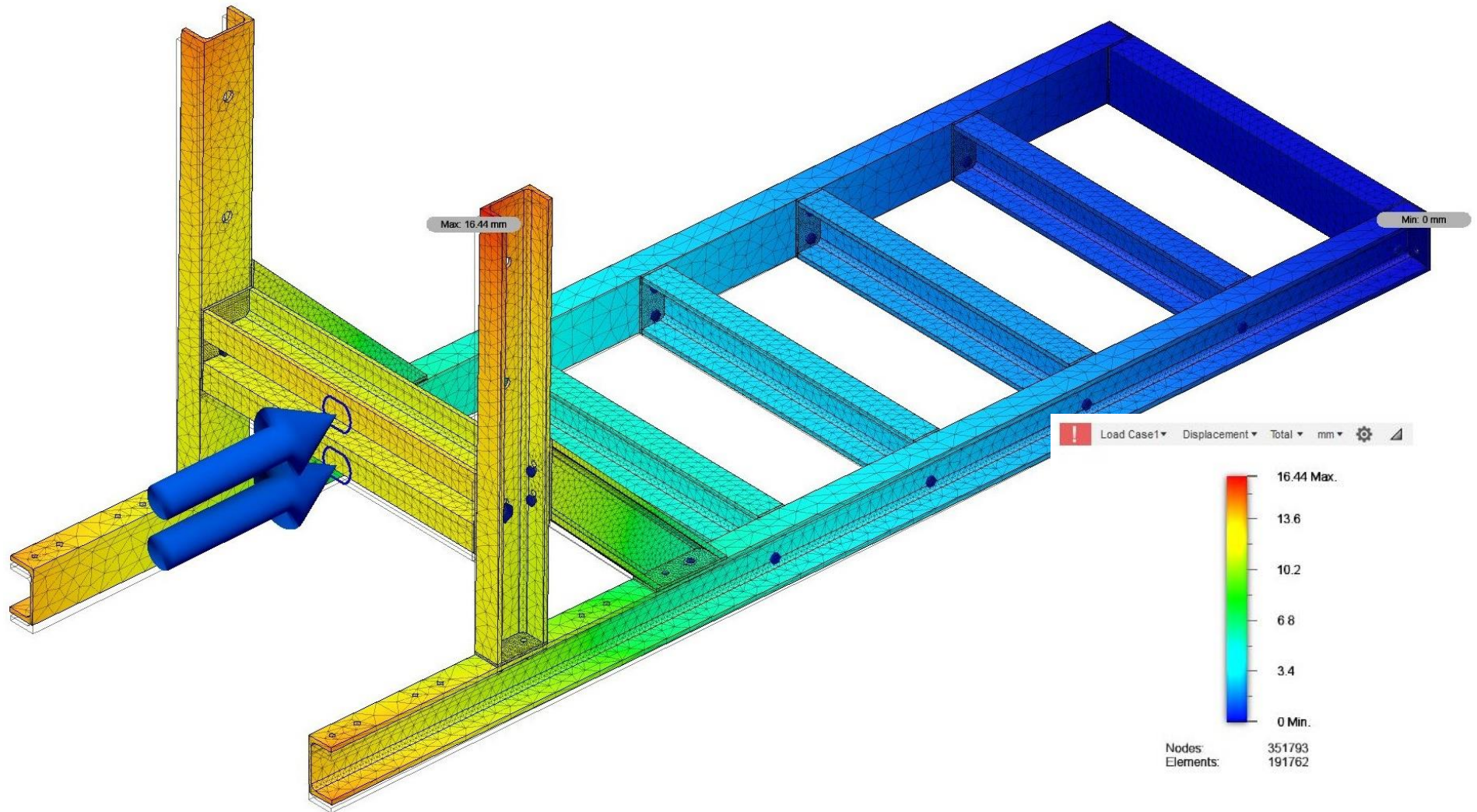


Figure C-3. Finite Element Analysis of pullout box base assembly at its standard vertical position with a jack load of 50 kN. Deflection was observed to be 16.5 mm.

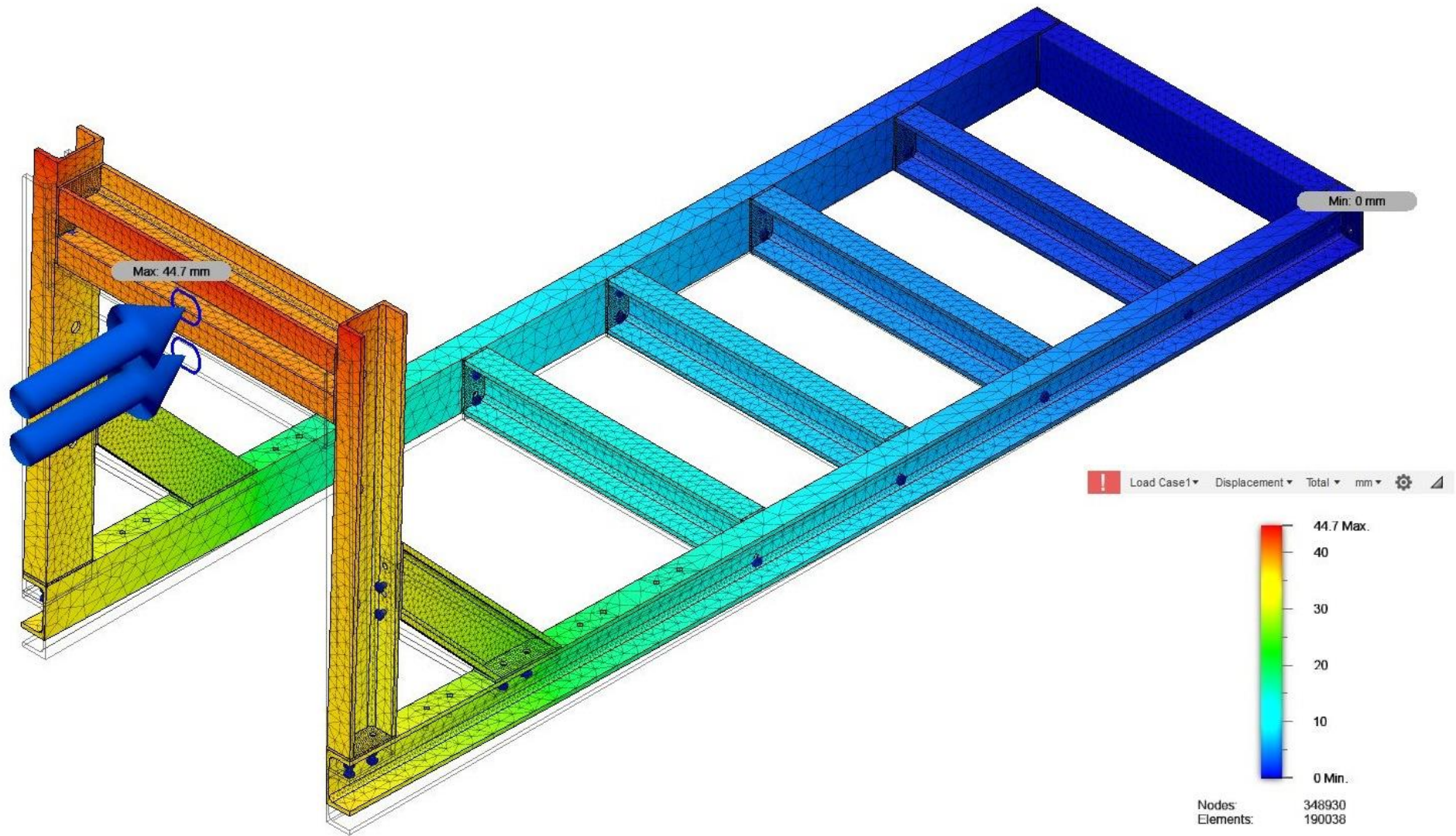


Figure C-4. Finite Element Analysis of pullout box base assembly at the least ideal position with a jack load of 50 kN. Deflection was observed to be 44.7 mm

Page left intentionally blank